

KINETIC MODELLING OF PYROLYSIS PROCESSES IN GAS AND CONDENSED PHASE

Mario Dente, Giulia Bozzano, Tiziano Faravelli, Alessandro Marongiu, Sauro Pierucci and Eliseo Ranzi*

Dipartimento di Chimica, Materiali e ingegneria Chimica, Politecnico di Milano,
Piazza L. da Vinci 32, 20133 Milano, Italy

I. Introduction	52
II. Kinetic Modelling of Pyrolysis Reactions	55
A. Automatic Generation of Pyrolysis Mechanism	64
B. Pyrolysis of Large Hydrocarbons	72
C. Detailed Characterization of Liquid Feeds	90
D. Extension of the Modelling to Liquid-Phase Pyrolysis	96
III. Fouling Processes: Formation of Carbonaceous Deposits and Soot Particles	100
A. Fouling and Coking Mechanisms in Pyrolysis Coils and TLE's	101
B. Evolution of Structure and Properties of the Deposit	107
C. Soot Formation	114
IV. Applications	124
A. Steam Cracking Process and Pyrolysis Coils	124
B. Visbreaking and Delayed Coking Processes	129
C. Thermal Degradation of Polymers	136
V. Conclusions	150
List of Symbols	151
Appendix 1. MAMA Program: Automatic Generation of Primary Lumped Reactions	152
A.1. Evaluation of End-Product Composition	152
A.2. Lumping of Components	155
A.3. Database Structure	157
A.4. Molecule Homomorphism Algorithm	159
A.5. Schematic Functionality of the Kinetic Generator	160
References	161

Abstract

The main goal of this paper is to discuss the common features in the development and validation phases of the reaction schemes able to describe pyrolysis processes in both gas and condensed phases. The

*Corresponding author. E-mail: eliseo.ranzi@polimi.it

complexity of these systems is due not only to the large number of elementary reactions involved but also to the difficulty of properly characterizing the reacting mixtures. This is typical of the pyrolysis process when liquid feedstocks, such as naphtha and gasoil, are vaporized and cracked to produce ethylene and alkenes. However, it is also true for the refinery processes involved in upgrading heavy feeds and in the combustion of liquid feeds, such as gasoline, diesel or jet propulsion fuels. Consequently, apart from the analysis of the chemistry involved in the reacting systems, another important step is the characterization of these complex hydrocarbon mixtures. High-temperature radical reactions, typical of pyrolysis processes, are characterized by their modular and hierarchical structure. This feature means that pyrolysis reactions can be studied by starting from the simpler systems and then progressively extending the simulation capability of the model to more complex situations. High-temperature pyrolysis of large hydrocarbon species rapidly gives rise to small radicals and species, and their interactions are common ground shared by all pyrolysis systems. The interactions of small hydrocarbon species, such as hydrogen, methane, ethane and ethylene, together with their parent radicals are the true core of the kinetic scheme and they constitute the first hierarchical step in all the pyrolysis models. The same mechanisms and similar radical reactions are also extended to the kinetic modelling study of the pyrolysis of liquid and condensed phases. Using a similar approach, it is possible to deal with the kinetic modelling of carbon residue and carbonaceous deposit formation on pyrolysis coils, and, more generally, on the metallic walls of different process units. These pyrolysis and condensation reactions help explain the soot and carbon particle formation in combustion processes. Always a similar kinetic approach and the same lumping techniques are conveniently applied moving from the simpler system of ethane dehydrogenation to produce ethylene, up to the soot formation in combustion environments. A brief discussion on the mathematical modelling of steam cracking, visbreaking and delayed coking processes shows the practical and direct interest of these kinetic models. The thermal degradation of the plastics, of very great environmental interest, is a further and final application example of pyrolysis reactions in the condensed phase and concludes this kinetic analysis.

I. Introduction

For several years now, detailed and complex radical reaction schemes have been widely used by the scientific and technical community to describe pyrolysis

and combustion processes. At the beginning of 1970s, the first detailed kinetic models for methane and methanol oxidation (Bowman, 1975; Seery and Bowman, 1970; Smoot *et al.*, 1976) were developed by taking advantage of the early stiff kinetic solvers (Gear, 1968), as Westbrook neatly summarized recently (Westbrook *et al.*, 2004). Using a detailed kinetic scheme of several thousand elementary steps to describe pyrolysis reaction chemistry was considered enormously innovative at the time and largely unknown to the scientific community at large (Dente *et al.*, 1970; Sundaram and Froment, 1978). The numerical solution of the very large ordinary differential equations (ODE) system of chemical component mass balances was obtained using a specifically conceived original and efficient numerical method (Dente *et al.*, 1979). More recently, theoretical concepts and methods, derived from vapour phase modelling experience and various modifications, were extended to describe pyrolysis reactions in the condensed phase. These applications first focused on refinery processes for heavy distillation residues, which essentially meant visbreaking and delayed coking. The second most important extension was to the thermal degradation of polymers. This kinetic analysis and approach also provided practical support for the kinetic studies on fouling phenomena in different process units.

Nowadays, improved computing facilities and, more importantly, the availability of the Chemkin package (Kee and Rupley, 1990) and similar kinetic compilers and processors have made these complex kinetic schemes more user-friendly and allows the study of process alternatives as well as the design and optimization of pyrolysis coils and furnaces. In spite of their rigorous, theoretical approach, these kinetic models of pyrolysis have always been designed and used for practical applications, such as process simulation, feedstock evaluations, process alternative analysis, reactor design and optimization, process control and so on. Despite criticisms raised recently by Miller *et al.* (2005), these detailed chemical kinetic models constitute an excellent tool for the analysis and understanding of the chemistry of such systems.

The main focus of this paper is to review and discuss certain features that are crucial to the various development and validation phases of these complex reaction schemes. In combustion practice as well as pyrolysis and refinery processes, the complexity of the reacting system is due not only to the large number of elementary reactions involved but also to the difficulty of properly characterizing the reacting mixture. This is typical of the pyrolysis process when liquid feedstocks, such as naphtha and gasoil, are vaporized and cracked to produce ethylene and alkenes. However, it is also true for the refinery processes involved in upgrading heavy feeds and in the combustion of liquid feeds, such as gasoline, kerosene, diesel or jet propulsion fuels. Consequently, another important step, apart from the analysis of the chemistry involved in the reacting systems, is the reliable characterization of these complex hydrocarbon mixtures. It is mostly for this reason that there is such great interest in the combustion

community in studying properly designed and defined mixtures of reference components (surrogate fuels) with the aim of analysing the decomposition and combustion behaviour of real transportation fuels in a reproducible way (Edwards and Maurice, 2001; Hudgens, 2003; Ranzi, 2006).

Gas-phase pyrolysis processes are characterized by high-temperature radical reactions. One relevant aspect of these complex and detailed reaction schemes is their modular and hierarchical structure (Westbrook and Dryer, 1984). This feature means that combustion or pyrolysis reactions can be studied by starting from the simpler systems and then progressively extending the simulation capability of the model to new and more complex situations. High-temperature pyrolysis of large hydrocarbons rapidly gives rise to small radicals and species, and their interactions are common ground shared by all pyrolysis systems. The interactions of small hydrocarbon species, such as hydrogen, methane, ethane and ethylene, together with their parent radicals are the true core of the kinetic scheme. In fact, these reactions constitute the first hierarchical step in the pyrolysis model. For example, successive dehydrogenation and condensation reactions of small alkenes, vinyl and allyl radicals are of vital importance in the characterization of ethylene formation from the degradation of all the different feeds, gases and liquids. Similarly, the high-temperature combustion of heavy fuels proceeds with the initial breaking down of the fuel to smaller radicals before the formation of the ultimate oxidation products. With the exception of certain resonance stabilized radicals, their decomposition rates are so fast that they form smaller unsaturated compounds. The smaller compounds, in rich conditions, can follow pyrolytic paths too and can form poly-aromatic hydrocarbons (PAH) and carbon particles. Pyrolysis reactions are thus critical not only when it comes to describing different refinery and petrochemical processes but also in extending the available databases to cover the decomposition behaviour of liquid fuels as well. The relative weight of these radical reactions is dependent on the operating conditions of the reacting system. The competitive nature of the pyrolysis and combustion process is of key importance. Thus, the gas-phase pyrolysis reactions of light hydrocarbon species hierarchically precede the kinetic models of heavier species.

As previously mentioned the same mechanisms and similar radical reactions can be extended to the kinetic modelling study of the pyrolysis of liquid and condensed phases. Using a similar approach, it is also possible to deal with the kinetic modelling of carbon residue and carbonaceous deposit formation on pyrolysis coils, and, more generally, on the metallic walls of different process units. These pyrolysis and condensation reactions help explain the soot and carbon particle formation in combustion processes. Finally, the last section of this chapter features brief discussion on the kinetic modelling of steam cracking, visbreaking and delayed coking processes. The thermal degradation of the plastics, of very great environmental interest, is a further example of pyrolysis reactions in the condensed phase and concludes this kinetic analysis.

II. Kinetic Modelling of Pyrolysis Reactions

It is now firmly established that free radical reactions dominate the thermal degradation of hydrocarbon species (Benson, 1976; Dente *et al.*, 1983; Poutsma, 2000; Savage, 2000). Only mechanistic radical kinetic schemes can provide reliable descriptions of the pyrolysis process.

In summary, the main reaction classes during pyrolysis are:

1. Initiation and termination (or recombination) reactions

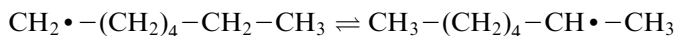
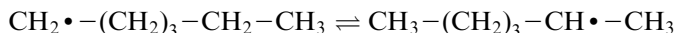
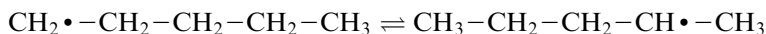


2. Propagation reactions

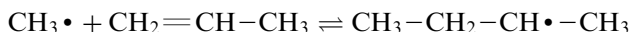
H-abstraction (or H-metathesis) on molecules



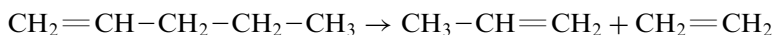
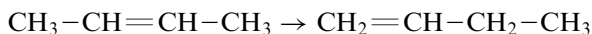
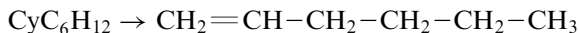
Alkyl radical isomerization via (1,4), (1,5) and (1,6) H-transfer



Addition of radicals to unsaturated molecules and alkyl radical decomposition



It is worthwhile pointing out that certain concerted path molecular reactions can play a significant role too. Typical examples are *cyclo*-alkane and olefin isomerization as well as dehydrogenation and “ene” decomposition via four- and six-centre reactions



There is an abundance of groundwork in the scientific literature regarding both the fundamental and applied chemical kinetics of pyrolysis processes.

The *n*-butane pyrolysis is analysed here as an initial, simple example of a pyrolysis reaction mechanism. It is important to note that the pyrolysis reactions of small hydrocarbons are fundamental to the proper understanding of the whole process. In fact, the pyrolysis mechanism displays a typical hierarchical structure and the small hydrocarbons must be analysed first. Fig. 1 shows the main and minor products from *n*-butane decomposition, under isothermal conditions, at 1,093 K and 1 atm. Ethylene, propylene and methane are the main products, while only trace amount of butenes, ethane, benzene and cyclopentadiene are observed. These model predictions have been confirmed and validated by several experimental measurements (Dente and Ranzi, 1983).

The most common initiation or homolysis reaction is the breaking of a covalent C–C bond with the formation of two radicals. This initiation process is highly sensitive to the stability of the formed radicals. Its activation energy is equal to the bond dissociation enthalpy because the reverse, radical–radical recombination reaction is so exothermic that it does not require activation energy. C–C bonds are usually weaker than the C–H bonds. Thus, the initial formation of H radicals can be ignored. The total radical concentration in the reacting system is controlled both by these radical initiation reactions and by the termination or radical recombination reactions. In accordance with Benson (1960), the rate constant expressions of these unimolecular decompositions are calculated from the reverse reaction, the recombination of two radical species to form the stable parent compound, and microscopic reversibility (Curran *et al.*, 1998). The reference kinetic parameters for the unimolecular decomposition reactions of *n*-alkanes for each single fission of a C–C bond between secondary

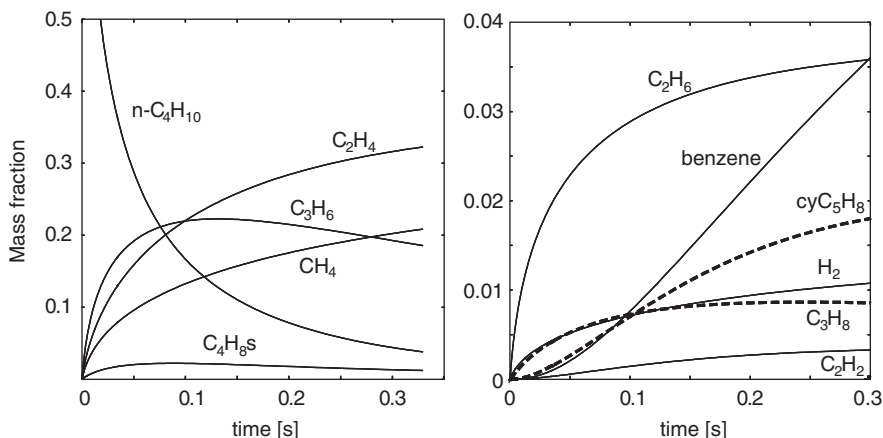
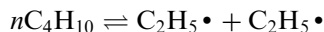


FIG. 1. Mass fractions of the main products from *n*-butane decomposition, at 1,093 K and 1 atm (Model predictions).

C-atoms, are

$$k_{\text{ref}} = 5.0 \times 10^{16} \exp\left(\frac{-81,000}{RT}\right) \quad [\text{s}^{-1}]$$

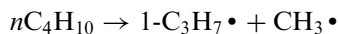
Thus, the initiation reaction of *n*-butane is



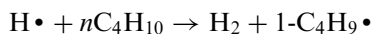
where the kinetic parameters suggested by Tsang (1978c), $k = 2.51 \times 10^{16} \exp(-82,000/RT)$, by Warnatz (1984), $k = 2 \times 10^{16} \exp(-81,200/RT)$, and finally by Dean (1985), $7.94 \times 10^{16} \exp(-80,150/RT)$, agree well with the reference rate parameters. About 2,000 kcal/kmol of extra energy is required to split off a terminal methyl group. Taking into account the hydrocarbon symmetry, it is therefore possible to assume

$$k = 10^{17} \exp\left(\frac{-83,500}{RT}\right) \quad [\text{s}^{-1}]$$

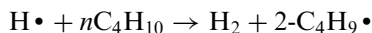
for the second initiation reaction of *n*-butane



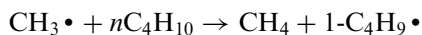
Once initiation reactions generate the propagating radicals, the primary and main products are explained simply by the H-abstraction reactions and the subsequent, fast decomposition of 1- and 2-butyl radicals. All the different H-abstracting radicals ($R\bullet$) can produce the two *n*-butyl radicals.



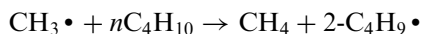
$$k = 1.29 \times 10^4 T^2 \exp\left(\frac{-6,500}{RT}\right) \quad [\text{m}^3/\text{kmol s}]$$



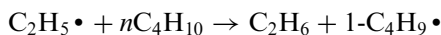
$$k = 0.86 \times 10^4 T^2 \exp\left(\frac{-4,000}{RT}\right) \quad [\text{m}^3/\text{kmol s}]$$



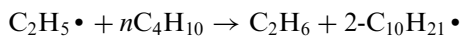
$$k = 2.34 \times 10^2 T^2 \exp\left(\frac{-7,500}{RT}\right) \quad [\text{m}^3/\text{kmol s}]$$



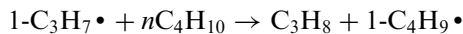
$$k = 1.56 \times 10^2 T^2 \exp\left(\frac{-5,000}{RT}\right) \quad [\text{m}^3/\text{kmol s}]$$



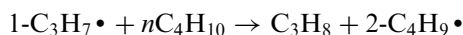
$$k = 1.40 \times 10^2 T^2 \exp\left(\frac{-10,500}{RT}\right) \quad [\text{m}^3/\text{kmol s}]$$



$$k = 0.92 \times 10^2 T^2 \exp\left(\frac{-7,700}{RT}\right) \quad [\text{m}^3/\text{kmol s}]$$

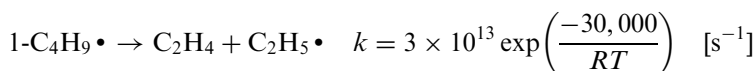
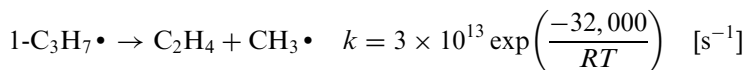


$$k = 0.81 \times 10^2 T^2 \exp\left(\frac{-9,400}{RT}\right) \quad [\text{m}^3/\text{kmol s}]$$

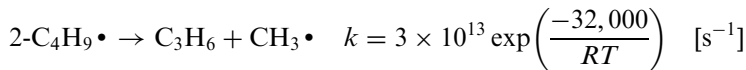


$$k = 0.54 \times 10^2 T^2 \exp\left(\frac{-6,600}{RT}\right) \quad [\text{m}^3/\text{kmol s}]$$

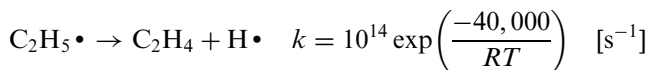
Butyl radicals decompose quickly to form ethylene and propylene. At high temperatures, alkyl radical decomposition reactions constitute an important reaction class and the prevailing fate of alkyl radicals. Take 1-propyl and 1-butyl radicals, for example. These primary alkyl radicals give rise to the following β -decomposition reactions:



These values agree closely with the ones proposed by Warnatz (1984), Dean (1985) and Tsang (1988). At the usual pyrolysis temperatures, these rate constants are $10^{6.5}$ and 10^7 s^{-1} , respectively, i.e. the lifetime of alkyl radicals is shorter than 10^{-6} s . Similarly, 2-butyl radical can form propylene and methyl radical,



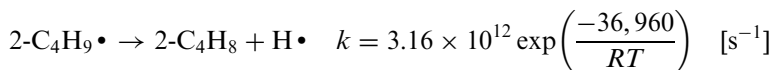
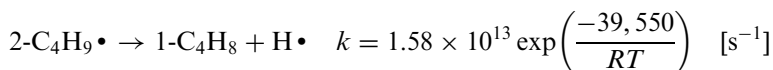
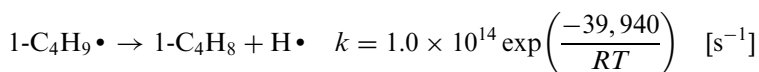
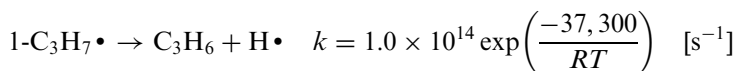
Via this mechanism, *n*-butyl radicals decompose directly to form ethylene and propylene, with ethyl and methyl radicals, respectively. The successive dehydrogenation reaction of ethyl radical forms ethylene and H radicals,



The high-pressure limit of the kinetic constant of this reaction clearly indicates that the dehydrogenation reactions are less favoured than the dealkylation ones.

Only about 3 wt% of ethane is observed in the steam cracking products, indicating that the formation of ethylene is the preferential fate of ethyl radicals. Note that most of ethane is formed via ethyl radical H-abstraction reactions, while less than 10% is due to the recombination reaction of methyl radicals. Similarly, propane formation is mostly due to the H-abstraction reactions of propyl radicals and only marginally to the recombination of methyl and ethyl radicals.

It is important to stress that all the alkyl radicals can also undergo dehydrogenation reactions with rate constants, which depend on the type of radical and the number of hydrogen atoms involved



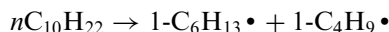
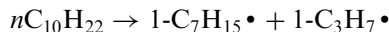
Of course, this high activation energy means that dehydrogenation reactions are less favoured than the side β -decomposition reactions (Dean, 1985; Weissman and Benson, 1984). This is why butene formation is limited to less than 2–3 wt%.

A complete analysis of the products reported in Fig. 1 requires some more comments on cyclopentadiene and benzene. Both are typical secondary products, and are mainly the result of successive addition and condensation reactions of alkenes and unsaturated radicals. Once a significant amount of ethylene and propylene is formed, vinyl and allyl radicals are present in the reacting system and form butadiene, via butenyl radicals. Successive addition reactions of vinyl and allyl-like radicals on alkenes and dialkenes sequentially explain the formation of cyclopentadiene and benzene. These reactions are discussed in-depth in the literature and will be also analysed in the coming paragraphs (Dente *et al.*, 1979). It seems worthwhile mentioning that these successive reactions and interactions of small unsaturated radicals and species constitute the critical sub-mechanism for the correct evaluation of ethylene selectivity. In fact, once the primary decomposition of the hydrocarbon feed has largely completed, the primary products and mainly small alkenes can be

involved in successive reactions with detrimental effect on the overall selectivity of the process.

The simple pyrolysis of *n*-butane gives only a partial idea of how complex pyrolysis mechanisms are. The pyrolysis of *n*-decane provides a further example of the complexity of pyrolysis reactions.

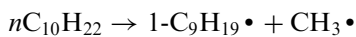
There are five different C–C bonds in the *n*-decane chain, and therefore there are five different initiation reactions. For symmetry reasons, it is possible to assume $k = 10^{17} \exp(-81,000/RT)$ [s⁻¹] for the following initiation reactions:



while for the reaction:



only $5 \times 10^{16} \exp(-81,000/RT)$ [s⁻¹] is assumed. Finally, $10^{17} \exp(-83,500/RT)$ [s⁻¹] is the kinetic constant of the last initiation reaction:



Once radicals are formed in the system, propagation reactions are the main basis of the initial feed decomposition. Figure 2 shows the complete reaction path of H-abstraction reactions on *n*-decane and itself provides proof of the complexity of the mechanism. All the different H-abstrating radicals (R•) can produce the five different isomers of *n*-decyl radical. These radicals can then isomerize and/or decompose.

The H-abstraction or metathesis reactions can be systematically described in their general form:



R and RH stand for all the possible H-abstrating radicals and for the corresponding saturated species. It is possible to assume that the rate constant for the reaction is only function of the H-abstrating radical (R•) and of the molecule from which H-atom is removed (R'H). As a first approximation, it is possible to decompose this kinetic constant as the product of two separate terms:

$$k_{\text{Habstr,ref}} \approx k_{\text{ref,R}}^0 C_{R'H}$$

where $k_{\text{ref,R}}^0$ represents the intrinsic reactivity of the radical and $C_{R'H}$ is the relative reactivity of the removed H-atom. This assumption simply means that the contributions for evaluating the rate constant only come from properties

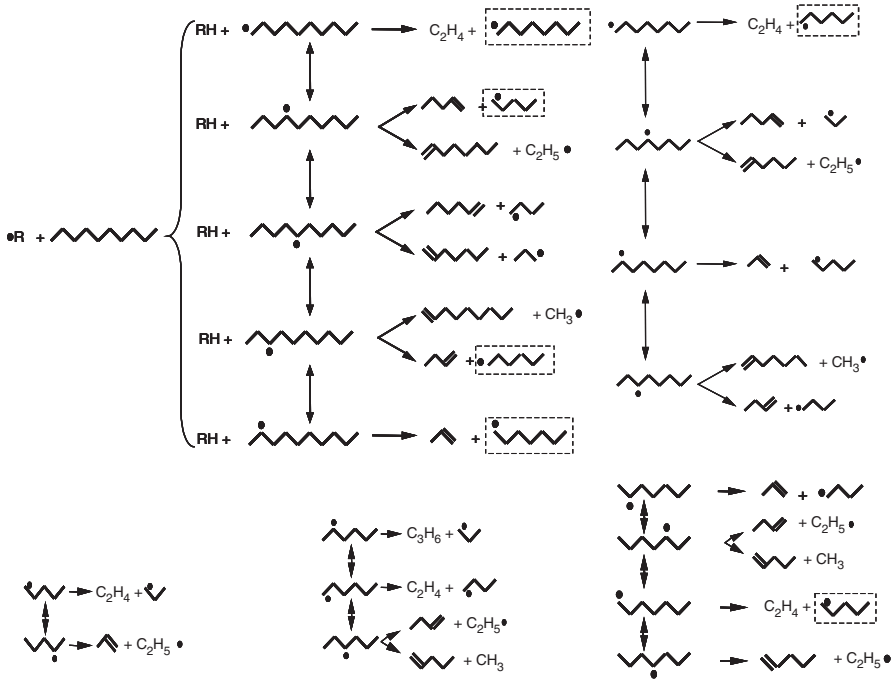
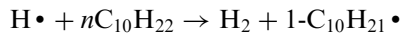
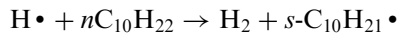


FIG. 2. H-abstraction reactions of *n*-decane and successive isomerization and decomposition reactions of alkyl radicals larger than C4.

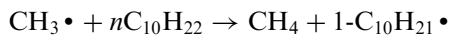
related to the abstracting radical and to the type of the hydrogen atom to be abstracted. The theoretical basis for this simplification lies partially in the assumption that the forces between atoms are very short range (Benson, 1976), i.e. in the order of magnitude of the bond lengths: each atom contributes constant amounts to the molecule properties. Details of this approach can be found elsewhere (Ranzi *et al.*, 1994). On this basis, the H-abstraction reactions on *n*-decane are estimated taking into consideration the presence of 16 secondary H-atoms, with the corresponding formation of the four different secondary radicals (*s*-C₁₀H₂₁, *s* = 2,5) and the presence of six primary H-atoms, with the formation of the primary *n*-decyl radical. Depending on the attacking radical, the estimated rate constants for each *n*-decyl isomer are



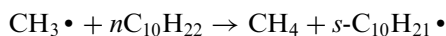
$$k = 6.43 \times 10^3 T^2 \exp\left(\frac{-6,500}{RT}\right) \quad [\text{m}^3/\text{kmol s}]$$



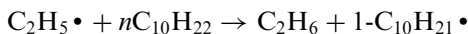
$$k = 8.60 \times 10^3 T^2 \exp\left(\frac{-4,000}{RT}\right) \quad [\text{m}^3/\text{kmol s}]$$



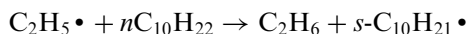
$$k = 1.17 \times 10^2 \text{T}^2 \exp\left(\frac{-7,500}{RT}\right) \quad [\text{m}^3/\text{kmol s}]$$



$$k = 1.56 \times 10^2 \text{T}^2 \exp\left(\frac{-4,900}{RT}\right) \quad [\text{m}^3/\text{kmol s}]$$



$$k = 0.69 \times 10^2 \text{T}^2 \exp\left(\frac{-10,500}{RT}\right) \quad [\text{m}^3/\text{kmol s}]$$

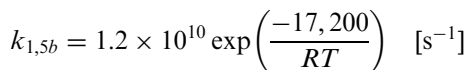
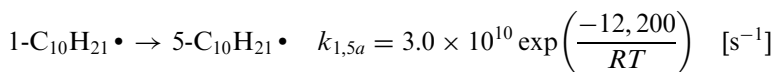
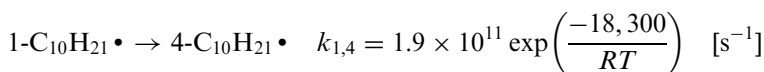


$$k = 0.92 \times 10^2 \text{T}^2 \exp\left(\frac{-7,700}{RT}\right) \quad [\text{m}^3/\text{kmol s}]$$

Similar H-abstraction reactions are easily evaluated for all the H-abstracting radicals.

Internal isomerization reactions also play an important role during pyrolysis. In fact, 1–4, 1–5 and 1–6 H-transfer reactions are easily explained on the basis of internal H-abstraction reactions, via five-, six- and seven-membered ring intermediates. The rate constants of these isomerization reactions are estimated in terms of the number of atoms in the transition-state ring structure (including the H-atom) and the type of sites involved in the H-transfer ([Benson, 1976](#)).

For instance, 1-decyl radicals can undergo the following isomerization reactions:



The (1,5) isomerization reaction can be explained on the basis of both a six- and a seven-membered ring intermediate due to the symmetry of position 5 and 6 of *n*-decane. The 1–6 H-transfer (seven-membered ring intermediate) is less important than other isomerization reactions. This is due to the extra activation energy for the ring strain and to the decrease in the A-factor for the tie-up of the additional rotor ([Benson, 1976](#); [Curran *et al.*, 1998](#); [Matheu *et al.*, 2003](#)).

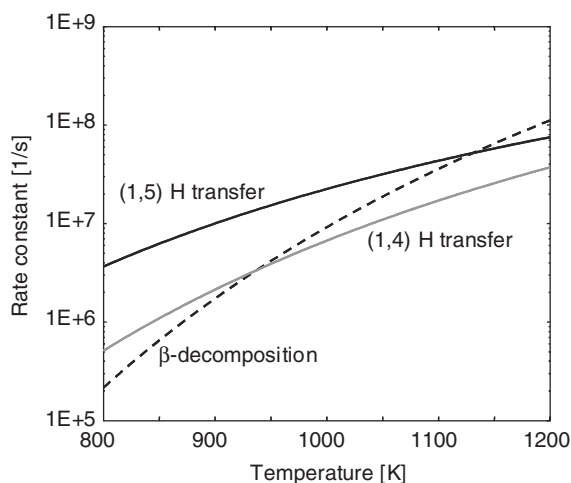
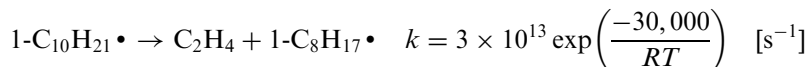


FIG. 3. Isomerization and decomposition reactions of alkyl radicals.

Figure 3 compares the rate values of these isomerization reactions with the 1-decyl radical β -decomposition:



In the temperature range of interest for steam cracking, isomerization and decomposition reactions compete and decomposition prevails only at temperatures higher than 1,100 K, while the 1–5 isomerization reaction dominates at temperatures lower than 900 K. Moreover, alkyl radicals can undergo competitive dehydrogenation reactions.

Besides these primary reactions, the successive decompositions of decyl radicals must also be taken into account as must the pyrolysis of the resulting alkenes. It is quite evident that a manual compilation of the whole set of reactions would be unmanageable, particularly when the molecular weight of the hydrocarbon components is increased.

As already observed above, the pyrolysis of naphthas and gasoils to produce light alkenes is a process whose chemical complexity is dictated both by the characterization of the hydrocarbon mixture and by the complete definition of the kinetic mechanism. Due to the large number of species involved and the need to take into account all the relevant interactions between the different species, the number of elementary reactions becomes very large. For this reason, it is useful to classify the reactions on the one hand and very convenient to apply automatic procedures in order to generate the kinetic scheme, on the other. Likewise, as the molecular weight of the molecules rises, it is not only useful but sometimes necessary to adopt carefully evaluated simplifying rules.

A. AUTOMATIC GENERATION OF PYROLYSIS MECHANISM

The use of computer generation systems in modelling the pyrolysis of large hydrocarbons is no longer considered simply an alternative to manual mechanism construction. It has become a necessity. The quantity of species and reactions becomes enormous, increasing molecular weight. This is particularly true if the focus is not merely on linear alkanes but also on other typical components of naphthas and gasoils, such as *iso*-alkanes or *cyclo*-alkanes, where the number of possible isomers increases exponentially with the number of carbon atoms in the molecule.

The generation of kinetic mechanisms is performed by computer programs which, at their best, decompose components via a defined set of rules. The procedures included in the programs can then be readily modified if changes in the understanding of the process require modifications to the available rules. It is important to stress, however, that this automatic generation is normally applied to the extension of existing kinetic schemes. Despite the fact that these programs are so easy to use and the relevance of the generated results, unresolved critical points in mechanism development still remain. These include, for instance, the proper definition of the species and reactions involved in the core of the kinetic mechanism where the interactions of small and stable species require greater direct in-depth analysis. The automatic generation of detailed mechanisms is not a feature peculiar to pyrolysis processes but has also been used extensively in different processes such as combustion, catalytic cracking and coking. Thus, many basic characteristics are worth determining not only in the pyrolysis area but also in other ones, as will be revealed in the description that follows.

Two different approaches are commonly referred to in the literature when it comes to the automatic generation of reaction mechanisms. The first approach involves combinatorial algorithms based mainly on the pioneering work of Yoneda (1979). These generate the whole set of possible reactions by only taking into account the congruence of the electronic configuration of reactants and products. Bond electron matrices are used to represent the chemical species and matrix operators describe all the possible reactions.

The second approach is simpler and generates the mechanism on the basis of specific reaction classes. Only a limited set of reaction rules is applied to all those molecules undergoing the same specific rearrangement. Reaction classes are founded on the basic principle that the reactivity of a molecule is based solely on the structural features around the bonds and atoms that change in the course of a reaction. These structural features are typically related to the influence of primary, secondary and tertiary H-atoms, to the stability of the formed radicals, and to the influence of neighbouring functional groups. Although this method easily produces reaction mechanisms, it does require a complete knowledge of the relevant reaction classes. As Blurock (Blurock, 2004) correctly observed, the goal of this mechanism generation system is to simulate

the procedures used for producing mechanisms by hand. It is a formalization of the procedures used to generate and manipulate all objects associated with mechanism development. This formalization leads to the automation of the steps and higher level operations as well as allowing more complex problems be dealt with. The tedious details, which could be error-prone if done by hand, are left to the system. Initial and partial applications to the steam cracking process date back to 1980s (Clymans and Froment, 1984; Dente and Ranzi, 1983; Froment, 1992; Hillewaert *et al.*, 1988). The approach was later extended to the catalytic cracking and hydropyrolysis processes of petroleum mixtures (Liguras and Allen, 1992). Quann and Jaffe (1992, 1996), in particular, proposed a very comprehensive example of a computer-generated reaction mechanism. Combustion processes also take this approach although they exhibit a more complex variety of phenomena and require a much higher number of species (intermediate and products) and reactions. This is as a result of the presence of oxygen as a further element together with carbon and hydrogen. Chevalier *et al.* (1988) proposed a detailed mechanism for the oxidation of *n*-hexadecane consisting of 1,200 species and 7,000 elementary reactions. Their computational technique, based on the LISP programming language, was also applied to the branched hydrocarbons such as *iso*-octane or different heptane isomers. Ranzi *et al.* (1997b) extended the automatic generation of pyrolysis reactions to combustion processes by including the interactions between alkyl radicals and oxygen with the aim of highlighting a few classes of primary propagation reactions responsible for the low-temperature phenomena during the hydrocarbon oxidation. Analogous to this, the research group in chemical kinetics in Nancy developed software (EXGAS) for the oxidation of alkanes, alkenes, ethers and *cyclo*-alkanes and mixtures of hydrocarbons. The programming of this system is based mainly on a referenced canonical tree-like description of molecules and free radicals, and can handle both acyclic and cyclic compounds (Warth *et al.*, 2000). Applications to normal and *iso*-alkanes up to *n*-hexadecane are referred to (Fournet *et al.*, 2001) and the extension to *n*-hexene was also discussed (Touchard *et al.*, 2004) recently.

Other characteristics besides the approaches described above, which may distinguish the automatic generators, are also adopted for the molecule and reaction paths descriptions.

Graph theory, substitution matrices and Boolean algebra have been extensively used for the automatic generation of the primary product distribution from the pyrolysis of hydrocarbon species. On this basis, Broadbelt and co-workers more recently proposed the NetGen program for automatic mechanism generation (Broadbelt *et al.*, 1994, 1995, 1996). A matrix representation of valence-bond connectivities is used to generate the chemical reactions. The unambiguous identification of different species is based on a general planar algorithm for the determination of homomorphism. The XMG (Exxon Mobil Mechanism Generation) generation code is the next extension of this work and was developed in cooperation with MIT (Green *et al.*, 2001; Grenda

et al., 1998, 2003). Despite the claims regarding the potential of these programs, they have mostly been applied to relatively small hydrocarbons. An interesting exception is the kinetic model of tetradecane pyrolysis, presented by De Witt *et al.* (2000).

A further key feature of each automatic generation of kinetic models is the rapid estimation of the thermodynamics properties and the rate constants. Thermochemistry generally refers to Benson's group additivity (Benson, 1976). Specific programs were developed by some of the research groups involved in this activity. In Nancy, specific heats, standard enthalpies of formation and entropies of molecules or free radicals were calculated using the software THERGAS (Muller *et al.*, 1995). The GAPP program and interface is a modified and improved version of the THERM program (Bozzelli and Dean, 1990; Ritter and Bozzelli, 1991).

As reaction rates are often expressed in a modified Arrhenius form, simple approaches like those based on linear free energy relationships, such as Evans–Polanyi, are adopted (Susnow *et al.*, 1997). Automatic generators usually refer to thermochemical kinetics methods (Benson, 1976) and the kinetic parameters rely on a limited number of reference rate constants and are extended to all the reactions of specific classes adopting analogy rules (Battin-LeClerc *et al.*, 2000; Ranzi *et al.*, 1995). Recently, extensive adoption of *ab initio* calculations of activation energies and reaction rates are adopted (Saeys *et al.*, 2003, 2004, 2006).

Finally, it is worth pointing out that one intrinsic limitation of these programs in terms of the automatic generation of pyrolysis mechanisms is the explosive number of possible reactions and intermediates products. The figures involved increase dramatically with the size of the initial radicals. While the number of end products can be controlled by adopting different solutions, such as lumping techniques (i.e. the grouping of species, generally isomers or homologous species, with the same functional groups and the same reactivity), the reduction of intermediate products as well as the grouping of the reactions involved depends on the hypothesis assumed about the interactions between the propagation paths of the different initial radicals. Specific hypothesis may lead to several reactions being expressed as a single equivalent one.

As an example of application of automatic generation, Table I gives the complete set of the primary propagation reactions of *n*-decyl radicals: isomerization, β -decomposition and dehydrogenation reactions. These reactions are produced directly by the MAMA program which was specifically developed for pyrolysis mechanism generation (Dente and Ranzi, 1983; Dente *et al.*, 2005; Pierucci *et al.*, 2005).

The main characteristics and peculiarities of this model are reported in Appendix 1. This automatic generation is performed quite simply on the basis of the definition of the different classes of primary reactions with the related small set of reference kinetic parameters, as reported in Table II.

TABLE I
PRIMARY PROPAGATION REACTIONS OF *n*-DECYL RADICALS

Isomerization reactions		
$\bullet\text{C-C-C-C-C-C-C-C-C} \rightarrow \text{C-C-C} \cdot \text{C-C-C-C-C-C-C}$	$1.89 \times 10^{11} \text{exp} (-18,300)$	
$\bullet\text{C-C-C-C-C-C-C-C-C} \rightarrow \text{C-C-C-C} \cdot \text{C-C-C-C-C-C}$	$3.00 \times 10^{10} \text{exp} (-12,200)$	
$\bullet\text{C-C-C-C-C-C-C-C-C} \rightarrow \text{C-C-C-C} \cdot \text{C-C-C-C-C-C}$	$1.20 \times 10^{10} \text{exp} (-17,200)$	
$\text{C} \cdot \text{C-C-C-C-C-C-C-C} \rightarrow \text{C-C-C-C} \cdot \text{C-C-C-C-C-C}$	$1.89 \times 10^{11} \text{exp} (-19,300)$	
$\text{C} \cdot \text{C-C-C-C-C-C-C-C} \rightarrow \text{C-C-C-C} \cdot \text{C-C-C-C-C-C}$	$3.00 \times 10^{10} \text{exp} (-13,200)$	
$\text{C} \cdot \text{C-C-C-C-C-C-C-C} \rightarrow \text{C-C-C} \cdot \text{C-C-C-C-C-C-C}$	$1.20 \times 10^{10} \text{exp} (-18,200)$	
$\text{C-C} \cdot \text{C-C-C-C-C-C-C} \rightarrow \text{C-C-C-C} \cdot \text{C-C-C-C-C-C}$	$1.89 \times 10^{11} \text{exp} (-19300)$	
$\text{C-C} \cdot \text{C-C-C-C-C-C-C} \rightarrow \text{C-C-C} \cdot \text{C-C-C-C-C-C-C}$	$3.00 \times 10^{10} \text{exp} (-13,200)$	
$\text{C-C-C} \cdot \text{C-C-C-C-C-C} \rightarrow \text{C-C-C-C} \cdot \text{C-C-C-C-C-C}$	$2.84 \times 10^{11} \text{exp} (-21,600)$	
$\text{C-C-C} \cdot \text{C-C-C-C-C-C} \rightarrow \text{C-C} \cdot \text{C-C-C-C-C-C-C-C}$	$3.00 \times 10^{10} \text{exp} (-13,200)$	
$\text{C-C-C} \cdot \text{C-C-C-C-C-C} \rightarrow \text{C} \cdot \text{C-C-C-C-C-C-C-C}$	$1.20 \times 10^{10} \text{exp} (-18,200)$	
$\text{C-C-C-C} \cdot \text{C-C-C-C-C} \rightarrow \text{C} \cdot \text{C-C-C-C-C-C-C-C}$	$1.89 \times 10^{11} \text{exp} (-19,300)$	
$\text{C-C-C-C} \cdot \text{C-C-C-C-C} \rightarrow \text{C-C} \cdot \text{C-C-C-C-C-C-C-C}$	$1.89 \times 10^{11} \text{exp} (-19,300)$	
$\text{C-C-C-C} \cdot \text{C-C-C-C-C} \rightarrow \text{C-C-C-C} \cdot \text{C-C-C-C-C-C-C}$	$4.50 \times 10^{10} \text{exp} (-15,500)$	
$\text{C-C-C-C} \cdot \text{C-C-C-C-C} \rightarrow \text{C} \cdot \text{C-C-C-C-C-C-C-C}$	$3.00 \times 10^{10} \text{exp} (-13,200)$	
$\text{C-C-C-C} \cdot \text{C-C-C-C-C} \rightarrow \text{C-C-C-C} \cdot \text{C-C-C-C-C-C-C}$	$1.80 \times 10^{10} \text{exp} (-20,500)$	
β -decomposition reactions		
$\bullet\text{C-C-C-C-C-C-C-C-C} \rightarrow \text{C}=\text{C} + \bullet\text{C-C-C-C-C-C-C-C}$	$1.00 \times 10^{14} \text{exp} (-30,000)$	
$\text{C} \cdot \text{C-C-C-C-C-C-C-C} \rightarrow \text{C-C}=\text{C} + \bullet\text{C-C-C-C-C-C-C}$	$1.00 \times 10^{14} \text{exp} (-31,000)$	
$\text{C-C} \cdot \text{C-C-C-C-C-C-C} \rightarrow \text{C}=\text{C-C-C-C-C-C-C} + \bullet\text{C}$	$1.00 \times 10^{14} \text{exp} (-33,000)$	
$\text{C-C} \cdot \text{C-C-C-C-C-C-C} \rightarrow \text{C-C-C}=\text{C} + \bullet\text{C-C-C-C-C-C}$	$1.00 \times 10^{14} \text{exp} (-31,000)$	
$\text{C-C-C} \cdot \text{C-C-C-C-C-C} \rightarrow \text{C}=\text{C-C-C-C-C-C-C} + \text{C} \cdot \text{C}$	$1.00 \times 10^{14} \text{exp} (-31,000)$	
$\text{C-C-C} \cdot \text{C-C-C-C-C-C} \rightarrow \text{C-C-C-C}=\text{C} + \bullet\text{C-C-C-C-C}$	$1.00 \times 10^{14} \text{exp} (-31,000)$	
$\text{C-C-C-C} \cdot \text{C-C-C-C-C} \rightarrow \text{C}=\text{C-C-C-C-C-C} + \text{C-C} \cdot \text{C}$	$1.00 \times 10^{14} \text{exp} (-31,000)$	
$\text{C-C-C-C} \cdot \text{C-C-C-C-C} \rightarrow \text{C-C-C-C-C}=\text{C} + \bullet\text{C-C-C-C}$	$1.00 \times 10^{14} \text{exp} (-31,000)$	
Dehydrogenation reactions		
$\bullet\text{C-C-C-C-C-C-C-C-C} \rightarrow \text{H} + \text{C}=\text{C-C-C-C-C-C-C-C}$	$1.00 \times 10^{14} \text{exp} (-39,500)$	
$\text{C} \cdot \text{C-C-C-C-C-C-C-C} \rightarrow \text{H} + \text{C}=\text{C-C-C-C-C-C-C-C}$	$1.00 \times 10^{14} \text{exp} (-41,000)$	
$\text{C} \cdot \text{C-C-C-C-C-C-C-C} \rightarrow \text{H} + \text{C}=\text{C-C-C-C-C-C-C-C}$	$1.00 \times 10^{14} \text{exp} (-41,000)$	
$\text{C-C} \cdot \text{C-C-C-C-C-C-C} \rightarrow \text{H} + \text{C}=\text{C-C-C-C-C-C-C-C}$	$1.00 \times 10^{14} \text{exp} (-41,000)$	
$\text{C-C} \cdot \text{C-C-C-C-C-C-C} \rightarrow \text{H} + \text{C-C-C}=\text{C-C-C-C-C-C-C}$	$1.00 \times 10^{14} \text{exp} (-41,000)$	
$\text{C-C-C} \cdot \text{C-C-C-C-C-C} \rightarrow \text{H} + \text{C-C-C}=\text{C-C-C-C-C-C-C}$	$1.00 \times 10^{14} \text{exp} (-41,000)$	
$\text{C-C-C} \cdot \text{C-C-C-C-C-C} \rightarrow \text{H} + \text{C-C-C-C}=\text{C-C-C-C-C-C}$	$1.00 \times 10^{14} \text{exp} (-41,000)$	
$\text{C-C-C-C} \cdot \text{C-C-C-C-C} \rightarrow \text{H} + \text{C-C-C-C}=\text{C-C-C-C-C-C}$	$1.00 \times 10^{14} \text{exp} (-41,000)$	
$\text{C-C-C-C} \cdot \text{C-C-C-C-C} \rightarrow \text{H} + \text{C-C-C-C-C}=\text{C-C-C-C-C}$	$1.00 \times 10^{14} \text{exp} (-41,000)$	

The resulting mechanism includes 16 isomerization, eight β -decomposition and nine dehydrogenation reactions, which are the primary propagation reactions of five different *n*-decyl radicals. As already discussed elsewhere, it is very easy to extend this generation to heavier species (Ranzi *et al.*, 2005). Of course, the complexity, or rather the number of elementary reactions, and the number of intermediate radicals and molecules in particular, rapidly increase with the number of C-atoms. The need to introduce the primary reactions of the primary products, such as alkenes, is also taken into account.

TABLE II
REFERENCE KINETIC PARAMETERS OF PYROLYSIS REACTIONS (UNITS ARE KMOL, M, S AND KCAL)

Initiation reactions: Unimolecular decomposition of C–C bonds			
<i>CH₃–C_{sec}</i>	<i>C_{sec}–C_{sec}</i>	<i>C_{sec}–C_{ter}</i>	<i>C_{sec}–C_{quat}</i>
$5 \times 10^{16} \exp(-83,500/RT)$	$5 \times 10^{16} \exp(-81,000/RT)$	$5 \times 10^{16} \exp(-80,000/RT)$	$5 \times 10^{16} \exp(-78,000/RT)$
H-abstraction reactions of alkyl radicals			
	<i>Primary H-atom</i>	<i>Secondary H-atom</i>	<i>Tertiary H-atom</i>
Primary radical	$10^8 \exp(-13,500/RT)$	$10^8 \exp(-11,200/RT)$	$10^8 \exp(-9,000/RT)$
Secondary radical	$10^8 \exp(-14,500/RT)$	$10^8 \exp(-12,200/RT)$	$10^8 \exp(-10,000/RT)$
Tertiary radical	$10^8 \exp(-15,000/RT)$	$10^8 \exp(-12,700/RT)$	$10^8 \exp(-10,500/RT)$
Isomerization reactions (Transfer of a primary H-atom ^a)			
	<i>1–4 H-transfer</i>	<i>1–5 H-transfer</i>	<i>1–6 H-transfer</i>
Primary radical	$10^{11} \exp(-20,600/RT)$	$1.58 \times 10^{10} \exp(-14,500/RT)$	$3.16 \times 10^9 \exp(-19,500/RT)$
Secondary radical	$10^{11} \exp(-21,600/RT)$	$1.58 \times 10^{10} \exp(-15,500/RT)$	$3.16 \times 10^9 \exp(-20,500/RT)$
Tertiary radical	$10^{11} \exp(-22,100/RT)$	$1.58 \times 10^{10} \exp(-16,000/RT)$	$3.16 \times 10^9 \exp(-21,000/RT)$
Alkyl radical decomposition reactions (to form primary radicals)			
	<i>Primary radical</i>	<i>Secondary radical</i>	<i>Tertiary radical</i>
	$10^{14} \exp(-30,000/RT)$	$10^{14} \exp(-31,000/RT)$	$10^{14} \exp(-31,500/RT)$
Corrections of decomposition rates to form			
<i>Methyl radical</i>	<i>Secondary radical</i>	<i>Tertiary radical</i>	<i>Allyl radical</i>
$\exp(-2,500/RT)$	$\exp(1,500/RT)$	$\exp(2,500/RT)$	$0.316 \times \exp(8,000/RT)$

^aCorrections for secondary and tertiary H-atoms are the same as for H-abstractions.

1. Lumping of Reactions

The previous paragraph highlights the rapid increase in the number of species and reactions as the molecular weight of the hydrocarbons rises. Appropriate reduction techniques are thus very useful in taking a more viable approach to the problem.

As previously discussed, alkyl radicals decomposition reactions constitute an important fate and reaction path of alkyl radicals. Due to the very short life-times of alkyl radicals, [Rice and Herzfeld \(1933, 1934\)](#) suggested a complete decomposition mechanism where all the radicals larger than methyl were considered instantaneously decomposed into alkenes and H and CH₃ radicals. In this mechanism, all the intermediate alkyl radicals decompose to directly form alkenes and smaller alkyl radicals. This would mean that the final ethylene production from a steam cracking process would be significantly overestimated when compared with the experimental measurements. For instance, the net and final result of the successive decomposition mechanism of 1-decyl radical would be 5 moles of ethylene and one H radical.

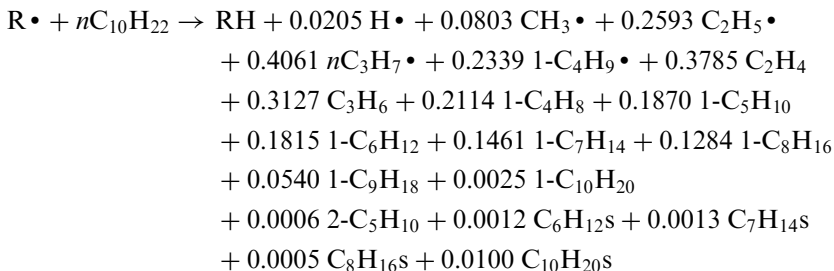
This typical feature of pyrolysis systems is very useful in improving the handling of the decomposition paths of large hydrocarbon species. Within the pressure and temperature range of the pyrolysis processes, the absence of interactions between large radicals and other species in the cracking mixture allows the direct substitution of *n*-decyl radicals with their primary isomerization and decomposition products, as shown in [Fig. 2](#). [Table III](#) reports the product distribution from the isomerization and β -decomposition reaction of *n*-decyl radicals, as a net result of the H-abstraction reactions on *n*-decane. These distributions, which were evaluated at three different temperatures, show a limited temperature effect. In fact, the largest deviations in product distribution relate to the increasing importance of the primary radical and its successive decomposition to form ethylene and *n*-octyl radicals. The greater stability of the 2-decyl radical is due to the single β -decomposition of this

TABLE III
TEMPERATURE EFFECT ON PRIMARY PRODUCT DISTRIBUTION FROM β -DECOMPOSITION REACTION OF
n-DECYL RADICAL

	800 K	1,000 K	1,200 K
C ₉ H ₁₈ + CH ₃ •	0.0424	0.0516	0.0588
C ₈ H ₁₆ + C ₂ H ₅ •	0.1478	0.1332	0.1193
C ₇ H ₁₄ + C ₃ H ₇ •	0.1519	0.1475	0.1346
C ₆ H ₁₂ + C ₄ H ₉ •	0.1519	0.1475	0.1346
C ₅ H ₁₀ + C ₅ H ₁₁ •	0.1479	0.1332	0.1193
C ₄ H ₈ + C ₆ H ₁₃ •	0.1492	0.1412	0.1359
C ₃ H ₆ + C ₇ H ₁₅ •	0.1526	0.1569	0.1677
C ₂ H ₄ + C ₈ H ₁₇ •	0.0563	0.0889	0.1300

secondary radical. Moreover, it is important to stress that at temperatures higher than 1,200 K the lifetime of alkyl radicals falls to less than 10^{-8} s and their internal distribution becomes of limited importance.

In principle, heavy radicals could undergo also H-abstraction, addition on unsaturated bonds and recombination reactions. It is quite easy to demonstrate how little relevance these reactions have compared with the isomerization and decomposition ones. This helps drastically reduce the total number of radicals and reactions to be considered. All of the intermediate alkyl radicals, higher than C₄, are supposed to be instantaneously transformed into their final products. With reference to the primary products of Table III, the heavy radicals from pentyl up to octyl undergo direct isomerization and decomposition reactions to form smaller radicals and alkenes. Therefore, large sections of the kinetic scheme can be reduced to a few equivalent or lumped reactions whilst still maintaining a high level of accuracy. The complete kinetic scheme shown in Fig. 2 can be then simply reduced to this single, equivalent or lumped reaction:



This stoichiometry is directly obtained at 1,040 K by solving the initial continuity equations for all the radical species. A better insight into this approach is given in Appendix 1 which also refers to the specific MAMA code. The MAMA program is actually much more than a simple automatic reaction mechanism generator. It may generate the reaction path, namely the isomerization and decomposition reactions of the intermediate species, but it also solves the overall system and evaluates the primary distribution products in accordance with the hypothesis of the autonomous fate of the large intermediate radicals. The net result is the generation of equivalent or lumped reactions that drastically reduce the overall dimension of the reacting system, in terms of both species and reactions. This equivalent stoichiometry lumps all the elementary reactions of Fig. 2 and, as already mentioned, it is only very slightly temperature dependent at the usual steam cracking process temperature (900–1,100 K). This simplification was also strongly supported by the recent findings of McGivervy *et al.* (2004) who analysed the decomposition of *n*-octyl radicals.

H radical formation occurs as a result of the dehydrogenation reactions of all the intermediate radicals. These dehydrogenation reactions, not reported in Fig. 2 as well as in Table III, also explain the drop in the formation of 2-pentene, 2- and 3-hexenes and so on.

This lumped reaction matches the general lumping definition discussed at the “Workshop on Combustion Simulation Databases for Real Transportation Fuels” (Hudgens, 2003) very well. The lumped reaction is a collection of elementary reactions expressed as an “equivalent” apparent single step reaction. A lumped reaction may be a stepwise reaction, involving a consecutive set of elementary reactions, the simplest example being $A \rightarrow I \rightarrow B$, where I is a steady-state intermediate. A lumped reaction may also be a set of related but dissimilar reactions, operating as alternative or parallel pathways, or $A \rightarrow \{In\} \rightarrow B$ where $\{In\}$ represents the set of parallel pathways. Finally, a lumped reaction may also be a set of similar reactions, operating collectively on similar molecular species, or $\{A\} \rightarrow \{I\} \rightarrow \{B\}$ where $\{A\}$, $\{I\}$ and $\{B\}$ are sets of similar reactants, intermediates and products, respectively.

2. Lumping of Species

The sets of similar reactants, intermediates and products in the previous lumped reaction are also an initial example of lumped species. Thus, lumped species $\{A\}$ are defined as a weighted mixture of several isomers:

$$\{A\} = \sum x_j A_j$$

Lumped species react in a similar way and their internal distribution remains almost unchanged with the reactions.

Thus, all the isomers of large hydrocarbon species should be conveniently grouped into a single lumped component. A large number of alkene isomers are formed during the pyrolysis of heavy alkanes. For instance, dehydrogenation reactions of branched alkyl radicals generate all the different branched alkenes. In order to avoid an unnecessary number of species, all these isomers are conveniently grouped and considered as a single lumped compound. The clear advantage of the automatic generation is that the internal splitting of the real components is stored and the impact on the final product distribution is correctly taken into account.

Apart this “horizontal” lumping among species with the same molecular weight, there is also another very convenient simplification: the lumping of homologous species with a different number of carbon atoms. Let us refer to this as “vertical” lumping, i.e. lumping of homologous species with different molecular weights. The reactivity and the product distribution of large hydrocarbons with n_C carbon atoms can be correctly and conveniently estimated with a linear combination of the reactivity and product distribution of the homologous species with (n_C-1) and (n_C+1) carbon atoms. This fact is clearly demonstrated in Fig. 4 where the selectivities of small radicals and alkenes obtained from the H-abstraction reactions of n -alkanes are reported as a function of the carbon number. A quasilinear tendency of the different products with the carbon number can be observed.

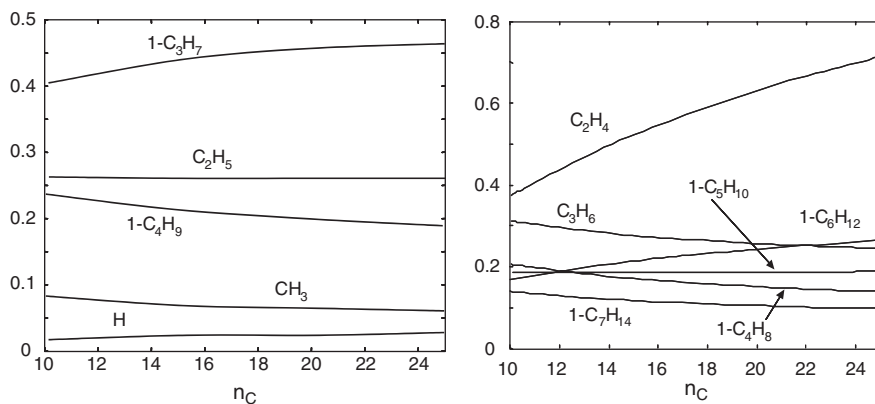


FIG. 4. Stoichiometric coefficients of small radicals and α -alkenes from the H-abstraction reactions of n -alkanes at 1,040 K, as a function of the carbon number.

Two other considerations can be drawn from the analysis of this figure:

- Ethylene selectivity increases with carbon number due to the importance of the β -decomposition of large intermediate radicals.
- 1-Pentene and, more importantly, 1-hexene selectivities also increase due to the internal (1–4) and (1–5) H-transfer reactions. 1-Propyl radical also increases for the same reason.

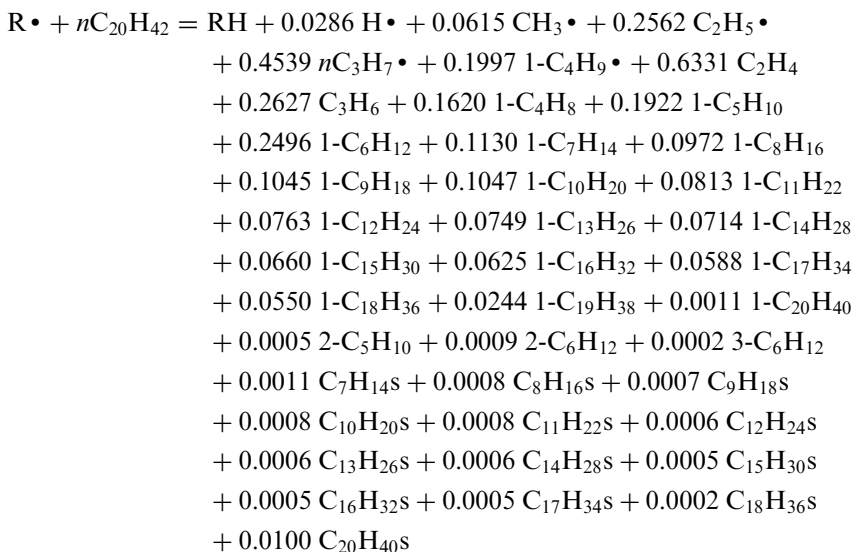
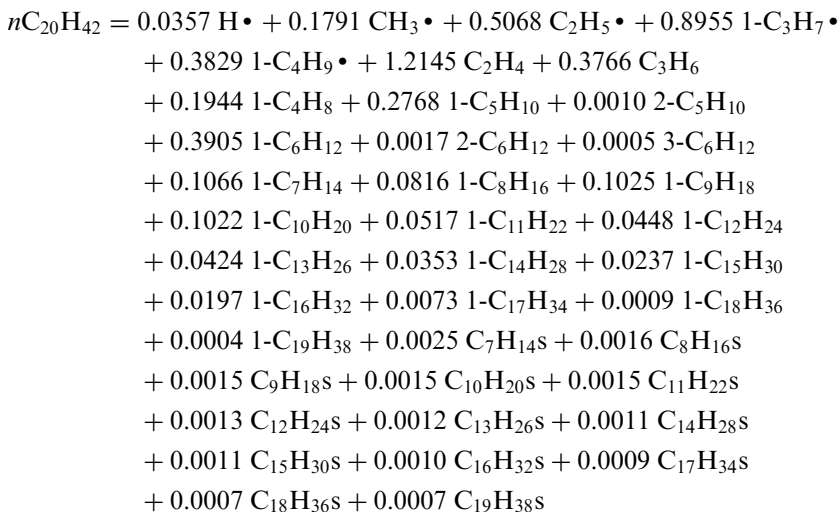
B. PYROLYSIS OF LARGE HYDROCARBONS

It is possible to analyse and to generate the primary pyrolysis reactions of the various hydrocarbon classes using the aforementioned kinetic parameters as a basis. Normal and branched alkanes, *cyclo*-alkanes and aromatics are briefly analysed in order to discuss the analogies and similarities, as well as the differences in their pyrolysis reactions. The previously mentioned assumptions relating to the autonomous fate of large alkyl radicals and the consequent lumping of reactions are consistently applied. The automatic generation of the primary pyrolysis reactions is obtained by applying the same rules and criteria already discussed when analysing the primary reactions of n -decane and once again using the reference kinetic parameters from Table II (Ranzi *et al.*, 2001).

1. Normal Alkanes

The clear advantage of this lumping approach is that the analysis of new components only requires the definition of the primary pyrolysis reactions. For large alkanes, only the initiation and H-abstraction reactions need to be defined.

Thus, the lumped stoichiometry of the initiation and H-abstraction reactions of *n*-eicosane, again evaluated by the MAMA program at 1,040 K, is simply:



Of course, α -linear-alkenes ($\text{1C}_n\text{H}_{2n}$) prevail but all the remaining linear alkenes ($\text{C}_n\text{H}_{2n}\text{s}$) are also formed as a result of the dehydrogenation reactions of all the intermediate radicals.

For the sake of simplicity and because their quantities are so tiny, these linear non α -alkenes are conveniently grouped. Table IV shows the temperature effect on the molar selectivities of the primary products from the H-abstraction

TABLE IV
TEMPERATURE EFFECT ON THE PRIMARY PRODUCT DISTRIBUTION FROM H-ABSTRACTION REACTIONS OF
n-EICOSANE (MOLAR SELECTIVITY)

T/K	940	990	1,040	1,090
H•	0.0172	0.0224	0.0286	0.0360
CH ₃ •	0.0645	0.0633	0.0615	0.0596
C ₂ H ₅ •	0.2790	0.2666	0.2562	0.2469
1-C ₃ H ₇ •	0.4358	0.4473	0.4539	0.4558
1-C ₄ H ₉ •	0.2035	0.2004	0.1997	0.2018
C ₂ H ₄	0.4036	0.5082	0.6331	0.7759
C ₃ H ₆	0.3043	0.2832	0.2627	0.2430
1-C ₄ H ₈	0.1883	0.1749	0.1621	0.1500
1-C ₅ H ₁₀	0.1957	0.1939	0.1922	0.1905
2-C ₅ H ₁₀	0.0004	0.0005	0.0005	0.0006
1-C ₆ H ₁₂	0.2418	0.2476	0.2496	0.2474
C ₆ H ₁₂ S	0.0008	0.0009	0.0011	0.0013
1-C ₇ H ₁₄	0.1260	0.1195	0.1130	0.1069
C ₇ H ₁₄ S	0.0009	0.0011	0.0013	0.0014
1-C ₈ H ₁₆	0.1049	0.1009	0.0972	0.0938
C ₈ H ₁₆ S	0.0006	0.0007	0.0008	0.0009
1-C ₉ H ₁₈	0.1087	0.1070	0.1045	0.1014
C ₉ H ₁₈ S	0.0005	0.0006	0.0007	0.0009
1-C ₁₀ H ₂₀	0.1113	0.1087	0.1047	0.1000
C ₁₀ H ₂₀ S	0.0005	0.0007	0.0008	0.0009
*1-C ₁₁ H ₂₂	0.1244	0.1219	0.1194	0.1169
*C ₁₁ H ₂₂ S	0.0007	0.0009	0.0011	0.0013
*1-C ₁₃ H ₂₆	0.1869	0.1850	0.1827	0.1798
*C ₁₃ H ₂₆ S	0.0010	0.0012	0.0015	0.0018
*1-C ₁₆ H ₃₂	0.2098	0.2090	0.2080	0.2067
*sC ₁₆ H ₃₂ S	0.0010	0.0013	0.0015	0.0018
*1-C ₂₀ H ₄₀	0.0597	0.0606	0.0616	0.0626
*C ₂₀ H ₄₀ S	0.0064	0.0082	0.0102	0.0125

*Lumped or equivalent compounds.

reactions of *n*-eicosane. Predicted ethylene selectivities move from 40.36% at 940 K up to 77.59% at 1,090 K, clearly indicating the prevailing importance of the decomposition reactions at high temperatures. The ethylene increase actually corresponds to a reduction in the heavier alkenes, particularly propene and butene. The higher ethylene selectivity at high temperature is mainly due to the increase in decomposition reactions with respect to isomerization ones. Heavy alkenes are also grouped using vertical lumping. H radical production is very low due to the high activation energy of the dehydrogenation reaction.

2. Branched Alkanes

Branched alkane decomposition becomes increasingly difficult, mainly as a result of the large number of possible isomers with the same molecular weight.

TABLE V
AVERAGE CARBON NUMBER, BOILING TEMPERATURES AND THE NUMBER OF PARAFFIN ISOMERS OF
DIFFERENT PETROLEUM FRACTIONS. ADAPTED FROM [ALTGELT AND BODUSZYNSKI \(1994\)](#)

Carbon no.	Boiling temperature (°C)	Paraffin isomers	Petroleum fraction
8	126	18	Naphtha and gasoline
10	174	75	Kerosene
12	216	355	Jet fuels
15	271	4,347	Diesel fuels
20	344	3.66×10^5	Light gasoil
25	402	3.67×10^7	Gasoil
30	449	4.11×10^9	Heavy gasoil
35	489	4.93×10^{11}	Atmospheric residue

TABLE VI
RELATIVE AMOUNT OF BRANCHED ISOMERS OF C_8H_{18} (WT%)

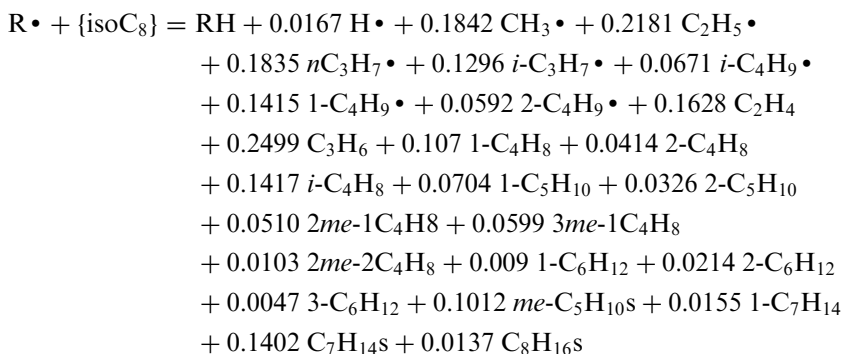
Origin	Ponca	Occidental	Texas	Internal weights
Isomers				
2-methylheptane	46.3	36.9	42.1	45.8
3-methylheptane	15.4	28.5	23.4	22.9
4-methylheptane	10.3	10.2	9.3	11.5
2,3-dimethylhexane	3.6	5.4	6.3	3.4
2,4-dimethylhexane	3.1	5.5	4.2	3.4
2,5-dimethylhexane	3.1	5.7	4.0	3.4
3,4-dimethylhexane	6.7	2.6	3.7	3.4
2,2-dimethylhexane	0.5	—	0.3	—
3,3-dimethylhexane	1.5	1.7	0.4	—
2,3,4-trimethylpentane	0.3	—	1.1	1.2
2,2,3-trimethylpentane	0.2	—	—	—
2,3,3-trimethylpentane	0.3	—	0.6	—
3-ethylhexane	4.6	3.5	3.1	3.8
2-methyl-3-ethylpentane	3.1	—	1.5	1.2
3-methyl-3-ethylpentane	1.0	—	—	—

Several simplifications, whose importance increases with carbon numbers, are thus introduced. The difficulties involved in a detailed description of feed components are primarily caused by the very large number of compounds in the petroleum fractions, as clearly outlined in [Table V](#).

One convenient simplification becomes clear when considering relatively simple or light components such as the branched C_8H_{18} . As shown in [Table VI](#), only a few isomers describe the whole fraction of branched alkanes with eight carbon atoms: three monomethyl-heptanes, ethyl-hexane and four dimethyl-hexanes with a tertiary C structure. In spite of the different origins of these feeds, there is clear regularity with regard to their composition. In fact,

monomethyl-heptanes prevail on dimethyl-hexanes and monoethyl-hexanes. Trimethyl-pentanes are less abundant and quaternary C-atoms are of very limited importance. On this basis, it is possible to empirically derive an internal distribution of the isomer mixture and to derive a lumped component $\{isoC_8\}$, as shown in the last column of Table VI. Of course, this internal distribution is a peculiarity of the virgin fractions and can change drastically after thermal or catalytic refinery processes.

Thus, for virgin feeds, a single equivalent or lumped component $\{isoC_8\}$ is defined by grouping all the different isomers with their relative weights, where the three mono-methyl-heptanes sum up to about 80% of the whole fraction. The corresponding lumped H-abstraction reaction, obtained by simply mixing the primary distribution products generated by MAMA program, has the following stoichiometry:



It is important to stress that this lumped reaction allows a significant reduction in both feed and intermediate species as well as in reactions, yet still retaining a very high level of accuracy in the prediction of the various products of pyrolysis.

It is quite difficult to find accurate and detailed analyses of single isomers for branched alkanes with more than 10 C-atoms in the literature. Nevertheless, GC analysis of heavy naphtha, kerosene and light gasoils indicates the prevailing presence of isoprenoid structures characterized by an average probability of methyl substitution of about 0.20 (Altgelt and Boduszynski, 1994).

One possible use of kinetic generators and the advantages associated with them can be demonstrated by considering the lumped component $\{isoC_{15}\}$. There are more than 4,000 different isomers, as reported in Table V: 12 different methyl-tetradecanes, 55 dimethyl- C_{13} (without quaternary C-atoms), 120 trimethyl- C_{12} , 126 tetra-methyl- C_{11} and so on. These numbers of different isomers are significantly reduced by accounting for the symmetry of the molecule. By accounting for mono-, di-, tri-, tetra- and penta-methyl isomers with the

proper relative weight, the lumped reaction of $\{isoC_{15}\}$ (well-defined mixture of different branched alkanes $C_{15}H_{32}$) becomes:

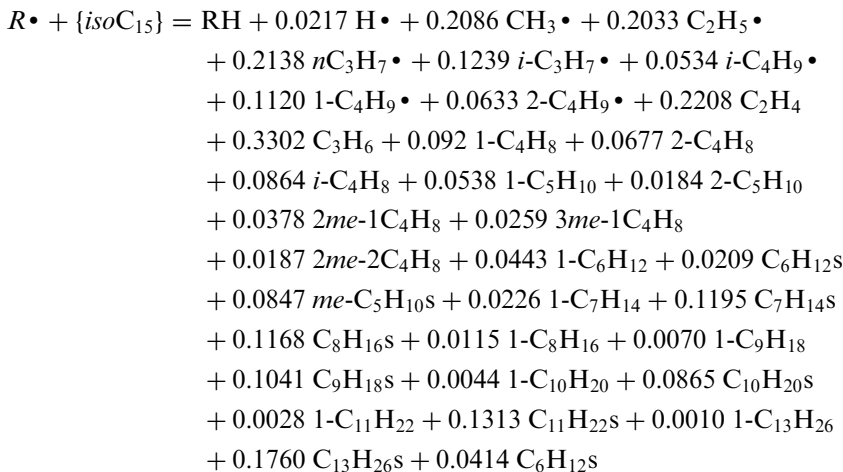
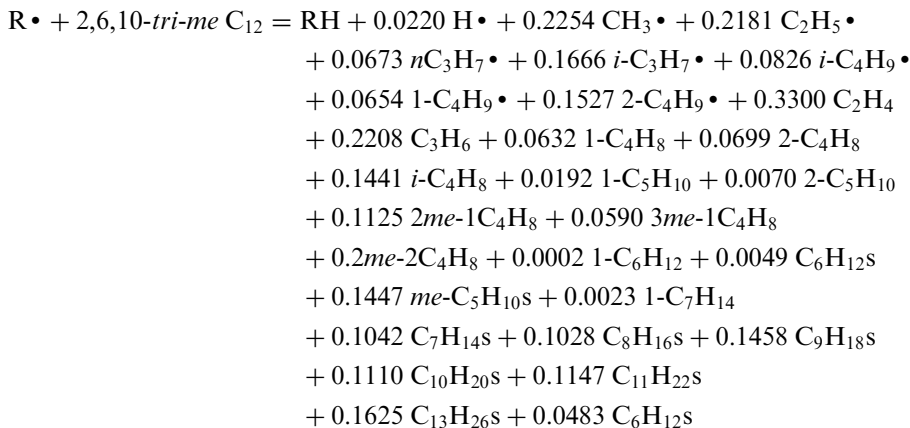


Figure 5 demonstrates the sensitivity of the primary products of this lumped H-abstraction reaction by varying the probability of methyl substitution, i.e. by varying the relative amount of the different classes of isomers (mono-, di-, tri-, tetra-methyl and so on). While ethylene and 1-butene selectivities decrease with the increase in degree of methyl substitution, methyl radical, 2-butene and isobutene formation is enhanced.

The isoprenoid structure hypothesis corresponds to an average of three methyl substitutions along the carbon chain. By comparison, the equivalent H-abstraction reaction of the 2,6,10-tri-methyl-dodecane, with a regular tri-isoprene structure, becomes:



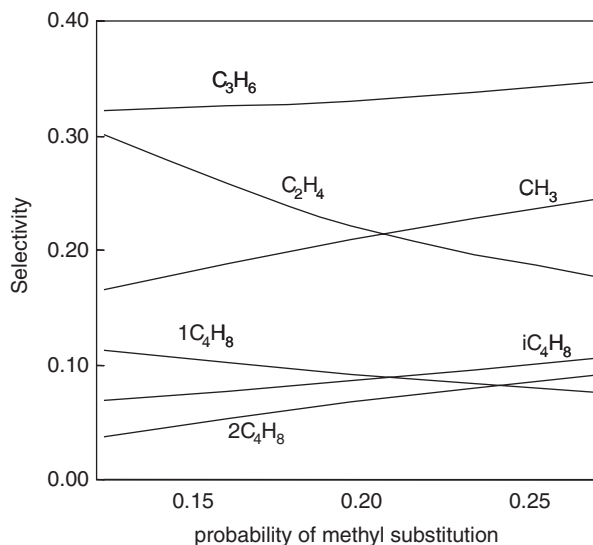


FIG. 5. Pyrolysis of lumped component of branched alkanes $\{C_{15}H_{32}\}$. Selectivity of methyl radical and small alkenes as a function of the probability of methyl substitution.

Due to the regular branched structure of this isomer, linear 1-alkenes heavier than 1-heptene are not present and the relative amount of propyl and butyl radicals is significantly different too. In other words, the lumped H-abstraction reaction of a single model component loses the variety of primary products obtained from the previous lumped $\{isoC_{15}\}$. It seems relevant to observe that to improve ethylene selectivity prediction, alkene components heavier than hexenes can be conveniently described with two different species, respectively corresponding to the true component $1-C_nH_{2n}$ and to a lumped mixture of the remaining normal and branched isomers.

As previously mentioned, the difference in the primary product distributions from homologous species decreases as the number of carbon atoms (n_c) becomes larger than 10–12. Therefore, branched alkanes heavier than C_{10} are also lumped species that contain not only isomers (with the same n_c) but also adjacent homologous species. For instance, all the different branched alkanes with 11 C-atoms are split equally between the two lumped components $\{isoC_{10}\}$ and $\{isoC_{12}\}$. As a result of this vertical lumping, only a few reference and lumped components are selected inside each family thus further decreasing the computation effort involved while maintaining prediction accuracy.

3. Cyclo-Alkanes and Alkenes

There is a great abundance of groundwork in the scientific literature on both the fundamental and applied chemical kinetics of pyrolysis reactions relating to

normal and branched alkanes. The pyrolysis of *cyclo*-alkanes, on the other hand, has received very little attention. Nevertheless, naphthas and liquid feeds contain large quantities of *cyclo*-alkanes, which consist of both alkyl *cyclo*-pentane and alkyl *cyclo*-hexane components.

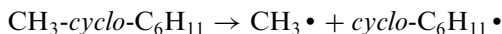
Cyclo-alkane pyrolysis involves a more complex overall reacting system due to the presence of new relevant reaction classes, such as the ring opening and the *cyclo*-addition reactions (Dente *et al.*, 2005; Green *et al.*, 2001; Matheu *et al.*, 2003; Pierucci *et al.*, 2005). While the ring opening can take advantage of the reference kinetic values of the β -decomposition reactions of alkyl radicals, new reference kinetic parameters need to be singled out for the internal isomerization of *cyclo*-alkyl radicals as well as the *cyclo*-addition reactions of alkenyl radicals. The result of the successive decomposition and *cyclo*-addition reactions of these radicals gives rise to several different isomers. Starting, for instance, from *cyclo*-hexyl radical, various methyl-cyclopentyl as well as various normal and branched hexenyl radicals are obtained.

Furthermore, the pyrolysis of *cyclo*-alkanes is a chain radical process where several molecular reactions also play a significant role. Specifically, the molecular isomerizations between *cyclo*-alkanes and alkenes are typical examples of four- and six-centre concerted reactions.

The complexity rises due to the number of intermediate components in the primary decomposition paths rapidly increasing with the molecular weight. The MAMA kinetic generator becomes very useful and practically essential in evaluating the net result of these reacting systems. With the focus on a reliable evaluation of the ethylene yields in commercial reactors, the complexity of these reacting system demands major simplifications if it is to describe primary product distribution and successive decomposition paths without requiring too great a computational effort.

Cyclo-alkanes are typically *cyclo*-pentanes and *cyclo*-hexanes with a certain degree of methylation and a single more or less long alkyl side chain. The C–C cleavage in the side chain follows the same rules and applies the same reference kinetic parameters as the initiation reactions of normal and branched alkanes.

The formation of *cyclo*-alkyl radicals with the radical position on the ring is the result of a C–C bond cleavage in the alkyl substituted position. For instance, the following model reaction:



is similar to the initiation reaction of *iso*-butane, and it is possible to refer to the same activation energy and to assume the following rate expression:

$$k = 5.0 \times 10^{16} \exp\left(\frac{-85,000}{RT}\right) \quad [\text{s}^{-1}]$$

This value agrees reasonably well with the rate suggested by Tsang (1978a)

$$k = 1.09 \times 10^{26} T^{-2.6} \exp\left(\frac{-90,400}{RT}\right) \quad [\text{s}^{-1}]$$

for *iso*-butane, although it is quite a lot faster than the one proposed by Brown and King (1989) for the demethylation reaction of methyl-*cyclo*-hexane:

$$k = 1.41 \times 10^{16} \exp\left(\frac{-88,000}{RT}\right) \quad [\text{s}^{-1}]$$

New reactions involve the cleavage of a C–C bond inside the ring to form biradical intermediates, which quickly rearrange themselves into molecular products: initiation, in this case, acts as an isomerization reaction to form alkenes. On the basis of available thermochemical evaluations (Benson, 1976), the suggested reference kinetic parameters are

$$\text{Cyclo-C}_5\text{H}_{10} \rightarrow \text{1-pentene} \quad k_{\text{cy5}} = 1.6 \times 10^{16} \exp\left(\frac{-83,500}{RT}\right) \quad [\text{s}^{-1}]$$

$$\text{Cyclo-C}_6\text{H}_{12} \rightarrow \text{1-hexene} \quad k_{\text{cy6}} = 1.6 \times 10^{16} \exp\left(\frac{-86,000}{RT}\right) \quad [\text{s}^{-1}]$$

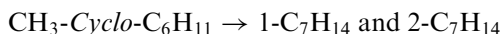
These parameters agree with the information in the literature:

$$\text{Cyclo-C}_5\text{H}_{10} \rightarrow \text{1-pentene} \quad k = 1.4 \times 10^{16} \exp\left(\frac{-85,400}{RT}\right) \quad [\text{s}^{-1}]$$

(Tsang, 1978b)

$$\text{Cyclo-C}_6\text{H}_{12} \rightarrow \text{1-hexene} \quad k = 5.0 \times 10^{16} \exp\left(\frac{-88,800}{RT}\right) \quad [\text{s}^{-1}]$$

(Tsang, 1978a)



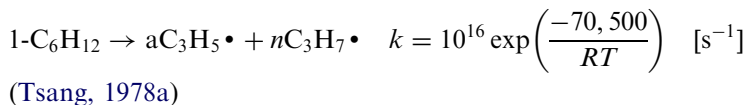
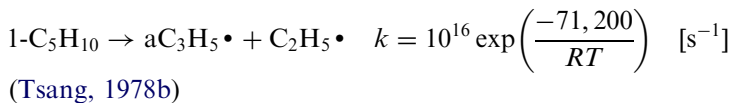
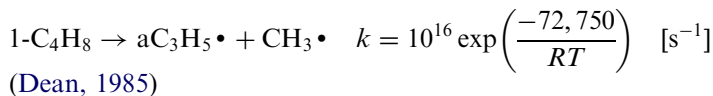
$$k = 2.5 \times 10^{16.4} \exp\left(\frac{-83,000}{RT}\right) \quad [\text{s}^{-1}]$$

(Brown and King, 1989)

The differences in the activation energies are due both to the strain energy of the *cyclo*-pentane ring and to the presence of methyl and alkyl substitutions on the ring.

From the above consideration it can be deduced that the initiation of *cyclo*-alkanes then turns into the initiation reactions of alkenes. In this situation, the weakest C–C bonds in the alkene skeleton are those forming allyl type radicals.

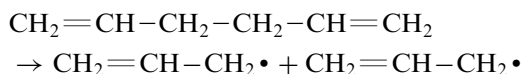
The following reactions are typical examples in this class:



For alkenes heavier than 1-pentene, the selected reference value for this initiation reaction is

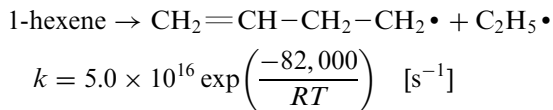
$$k = 10^{16} \exp\left(\frac{-71,200}{RT}\right) \quad [\text{s}^{-1}]$$

The activation energy adopted here is obtained by correcting the bond energy with the contribution of the formation of a resonantly stabilized radical. This correction agrees with the data proposed for the formation of two allyl radicals as in the case of 1,5-hexadiene initiation reaction



Dean (1985) suggests $1.58 \times 10^{15} \exp(-57,000/RT)$ which is also confirmed as $6.3 \times 10^{14} \exp(-57,630/RT)$ by Roth *et al.* (1991).

Initiation through the decomposition of various C–C bonds is significantly less important and is similar to alkane species decomposition:



H-abstraction reactions of *cyclo*-alkanes follow the same rules and apply the same reference kinetic parameters as the analogous reactions of normal and branched alkanes. For example, Fig. 6 shows the main *cyclo*-hexyl radical pyrolysis pathways. For simplicity's sake, most of the dehydrogenation reactions are not reported.

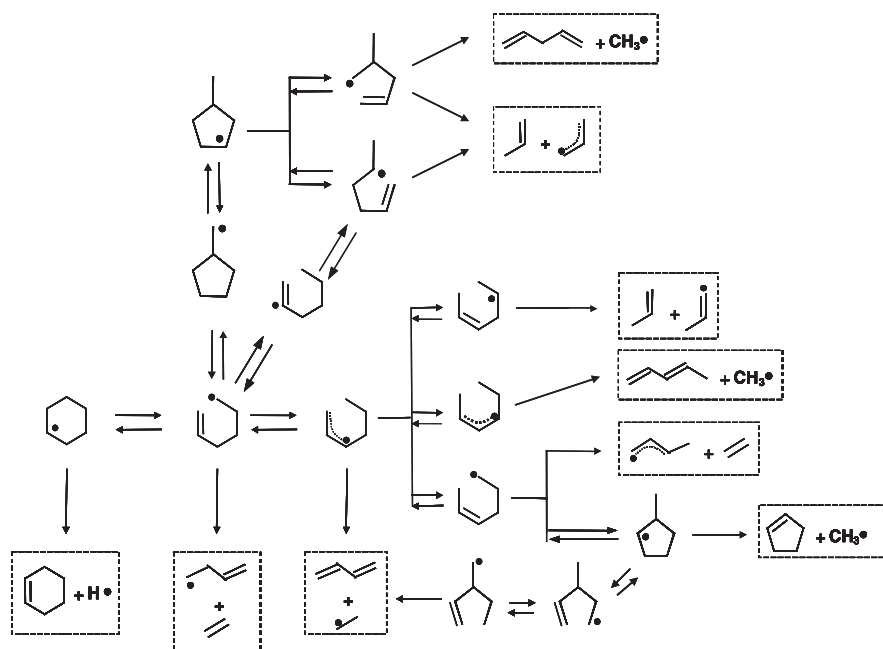


Fig. 6. Primary propagation path of *cyclo*-hexyl radical.

Once again, these reaction paths follow elementary steps with very simple and predefined rules. They may be simply classified as: isomerization and decomposition reactions.

Isomerization reactions include:

- Ring decomposition and the reverse *cyclo*-addition reactions
- 1-4, 1-5, 1-6 H-transfer reactions via five-, six- and seven-membered ring intermediates. These reactions are favoured when forming allyl or similar resonantly stabilized radicals (RSR).

Decomposition reactions include:

- β -decomposition reactions
- Dehydrogenation reactions.

A simple inspection of the scheme reported in Fig. 6 demonstrates two things. Firstly, each reaction step falls into the list reported above, and secondly, the more the initial radical carbon number increases, the larger the number of possible reactions and the greater the pool of all the intermediate and final species.

Several kinetic parameters of these propagation reactions are taken directly from the analogous reactions of alkyl radicals. For instance, the kinetic parameters of the dehydrogenation reaction of cyclohexyl radical to form cyclohexene

$$k_1 = 2.0 \times 10^{14} \exp\left(\frac{-39,500}{RT}\right) \quad [\text{s}^{-1}]$$

are the same parameters used for the dehydrogenation reaction of 3-pentyl radical to form 2-pentene:

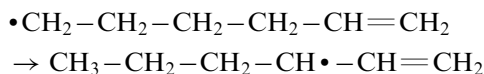


Similarly, the kinetic parameters of the decomposition reaction of the 5-hexen-1-yl radical to form C_2H_4 and the 3-butenyl radical

$$k_2 = 10^{14} \exp\left(\frac{-30,000}{RT}\right) \quad [\text{s}^{-1}]$$

are the same parameters used for the β -decomposition reactions of primary alkyl radicals to form ethylene and smaller primary radicals. The presence of a double bond inside the radical does not affect the reaction itself until the double bond is far enough from the reaction zone.

The isomerization reaction to form the resonantly stabilized hexenyl radical:



applies the same estimation rules common to all alkyl radicals. It is thus possible to estimate the following rate parameters for the direct and reverse reactions, respectively

$$k_{\text{for}} = 1.58 \times 10^{11} \exp\left(\frac{-15,500}{RT}\right) \quad [\text{s}^{-1}]$$

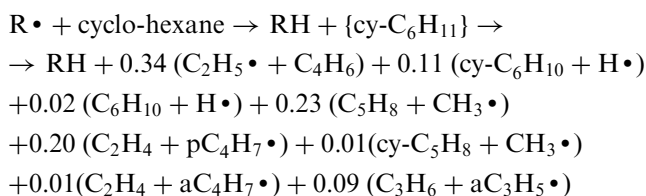
$$k_{\text{rev}} = 3.16 \times 10^{11} \exp\left(\frac{-29,000}{RT}\right) \quad [\text{s}^{-1}]$$

These kinetic parameters take into account the formation of a five-membered ring intermediate, the H-abstraction reaction of two H-atoms of allyl type and the formation of the resonantly stabilized 1-hexen-3-yl radical. These facts explain why the reverse isomerization reaction requires greater activation energy. As clearly shown in Fig. 6, there is a new class of important reactions, i.e. ring decomposition (e.g., *cyclo*-hexyl to form hexenyl radical) and the reverse *cyclo*-addition reaction. The activation energies of ring decomposition to form primary radicals are 31,500 and 28,000 kcal/kmol respectively for the

six- and five-membered ring cleavage. The reverse *cyclo*-addition reactions (through the addition of a primary radical) require 8,000 and 13,500 kcal/kmol for the formation of a five- and six-membered ring respectively (Matheu *et al.*, 2003). Successive isomerization and β -decomposition reactions of these radicals increase the complexity of the overall mechanism and explain the primary formation of propene, butadiene, pentadiene and cyclopentene from *cyclo*-hexane.

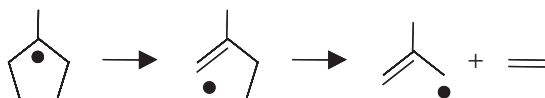
The complete set of the reference kinetic parameters for *cyclo*-alkane and alkene pyrolysis is reported in Table VII.

The overall *cyclo*-hexyl radical isomerization and decomposition mechanism, already shown in Fig. 6, is once again reduced to a single equivalent reaction which lumps all the intermediate propagation and decomposition steps:



This initial product distribution, evaluated by MAMA at 1,040 K, shows the importance of butadiene formation through the decomposition of 1-hexen-3yl radical, and also confirms that this stoichiometry is only slightly temperature dependent in this case too.

The analysis of the primary decomposition products from the decomposition of methyl-*cyclo*-pentane requires the addition of only a few reactions to the scheme shown in Fig. 6. Three methyl-*cyclo*-pentyl radicals were already formed from the successive isomerization reactions of *cyclo*-hexyl-radical, and thus only the tertiary radical, with its isomerization and decomposition reactions to form methyl-allyl radical and ethylene, needs to be included



The net result of the H-abstraction, propagation and decomposition reactions of methyl-*cyclo*-pentane becomes

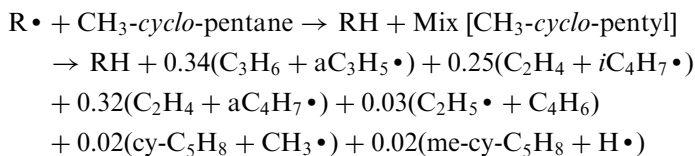


TABLE VII
REFERENCE KINETIC PARAMETERS FOR THE PYROLYSIS OF CYCLO-ALKANE AND ALKENES (UNITS ARE: KCAL, KMOL, L, S)

H-abstraction reactions			
	Primary H-atom	Secondary H-atom	Primary allyl H-atom
Primary alkyl radical	$10^8 \exp(-13,500/RT)$	$10^8 \exp(-11,200/RT)$	$10^8 \exp(-10,500/RT)$
Primary allyl radical ^a	$3.16 \times 10^8 \exp(-22,500/RT)$	$3.16 \times 10^8 \exp(-19,000/RT)$	$3.16 \times 10^8 \exp(-18,500/RT)$
Isomerization reactions of allyl radicals (Transfer of a primary H-atom)			
	<i>1-4 H-transfer</i>	<i>1-5 H-transfer</i>	<i>1-6 H-transfer</i>
Primary radical ^b	$10^{11} \exp(-28,000/RT)$	$1.58 \times 10^{10} \exp(-23,500/RT)$	$3.16 \times 10^9 \exp(-28,500/RT)$
	<i>5-membered ring</i>	<i>6-membered ring</i>	
Cyclo-addition reactions	$10^{11} \exp(-13,500/RT)$	$1.58 \times 10^{10} \exp(-8,000/RT)$	
Cyclo-alkyl radical decomposition	$5 \times 10^{13} \exp(-28,000/RT)$	$10^{14} \exp(-31,500/RT)$	
Reactions (to form primary radicals)			
Allyl radical decomposition reactions (to form conjugated dienes)		$5 \times 10^{13} \exp(-35,000/RT)$	

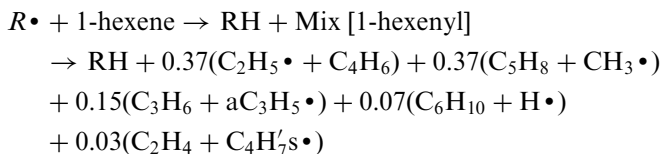
^aCorrections for secondary and tertiary radicals are the same as for alkyl radicals.

^bRate values for secondary and tertiary radicals are obtained by adding 1,500 and 2,000 kcal/kmol to the activation energies.

The lumped radical Mix [CH_3 -*cyclo*-pentyl] is the mixture of the four different alkyl radicals derived from the H-abstraction reactions on methyl-*cyclo*-pentane



Figure 6 also describes the 1-hexene reactions. Thus, the H-abstraction reactions of 1-hexene simply become



The system becomes increasingly complex as the molecular weight rises. Figure 7a and 7b show the distributions of small alkenes and radicals from the decomposition, at 1,040 K, of the series of 1-methyl-4-alkyl-*cyclo*-hexanes vs. the carbon number (from 1,4-dimethyl-*cyclo*-hexane up to 1-methyl-4-heptyl-*cyclo*-hexane).

The analysis of the primary decomposition and isomerization of *cyclo*-alkanes is limited to 14 C-atoms due to the large number of possible isomers and to the resulting dimension of the overall problem. Nevertheless, it should be pointed

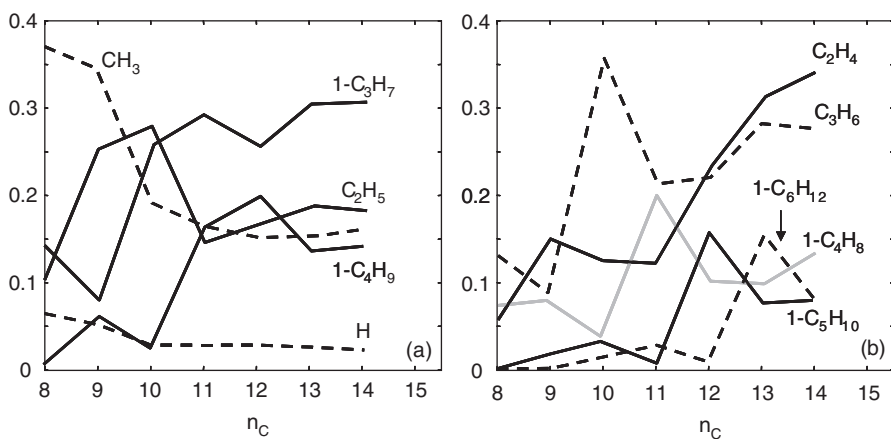
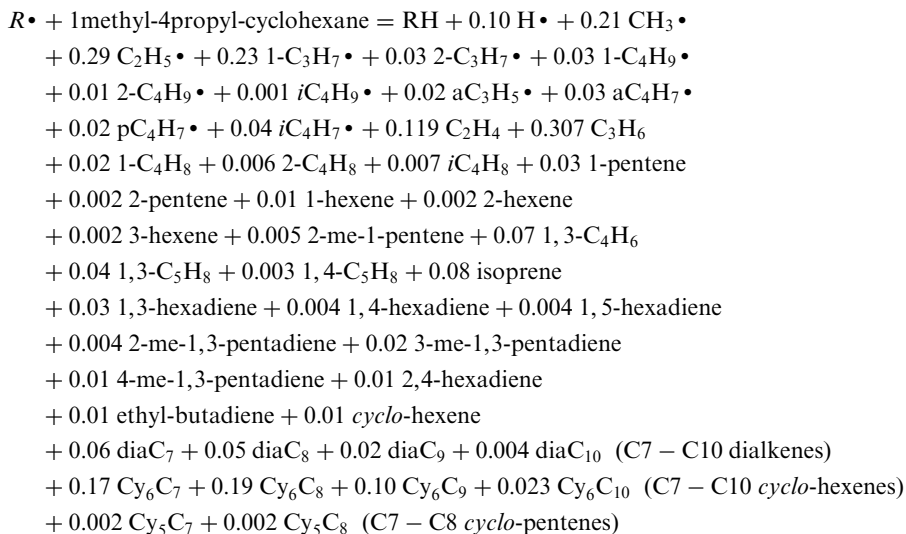


FIG. 7. Panel (a): primary selectivity of small radicals from the decomposition of 1-methyl-4-alkyl-*cyclo*-hexanes vs. carbon number; panel (b): primary selectivity of alkenes from the decomposition of 1-methyl-4-alkyl-*cyclo*-hexanes vs. carbon number.

out that the trend for small alkenes and radicals is asymptotic for C-atoms higher than 12–13. A complete and detailed description of heavier species soon becomes unmanageable. For this reason, the stoichiometry of the primary reactions of heavier homologous species is obtained using simpler extrapolation rules.

The detailed analysis of the primary product distribution from 1-methyl-4-propyl-cyclohexane (10 C-atoms) is useful for a better understanding of the relative importance of intermediate species. It can also provide useful information regarding the choice of intermediate lumped components.

Thus, MAMA gives the following result for the H-abstraction reaction:



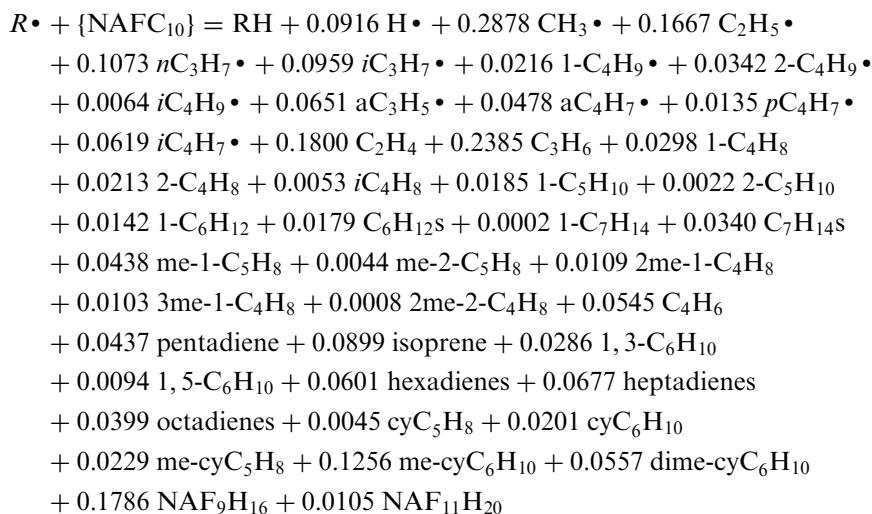
In order to simplify this stoichiometry, several species heavier than C6 are conveniently grouped into families of homologous species.

The following considerations can be singled out:

- Unsaturated radicals constitute more than 10% of the radical pool
- There is a significant production of conjugated di-alkenes and alkyl-cyclo-hexenes.

Both *cyclo*-hexane and *cyclo*-pentane components must be considered. As in the case of branched alkanes, the virgin feeds for *cyclo*-alkanes are relatively regular, once again due to the same diagenesis process. *Cyclo*-hexane rings are more abundant than *cyclo*-pentane ones. The probability of methyl substitutions is about 20%, on both the side chain and the naphthenic carbon. Moreover, experimental distributions of these components indicate the prevailing presence of a single long alkyl chain and several methyl substitutions.

On this basis, the fraction of the C10 *cyclo*-alkane isomers has been assumed as a single equivalent component with a default internal composition. MAMA analyses the primary propagation reactions of the real isomers of the mixture, groups and lumps all the stoichiometries, and generates the equivalent stoichiometry of the lumped component, once again using the same reference kinetic parameters. After processing by MAMA, the following lumped reaction represents the H-abstraction reaction of the lumped component {NAFC₁₀}:

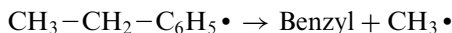


Analysis of this product distribution quite clearly reveals the importance of diolefins and unsaturated *cyclo*-alkanes. These components must therefore be described along with their successive pyrolysis reactions which soon move toward the formation of aromatic species.

4. Aromatics

The alkyl aromatic propagation reactions are automatically generated by the MAMA program in this case also and only a few new reactions need to be discussed. The formation of RSR is the first important feature. In fact, the H-abstraction reactions to form benzyl and benzyl-like radicals are the favoured ones with respect to H-abstraction on aromatic sites.

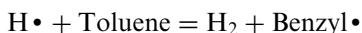
Similarly, the formation of RSR is also favoured in the initiation reactions. The kinetic parameters $6.1 \times 10^{15} \exp(-75,000/RT)$ [s⁻¹] suggested by Baulch *et al.* (1992) for the model reaction:



were used. The same authors suggest the following kinetic parameters:

$$k = 0.398 \times T^{3.44} \exp\left(\frac{-3,100}{RT}\right) \quad [\text{m}^3/\text{kmol s}]$$

for the H-abstraction reactions of H radical on toluene, to form benzyl radical:



These values are very similar to the ones of the H-abstraction from propene to form allyl radical (Tsang, 1992). Successive reactions of aromatics include the substitutive addition reactions that progressively favour the dealkylation reactions of aromatic species. The kinetic parameters for the reference reaction $\text{H} \bullet + \text{Toluene} \rightarrow \text{CH}_3 \bullet + \text{Benzene}$

$$k = 5.78 \times 10^{10} \exp\left(\frac{-8,090}{RT}\right) \quad [\text{m}^3/\text{kmol s}]$$

are taken from Baulch *et al.* (1994) whilst the kinetic parameters for the reverse reaction become (Robaugh and Tsang, 1986):

$$k = 1.2 \times 10^9 \exp\left(\frac{-16,000}{RT}\right) \quad [\text{m}^3/\text{kmol s}]$$

Other important reactions refer to vinyl and allyl radical addition reactions on alkyl aromatic species. These substitutive addition reactions also contribute to a progressive dealkylation of the aromatic species. The reference kinetic parameters of these reactions are respectively

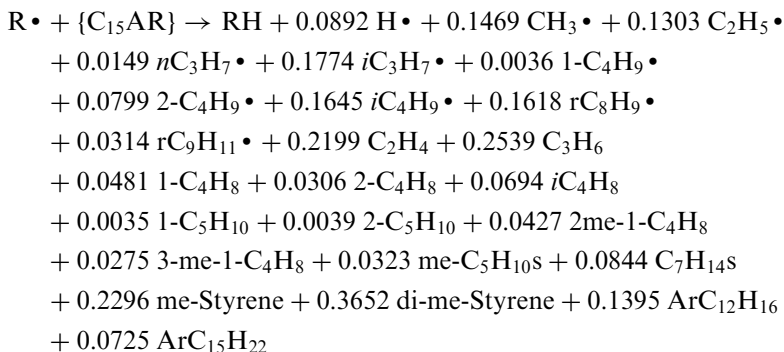
$$k_{\text{vinyl}} = 1 \times 10^9 \exp\left(\frac{-6,000}{RT}\right) \quad [\text{m}^3/\text{kmol s}]$$

$$k_{\text{allyl}} = 2 \times 10^9 \exp\left(\frac{-25,000}{RT}\right) \quad [\text{m}^3/\text{kmol s}]$$

The differences in activation energies caused by the additions of the different radicals reflect the different levels of stability of the attacking radicals.

β -decomposition and chain cleavages of alkyl side substitution still refer to previously discussed kinetic parameters. On this basis and once again using the MAMA program, the following stoichiometry is obtained for the H-abstraction reaction of the lumped component $\{\text{C}_{15}\text{AR}\}$. This component is a mixture of several isomers $\text{C}_{15}\text{H}_{24}$ with the prevailing presence of only one long side chain

with the usual methyl substitutions considered once again also.



The end primary products of this reaction include a significant quantity of RSR, referred to here as $rC_8H_9 \bullet$ and $rC_9H_{11} \bullet$, as well as methyl- and di-methylstyrene together with larger unsaturated aromatic components, once again lumped into $ArC_{12}H_{16}$ and $ArC_{15}H_{22}$. As clearly set out by Tsang (2004) with regard to the aromatic compounds, a resonance stabilized radical is formed once the alkyl side chains have been reduced to one carbon, and there is general agreement that the condensation of such long-lived radicals play an important role in the formation of PAH. As it will be discussed in the next paragraph, these species are important precursors of carbon deposition in the pyrolysis coils and are also important intermediates in the ultimate formation of soot particles in combustion processes. This is why there has been considerable work on the benzyl radical (Braun-Unkhalff *et al.*, 1990; Ellis *et al.*, 2003) (Frisch *et al.*, 1995) and it is clear that isomerization processes, quite rapidly releasing H-atoms, are competitive with condensation reactions.

C. DETAILED CHARACTERIZATION OF LIQUID FEEDS

As previously mentioned, pyrolysis feedstocks are usually made up of complex hydrocarbon mixtures derived from the refinery. An example of this complexity has been already given in Table V in which boiling temperatures and the number of paraffin isomers are compared with the carbon numbers of various petroleum fractions (Altgelt and Boduszynski, 1994).

1. Naphtha, Kerosene and Light Gasoil Fractions

Commercial naphthas are complex mixtures of a large number of different isomers and are generally characterized by specific gravity and boiling curves (TBP curves or ASTM D86). The relevant properties of different straight run naphthas are reported in Table VIII. The sulphur content is usually lower than 2% and nitrogen is in the order of a few ppm. Light and heavy naphthas are

TABLE VIII
MAJOR PROPERTIES OF STRAIGHT-RUN NAPHTHAS ADAPTED FROM AALUND (1976A, B)

Origin	Arabian	Iranian	U.S.S.R.	Indonesia	Algeria	Nigeria	Lybia	Ecuador
<i>Property</i>								
Boiling range (°C)	100–150	93–149	77–155	110–193	95–175	75–175	65–110	77–154
Gravity	0.7366	0.7389	0.7389	0.7861	0.7523	0.7792	0.7624	0.7459
P	70.3	53	60	43.8	63.8	27.5	77	49.4
N	21.4	34	32.4	29.1	25	58.5	18	43.9
A	8.3	13	7.6	27.1	11.2	14	5	6.7
Sulphur (wt%)	0.0028	0.13	0.03	0.01	—	0.01	0.0008	0.015
Yield (vol %)	6.8	9.6	12.58	17.9	18.11	8.7	11.67	11.91

TABLE IX
REGULARITY OF NAPHTHA COMPOSITION ADAPTED FROM SMITH (1968)

Ratio (vol %) of hydrocarbons to <i>n</i> -hexane	Minas	Beaver Lodge
<i>n</i> -pentane	0.69	0.82
<i>n</i> -hexane	1.00	1.00
<i>n</i> -heptane	1.23	1.10
<i>iso</i> -pentanes	0.53	0.52
<i>iso</i> -hexanes	0.81	0.68
<i>iso</i> -heptane	0.81	0.61
<i>cyclo</i> -pentanes	0.41	0.31
<i>cyclo</i> -hexanes	0.99	0.86
Benzene plus toluene	0.06	0.38

mainly aliphatic but they also contain a significant quantity of *cyclo*-alkanes. The aromatics may account for as much as 10–20% and most of these are alkyl-benzenes. When naphtha with a high aromatic content is cracked in a pyrolysis plant, alkene production decreases as it is difficult to convert aromatic hydrocarbons.

Naphtha can constitute from 10 to 35 volume percent of crude oil. Despite this difference, considerable similarities were observed in different crude oils if the comparison uses the ratios of each hydrocarbon to the volume percent of *n*-hexane (Smith, 1968). Table IX gives a very simple example of this by demonstrating the similarity between two different naphthas.

The fact that the relative presence of alkane and *cyclo*-alkane hydrocarbons in naphtha fractions is so similar suggests that the most of the oil has undergone the same sequence of reactions or diagenesis. The difference in the naphtha volume fraction inside the oil as well as the larger difference in the aromatic components, however, may indicate the extent to which the diagenesis has proceeded. This is why it is important to define the PONA index, i.e. the relative amount of paraffins, olefins, naphthenes and aromatics, so that the relative sizes

of the different fractions can be characterized. It is also important to specify both normal and branched alkanes. Alkenes are rarely contained in straight-run petroleum fractions; however, substantial amounts are present in certain refinery streams.

Naphtha feed is often characterized using PINA analysis that simply is the weight % of *n*-paraffin, *iso*-paraffin, naphthene and aromatic compounds. If the typical commercial indexes (specific gravity, PINA analysis and TBP curves or ASTM D86) are used properly, it is possible to empirically derive detailed naphtha composition by referring to the four different hydrocarbon classes and only to a limited number of reference components within each class. In fact, the PINA information indicates the relative abundance of the four different classes directly. The specific gravity and boiling curve allow the specification of the initial and final cuts of the hydrocarbon mixture as well as the relative presence and distribution of the reference pseudo components inside each fraction.

n-Alkanes from *n*-butane up to *n*-decane can be assumed as real components. However, *iso*-alkanes, *cyclo*-alkanes (heavier than C₆–C₇) and aromatics (from xylenes) are described with lumped components for each carbon number for the sake of convenience. As already mentioned, the analysis and comparison of different virgin feeds shows that significant regularities in the internal distribution of the different isomers can be singled out fairly independently of the crude origin. This fact has already been observed in Table VI for the isomers of the branched octanes. The same approach and similar internal distributions can be defined for all the lumped components as well as for *cyclo*-alkanes and aromatics. This means that the feed is described on the basis of a limited number of reference components defined as fixed mixtures of real isomers. This simplified but still reliable composition of the naphtha feed reduces the total number of species and reactions and makes it possible to deal with the complexity of the pyrolysis system.

Kerosene is the generic name for the lighter end of a group of petroleum substances known as middle distillates, the heavier end being gasoils. Kerosene can be divided into two basic types of kerosenes (straight-run and cracked) but subsequent treatments often blur this simple distinction. Kerosenes obtained from crude oil by atmospheric distillation are known as straight-run kerosenes. The typical distillation range of 145–300°C for kerosenes is such that benzene and *n*-hexane concentrations are always below 0.01% by mass. The main components of kerosenes are normal, branched and *cyclo*-alkanes. They normally account for at least 70% by volume of a process stream. Aromatic hydrocarbons, mainly alkylbenzenes and alkylnaphthalenes, will not normally exceed 25% by volume of kerosene streams (CONCAWE, 1995).

In the case of kerosene and light gasoil also, density, TBP or ASTM D86 distillation curves and PINA analysis (if available) are used, and empirical correlations are derived to yield a detailed picture of hydrocarbon mixture composition. The aromatic fraction can vary greatly for the different feeds, and information, such as the H/C of the feed, is important when PINA is not available.

Vertical lumping is also applied for components with more than 10 carbon atoms. The MAMA program generates the primary propagation reactions, i.e. the lumped initiation and H-abstraction reactions, for all these reference components. The overall resulting stoichiometry of these lumped species is simply obtained by averaging and weighting the lumped stoichiometries of the individual isomers, once again with regard to their internal composition.

2. Heavy Gasoils

The first difficulty in extending the kinetic model to very heavy feeds, and then vacuum oils and crude distillates containing feed components up to 35 C-atoms, involves a proper description of the cracking mixture. Altgelt and Boduszynski's book (Altgelt and Boduszynski, 1994) made an important contribution to this and remains a highly relevant reference work. Specific gravity, boiling points, viscosities, aniline points, UOP factor and hydrogen contents of the fractions are the usual characterization indexes. As Watson *et al.* (1935) discovered in their pioneering study, if two of these properties are known for any particular feedstock, the others can be more or less accurately approximated. This fact supports the idea that it is possible to derive some information on the internal composition of the fraction from these data. Much higher concentrations of certain petroleum compounds are found than others of similar structures. These survived the diagenesis of petroleum with fewer changes than the remainder. They are known as "biomarkers" or "molecular fossils" and are a further index of the regularities inside the oil fractions. They also support to some extent the idea that the internal detailed composition of the oil fractions can be derived by using only a few industrial indexes such as gravity, boiling curve and H/C data.

The n-d-M method (refractive index, density and molecular weight) is another way of calculating the distribution of carbon atoms in paraffinic, aromatic and naphthenic groups. Simple empirical correlations established by Tadema allow this group type characterization (Van Nes and Van Westen, 1951) to be completed. NMR, particularly the combination of ¹H- and ¹³C-NMR and elemental analysis, allows the determination of numerous average structural groups in a petroleum fraction, such as all the aromatic and aliphatic hydrocarbons. Oka and co-workers (Chang *et al.*, 1982; Oka *et al.*, 1977) assessed relevant steps towards so-called computer-assisted molecular structure construction (CAMSC), i.e. an accurate selection of reference components capable of describing the average properties of the mixture.

Parallel to this, it is also important to define the description level required by the model for it to be reliable and effective. Liguras and Allen (1989, 1992) quite correctly observe that one of the key issues in developing ideal characterization and kinetic models for hydrocarbon fractions is determining the point at which increasing the number of model compounds no longer enhances the model predictions. According to Krambeck (1992), the most important application of

detailed compositional analysis is in developing the reaction networks and the kinetic models of hydrocarbon processes. This means that a lumped composition of the feed must be derived. Adequacy and accuracy are the two key features of this lumped composition. Adequacy means that the lumped composition must have sufficient detail to determine all product properties of interest. Different feedstocks with the same lumped composition must yield reaction products with the same lumped composition. This is the first guarantee of accuracy.

On this basis, the detailed characterization of heavy oil fractions first requires the selection of model components. The following relevant classes of model components were selected:

<i>n</i> - and <i>iso</i> -alkanes		C_nH_{2n+2}
<i>cyclo</i> -alkanes:	mono-naphthenes	C_nH_{2n}
	di- and poly-	$C_nH_{2n-2}-C_nH_{2n-4}-C_nH_{2n-6}$
aromatics:	alkyl-benzenes	C_nH_{2n-6}
	alkyl-tetralines	C_nH_{2n-8}
	and -indanes	
	alkyl-naphthalenes,	$C_nH_{2n-12}-C_nH_{2n-18}$
	-phenanthrenes	
	alkyl-crysenes	C_nH_{2n-24}

Once again using vertical lumping, only one reference component every five C-atoms can be selected in the range between 20 and 35 carbon atoms, for each family. These components are schematically reported in Fig. 8. Primary distribution products for all these species are generated by the MAMA program, using the same rules and procedures previously discussed.

Figure 9 drastically simplifies the major reaction paths of alkyl-naphthalene components. Via H-abstraction and successive decomposition reactions, they can easily form, either naphthalenes with unsaturated side chains (vinyl, allyl or alkenyl side chains) or RSR and smaller decomposition products. The preferential radical attack on the alkyl side chain is in the benzyl position due to the weak hydrogen bond. This makes it easy to justify either the formation of RSR or the successive β -decomposition reaction to form vinylnaphthalene. The net result of the successive recombination and condensation reactions of these aromatic species is the formation of PAH of increasing molecular weight with a progressively lower hydrogen to carbon ratio.

Similar reaction mechanisms are also considered for the other classes of aromatic species. The reacting system gradually moves towards more stable species. These are light gases (H_2 and CH_4) and increasingly heavier poly-condensed aromatic species with a low degree of side substitutions and progressively lower hydrogen to carbon ratios. Thus, heavy gasoils at high severities, i.e. after long residence times at high temperatures, produce a fuel

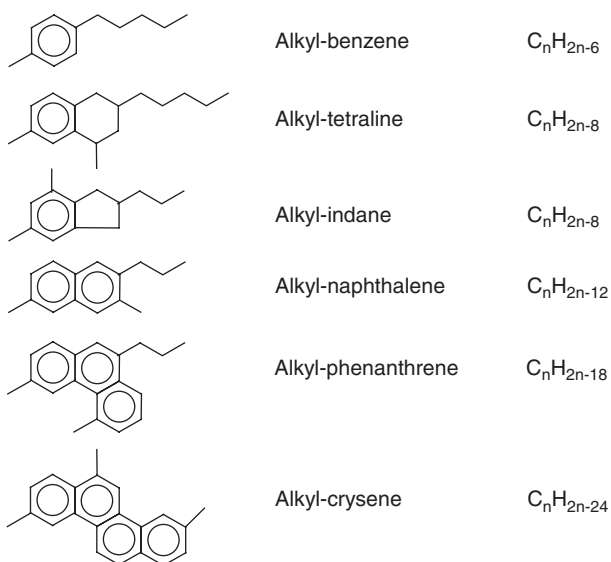


FIG. 8. Classes of model components in aromatic fractions of gasoil feeds.

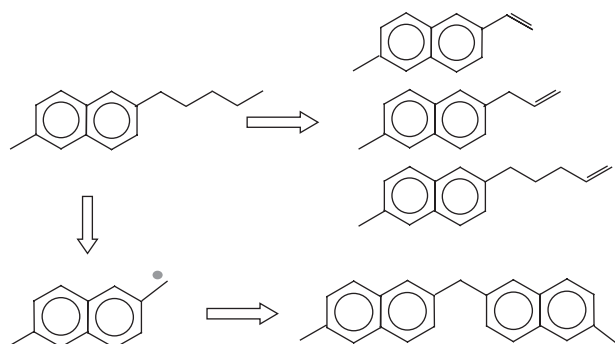


FIG. 9. Major reaction paths of alkyl-naphthalenes.

oil fraction (C_{12}^+) largely consisting of naphthalene, phenanthrene, crsenes and heavier aromatic condensed species too.

The description of the fuel oil fraction is also a first step towards the understanding of the fouling phenomena in cracking coils and in transferline exchangers. Fouling phenomena and carbon deposition on the pyrolysis coils mostly follow a heterogeneous process. They require the description of the liquid-phase transformation of the carbon macro-polymer structure and its progressive degradation and dehydrogenation to coke, as will be discussed in the coming paragraphs.

3. Crude Distillation Residues

There are analogies between the characterization of crude distillation residues and the previous feeds. The main difference is that for atmospheric and vacuum distillation residues of crude PINA and H/C can be estimated only through the kind of analysis (such as NMR) not normally available in refineries. Moreover, their final boiling point is not defined and the internal distribution of the different hydrocarbon classes of alkanes, *cyclo*-alkanes and aromatics has to be deduced in a different way. Inside each macro-class, the relative amount of the components can be derived from the following statistical distribution:

$$\frac{df}{dn_c} = \frac{1}{n_{c,av} - n_{c,min}} \exp \left[-\frac{n_c - n_{c,min}}{n_{c,av} - n_{c,min}} \right]$$

where f is the fraction of the components with n_c C-atoms, $n_{c,av}$ and $n_{c,min}$ are the average and the minimum number of C-atoms, respectively. Lumped components group sections of 5 to 10 carbon atoms, while a few pseudo components are assumed to represent the heavier fractions up to 200 C-atoms. This statistical distribution, which is also useful for heavy gasoils, was obtained after careful analysis and processing of the data available in the literature (Ali *et al.*, 1985).

Only a small number of experimental data are used to define the feed characteristics: atmospheric equivalent initial boiling point (AEBPI), kinematic viscosity, specific gravity, sulphur content and CCR (Conradson Carbon Residue). AEBPI defines $n_{c,min}$ and the viscosity of the residue $n_{c,av}$. Specific gravity and CCR are essential to defining the relative fraction of the three hydrocarbon classes. Sulphur content is used for correcting the effective specific gravity of the hydrocarbon fraction. The specific gravity of different hydrocarbon classes is defined by means of group contribution methods. In the case of heavy components, experimental data are not available; when the number of C-atoms and of rings increases over a certain amount, specific group contributions have to be derived.

Figures 10 and 11 show some examples of model predictions of the feedstock characterization of crude distillation residues. Figure 10 compares model predictions with the experimental distillation curves of three Arabian atmospheric residues. Figure 11 shows the model ability in predicting the aromatic carbon content and the H/C of different feeds in comparison with some NMR data. A more detailed description and discussion of this residue characterization is reported elsewhere (Bozzano *et al.*, 1995, 1998).

D. EXTENSION OF THE MODELLING TO LIQUID-PHASE PYROLYSIS

The interest here is focused mainly on heavy hydrocarbons feedstocks, as in the case of certain refinery processes, and on polymer thermal degradation. A radical chain mechanism is also involved in the liquid- or condensed-phase pyrolysis. This is once again characterized by initiation, radical recombination

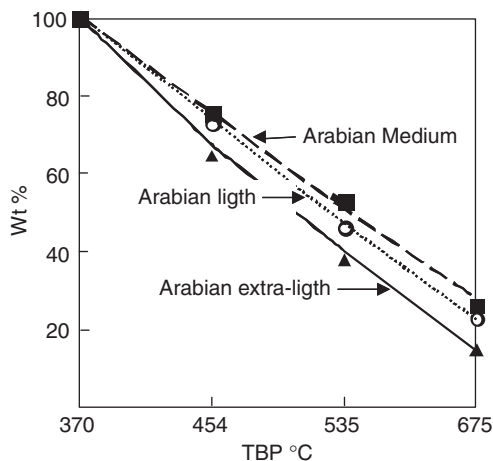


FIG. 10. Predicted and experimental distillation curves of Arabian residues (Ali *et al.*, 1985).

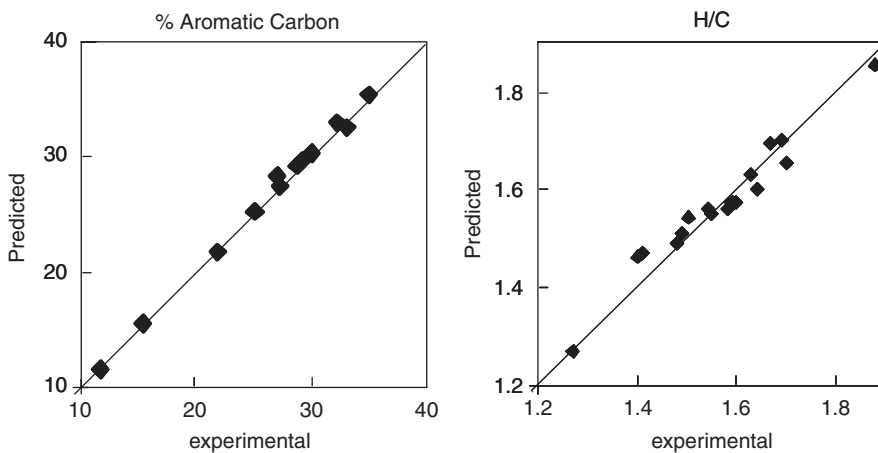


FIG. 11. Scatter diagrams of experimental and predicted values of aromatic carbon atoms and H/C in several residues.

and propagation reactions (i.e. β -scission, H-abstraction, radical isomerization, and substitutive addition of radicals onto unsaturated molecules). Thus, liquid-phase pyrolysis presents close analogies with the gas-phase pyrolysis. Because of the sterical hindrance in the liquid phase, the molecular rotation of large C–C segments is greatly inhibited and internal isomerization reactions of alkyl radicals are less important, in terms of the evaluation of the overall degradation process. For this reason, concerted path molecular reactions can be neglected too.

When the same reaction is “moved” from the gas to the liquid phase, frequency factor and activation energy need to be modified in principle because of

the condensed state. In fact, the transition state entropy and enthalpy change in passing from gas to the liquid phase. The transposition to the liquid phase of rate constants can be evaluated (Benson, 1960) from

$$\frac{k_{\text{liq}}}{k_{\text{gas}}} = \exp\left(\frac{\Delta S_{\text{liq}}^{\#} - \Delta S_{\text{gas}}^{\#}}{R}\right) \exp\left(-\frac{\Delta H_{\text{liq}}^{\#} - \Delta H_{\text{gas}}^{\#}}{RT}\right)$$

where $\Delta S_{\text{liq}}^{\#} - \Delta S_{\text{gas}}^{\#}$ = entropy variation of the transition state in passing from liquid to gas phase (this variation is typically negative). $\Delta H_{\text{liq}}^{\#} - \Delta H_{\text{gas}}^{\#}$ = enthalpy variation of the transition state in passing from liquid to gas phase (this is typically negative and about equivalent to the hypothetical heat of evaporation of the transition state).

The corrections are significant if the absolute value of reaction energy is very large; thus, they mainly affect initiation reaction and radical recombinations. The first consideration regards initiation reactions. Unlike the case of gas phase, the entropy change is related to the fact that when the two radicals are formed, they remain “caged” and cannot fully develop their translational and external rotational degrees of freedom (internal rotations and vibrational frequencies remain more or less the same in the reactant and in the transition state).

Just to give few examples, some initiation reactions related to C–C bond cleavage in heavy hydrocarbon and/or polymer decomposition in the liquid phase are reported (consequent to the application of the rule of simulating a fictitious condensation of the transition state).

1. Secondary–secondary carbon bond cleavage:

$$k = 7.94 \times 10^{14} \exp\left[-\frac{81,000 + F(n_c)}{RT}\right] \quad [\text{s}^{-1}]$$

2. Allyl (or Allyl-like and Benzyl-like)–primary carbon bond cleavage:

$$k = 3.16 \times 10^{13} \exp\left[-\frac{72,000 + F(n_c)}{RT}\right] \quad [\text{s}^{-1}]$$

Activation energies are corrected by means of the following approximated function:

$$F(n_c) = 1,140 \sqrt{\frac{200 \cdot n_c}{(200 + n_c)}} \quad [\text{kcal/kmol}^{-1}]$$

where n_c is the number of carbon atoms of the heavy component or simply the number of carbon atoms characterizing the so-called flow unit (Van Krevelen, 1976) for the diffusion in the molten polymer.

Rate constants of propagation reactions can be evaluated as in the case of gas phase because the “caging effect” previously mentioned is negligible.

For termination reactions, it is more convenient to make use of the collision theory with an orientation factor. The molecule mobility in liquid phase intuitively is reduced. When radicals approach with the proper orientation, their recombination is very fast but their mobility is low; therefore, the radical recombination is diffusionally limited. The number of collisions between radicals per unit time (Benson, 1960) is provided by $4\pi r_A D_{AS} C_{AS}$ (where r_A is the distance among the atoms containing the radical positions, typically C-atoms, D_{AS} is the diffusion coefficient of the radical in the surrounding area, C_{AS} is the radical concentration in the surrounding area).

The previous expression represents the number of collisions for the single radical A. By multiplying for the number of molecules per unit volume, the number of collisions is obtained

$$v_{\text{coll}} = \frac{1}{2} 4\pi r_A D_{AS} \left(\frac{N_{AV}}{1,000} \right) C_{AS}^2 = k_{\text{coll}} C_{AS}^2 \quad [\text{kmol/m}^3 \text{ s}]$$

where N_{AV} is the Avogadro number and the 1/2 factor is included to avoid counting the collisions twice. k_{coll} is the collision constant ($\text{m}^3/\text{kmole/s}$). The fraction of collision with orientation favourable to the coupling is the same as in the gas phase. The self-recombination constant is therefore provided by

$$k_{AA} = k_{\text{coll}} \cdot \Phi_{AA}^2 \quad [\text{m}^3/\text{kmol s}]$$

where Φ_{AA}^2 is the orientation factor of the collision for effective recombination. The traditional symmetry rule is valid for the recombination A–B

$$k_{AB} = 2\sqrt{k_{AA} \cdot k_{BB}} \quad [\text{m}^3/\text{kmol s}]$$

This rule has the obvious advantage of drastically reducing the number of useful recombination constants simply related to the self-recombinations. The k_{coll} evaluation deserves some further consideration. First of all, the Stokes–Einstein theory suggests that when molecules are not too “long” (the exclusion regards the case of polymers or that one of solvents with extended linear backbones), the diffusion coefficient is

$$D_{AS} \cong \frac{kT}{3\pi\mu_S r_A} \quad [\text{m}^2/\text{s}]$$

where k is the Boltzmann constant. According to the Eyring theory, the liquid viscosity μ_S is estimated as

$$\mu_S \cong \frac{N_{AV} h}{\tilde{V}_S} \exp\left(\frac{E_V}{RT}\right) \quad [\text{kg/m s}]$$

where h = Planck constant, \tilde{V}_S = liquid molar volume, E_v = energy required for the viscous motions. The latter can be approximately estimated as $E_v \approx 0.36 \Delta H_{ev}$ where ΔH_{ev} is the heat of vaporization of the liquid at its normal boiling point, T_b . When ΔH_{ev} is not available, the simple Trouton rule $\Delta H_{ev} \approx 21 T_b$ can be applied.

In the case of molten polymers, oligomers or solvents characterized by highly extended linear backbones, the proposed expression is the same but E_v corresponds to the so-called unit of flow energy, i.e. the energy needed to move the proper segment of the chain in the viscous flow (Van Krevelen, 1976). The same concept is applied also to \tilde{V}_S , which becomes the molar volume of the “segment”.

Therefore, by combining the given expressions, it follows that

$$k_{\text{coll}} \approx \frac{2kT}{3h} \tilde{V}_S \exp\left(-\frac{E_v}{RT}\right) \quad [\text{m}^3/\text{kmol s}]$$

where \tilde{V}_S = the molar volume of the liquid or of the polymer segment = W_S/ρ_S (with W_S = the average molecular weight of the liquid (kg/kmole), ρ_S = liquid density (kg/m³)). Therefore

$$k_{\text{coll}} \approx 10^{10.2} T \cdot \tilde{V}_S \exp\left(-\frac{E_v}{RT}\right) \quad [\text{m}^3/\text{kmol s}]$$

Note that the self-recombination kinetic constant follows an Arrhenius-type formula where E_v assumes the role of activation energy.

By applying the given formulas at 450 K, the recombination constant of macro-radicals in molten polymethylene becomes

$$k_{AA} \approx 10^{10.3} \exp\left(-\frac{5,800}{RT}\right) \quad [\text{m}^3/\text{kmol s}]$$

where the estimated orientation factor is $\Phi_{AA}^2 = 10^{-2.2}$.

III. Fouling Processes: Formation of Carbonaceous Deposits and Soot Particles

The formation of carbonaceous deposits and the formation of soot particles are two different aspects of the same pyrolysis reactions involving a complex sequence of condensation and dehydrogenation reactions.

Fouling processes on surfaces are common to all equipment involving hydrocarbon feeds at temperatures over $\sim 300^\circ\text{C}$. They are therefore widespread inside pyrolysis coils because they both operate at high temperatures and are fed by hydrocarbon fractions, which are responsible for the deposit formation. Fouling in pyrolysis coils has always had a negative impact on the behaviour of

the process. Deposit formation reduces heat transfer and increases tube skin temperatures so that the maximum allowable value is approached, limiting the total run-time. Moreover, the furnace thermal efficiency as well as the reaction volume inside the coils is progressively reduced. The pressure drop increases with a detrimental effect on process selectivity. The thermal efficiency of the downstream transfer line heat exchangers (TLE) is reduced too due to the progressive fouling of the tubes. The experimental information from industrial furnaces usually refers to the evolution of pressure drops and external tube skin temperature vs. on-stream time.

However, fouling is present not only in gas- and liquid-phase pyrolysis processes, but also in several other systems. In fact, the mechanisms involved in the formation and growth of the deposit are quite similar in coils, heat exchangers surfaces and drums of delayed coking, in the formation of PAH and soot in combustion processes as well as in the formation of nano and micro-fibres. In all these cases, despite different temperature levels ranging from 300°C up to more than 1,500°C, the continuous degradation towards char and coke formation plays a common role (Bozzano *et al.*, 2002). It is clear from this scenario that an understanding of the phenomena and their modelling is fundamental to improving not only the design of pyrolysis coils and cracking furnaces but also the operation of the heat exchangers and other process units.

The deposit grows as a consequence of the continuous addition of new species, molecules or radicals from the process fluid; these form a polymeric layer at the process fluid side. This layer has a relatively soft consistency (rubbery or glassy, depending on the temperature and time). It is then progressively dehydrogenated, causing it to release gases and its specific volume to shrink in many cases. This gives rise to morphological and structural modifications of the deposit, which becomes increasingly porous because of the formation of micro- and nano-fractures. As a consequence of these phenomena, the bulk of the deposit progressively assumes the characteristics of disordered graphite with time and temperature, and only then it can be defined as coke. While the deposit is progressively transformed into coke, the fouling process continuously increases its thickness. Thus, the deposit changes in nature, composition and properties not only with the time but also along the thickness.

On this basis, the fouling mechanisms must be discussed first and only then can the successive transformation of the deposit be analysed, with particular attention to the evolution of its structure and properties.

A. FOULING AND COKING MECHANISMS IN PYROLYSIS COILS AND TLE'S

Feed composition, operating conditions, equipment geometry, materials and their treatments are the main variables influencing the fouling rate. Firstly, qualitative information on deposit formation is obtained by a direct analysis of the morphology of the material. Coke samples from both industrial and

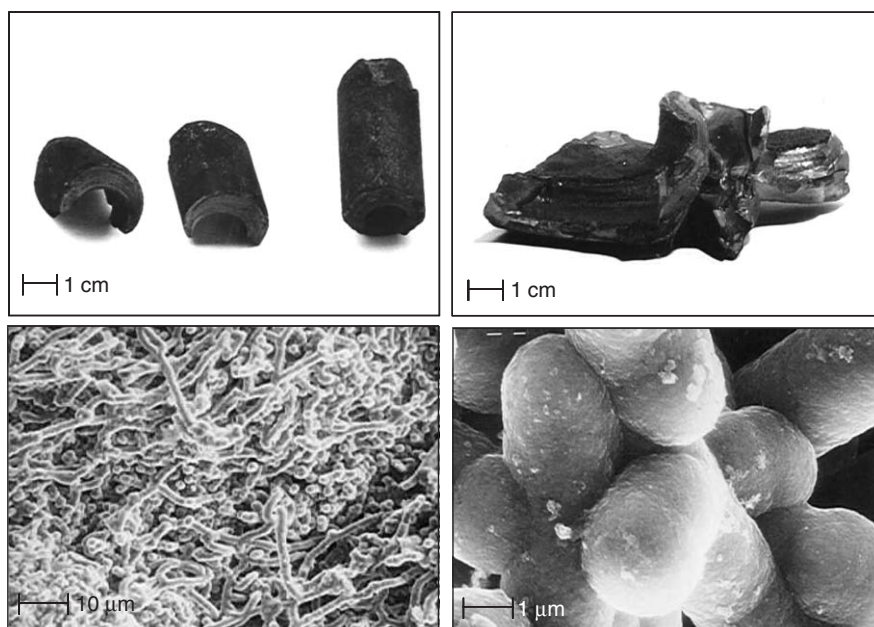


FIG. 12. Coke deposit in tubes and tubesheet of TLE of an ethane cracker.

lab-scale devices often show two different regions inside the deposit. There is a very thin polymeric layer close to the metal surface ($50\text{--}80\text{ }\mu\text{m}$) characterized by a fibrous structure with large void fractions and low thermal conductivity. Figure 12 gives a sample of the coke deposit from the tubes and the tubesheet of a TLE of an ethane cracker. Micro-fibres are present on the metal side of these deposits. The typical diameters of these fibres are in the order of a few μm with a length of some tens of μm . The second layer, close to the process side, is more compact and does not have this fibrous structure. Albright *et al.* (Albright and Marek, 1988, 1992; Albright *et al.*, 1979) discussed the morphology of several coke samples not only from steam cracking coils and TLE's but also from laboratory devices feeding ethylene, acetylene and butadiene at moderate temperatures. Similar studies and results were also obtained on coke samples coming from the pyrolysis coils and TLE's of crackers fed with naphtha and ethane (Dente and Ranzi, 1983).

After the pioneering work done by Dente and Ranzi (1983), the different mechanisms and features of fouling processes were more fully understood and clearly singled out (see for instance Albright, 2002; Albright and Marek, 1988; Blaikley and Jorgensen, 1990; Cai *et al.*, 2002; Chan *et al.*, 1998; Dente *et al.*, 1983; Froment, 1990; Kopinke *et al.*, 1988; Wauters and Marin, 2002; Zou *et al.*, 1987).

The fouling process consists of at least two mechanisms that contribute to the formation of the deposit: an initial catalytic mechanism, followed by a radicalic

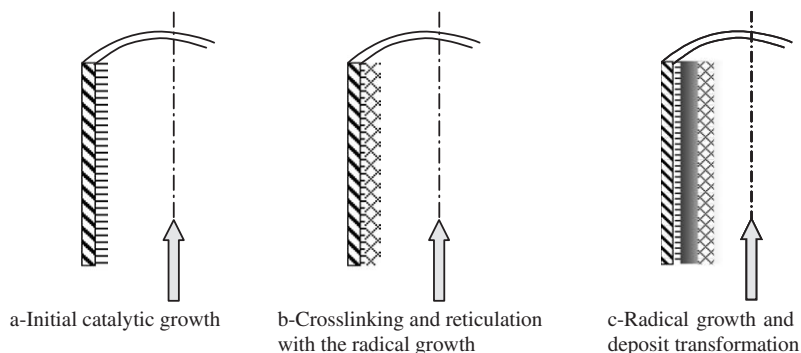


FIG. 13. Relevant steps in the fouling process and deposit formation.

one, which becomes more relevant when crosslink and reticulation reactions inside the deposit, increase the diffusion resistances of the monomers. This hinders their access to the catalytic sites on the metal surface. A simple outline of the evolution of the carbonaceous deposit over time is shown in Fig. 13. During continuous radical growth, the existing deposit progressively develops into more dehydrogenated structures (panel c).

1. Catalytic Mechanism and Initial Growth

Several researchers have studied the fouling of metal surfaces at moderate temperatures by analysing the effect of different feed components. The pyrolysis coil metals (and their oxides) act as a heterogeneous poly-addition catalyst, forming an initial fouling deposit very similar in its morphology to the polymers initially formed with traditional Ziegler–Natta catalysts. The transition metals of the coil surfaces are very good polymerization catalysts and promote this initial deposit formation. All the molecules containing vinyl groups can polymerize on the active sites. When a relatively uniform layer is formed on the metal surface, the catalytic mechanism turns out to be controlled by the diffusion of the monomer into the polymeric layer and a different radical mechanism rules the further fouling process. This now generally accepted conclusion means that the deposit growth can be described by means of at least two different contributions: first a catalytic mechanism and then a radicalic or pyrolytic one (Bach *et al.*, 1995; Barendregt *et al.*, 1981; Goossens *et al.*, 1978; Ranzi *et al.*, 1985; Zimmerman *et al.*, 1990).

This model is also supported by experimental data indicating a larger growth rate in aged coils (already decoked) with respect to new ones. The greater roughness and the higher metal oxide content increase both the metal surface and the number of active sites so that the catalytic mechanism is enhanced. Catalytic growth consists of the continuous addition of vinyl and vinyl-like compounds on the metal sites; these form polymer fibres with a “metallic head”

at their end, which eventually detaches from the wall surface. This is probably due to the initial formation of carbides, which can cause nano-fractures in the surface and generate catalyst particles that encourage carbonaceous fibre formation (Lobo and Trimm, 1973). This mechanism is supported by the analysis of coke layers near the metal surfaces where the metal atoms remain quite dense up to about 50 μm from the surface (Albright and Marek, 1988). Metal inclusions can be also responsible for fibre branching. Very similar findings and structures are also observed in the formation of carbon nano-tubes and micro-fibres in counter-flow diffusion flames (Helveg and Hansen, 2006; Helveg *et al.*, 2004; Merchan-Merchan *et al.*, 2003).

At the beginning of this catalytic growth, the metal surface is not limited by diffusion of monomer species; typical monomers are unsaturated molecules with a terminal vinyl group and are not only aromatics. With the proper sterical orientation, the monomers can add to the growing polymer chains. Polymer fibres then start to cover the metal surface. They grow and assemble so that diffusion resistances limit the further growth. The catalytic mechanisms progressively slow down, and dealkylation and dehydrogenation reactions increase in the formed polymer.

This situation can be clearly seen when observing the time evolution of the tube metal temperature of the pyrolysis coils: there is a fast initial increase and then a reduced asymptotic slope. Note that although the initial slope is initially related to the catalytic rate, it is also due to the relatively low thermal conductivity of the initial fibrous material as a result of the large void fraction. The thickness of this layer is in the order of 20–40 μm . The evolution of the fluid temperature over time either at the TLE outlet or in visbreaking processes and in delayed coking furnaces shows a very similar behaviour.

As recently summarized by Cai *et al.* (2002), this mechanism requires the presence of catalytic sites on wall surfaces at proper temperatures. On both new and aged metallic surfaces, there are significant populations of catalytic sites where ethylene and olefins can be preferentially adsorbed. Fe and Ni on metal surfaces help coke formation/deposition. The effect of tube materials on coke deposition under TLE conditions was also clearly demonstrated by Bach *et al.* (1995) who measured and compared the coking rates of 12 different kinds of steels. The steels can be further divided into three categories: low-alloyed and unalloyed steels consisting almost completely of iron; alloyed but nickel-free steels and commonly used high-temperature CrNi steels. The coking rates were the highest for unalloyed and low-alloyed steels, and lowest for CrNi steels. The high iron content and absence of Cr in the low or unalloyed steels are the primary reasons for rapid coke formation. Zychlinski *et al.* (2002) confirm this catalytic effect with their analysis of fouling processes on conventional and coated HP 40 materials. The results show that the Cr-based coating decreases coke formation in the radiant zone of a steam cracker by up to 90% and 80%, using ethane and naphtha, respectively, as feedstock.

2. Radical and Concerted Path Growth

After the catalytic formation of a basis substrate, a radical mechanism (also referred to as the pyrolytic mechanism) takes place with a reduced growth rate. This second mechanism is active in the bulk of the formed polymer, close to the fluid interface, and becomes more important at high temperatures. The Diels–Alder or concerted path reactions also give a major contribution.

Three main classes of addition reactions contribute to this mechanism:

1. Additions of radicals contained in the process fluid on unsaturated sites of the deposit surface (see Fig. 14)
2. Addition of acetylene, dienes and unsaturated molecules on the deposit surface: Diels–Alder reactions (see Fig. 15)
3. Addition of aromatic and polycyclic aromatic molecules with alkyl side chains on radical positions of the deposit surface (see Fig. 16).

These three classes of reactions consist of two consecutive steps: an initial addition of species from the process side on the coke surface and a successive release of small species (H_2 , alkyl side chain, CH_3 or H) with the continuous growth of the original aromatic structure. Successive dealkylation and dehydrogenation reactions further contribute to this coke formation mechanism.

The relative importance of the three reaction classes depends on the operating conditions. The first reaction class is more important at high temperatures as the

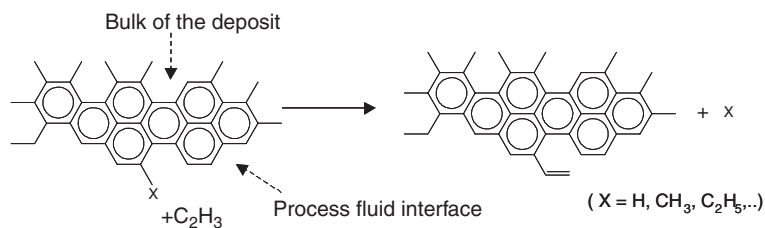


FIG. 14. Addition of unsaturated radicals on the surface of the polymer layer.

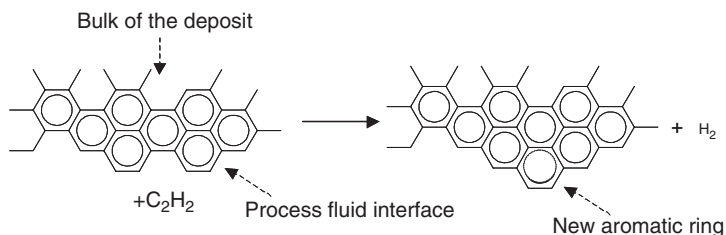


FIG. 15. Addition of unsaturated molecules on the surface of polymer layer (Diels–Alder reaction).

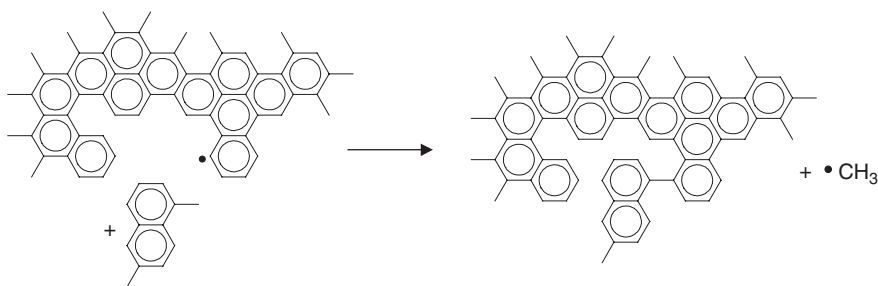


FIG. 16. Addition of an aromatic molecule on radical positions of the deposit surface.

radical concentration increases with temperature. Vinyl and vinyl-like radicals, aromatic and poly-aromatic phenyl-like radicals are the major precursors and are responsible for the growth.

Unsaturated hydrocarbons can add to the deposit-forming cyclic structures with five or six C-atoms through Diels–Alder reactions. The successive dehydrogenations produce polycyclic aromatic structures. In the third reaction class, aromatic species add to macro-radicals of the surface. Note that these radicals are greatly stabilized by the aromatic resonance. Thus, the third reaction class is more important at lower temperatures, typically, in TLE, visbreaking and delayed coking units.

The growth rate depends on the concentration values of the various reacting species at the interface. For gas phase pyrolysis, these concentrations are controlled by their solubility inside the soft layer of the deposit. In fact, only the external layer can be considered as a polymer in a molten or rubbery state. It has not yet been subject to sufficient dealkylation or dehydrogenation reactions, which create a progressive stiffness. For this reason it is important to properly evaluate the solubility of gaseous reactants in the polymer. For both vapour and liquid processes, the reactant concentrations inside the deposit rapidly decrease due to the increasing diffusion limitations. In fact, moving from the external to the inner layers, the polymer becomes increasingly cross-linked, approaching a glassy to solid state. The deposit structure becomes similar to disordered graphite. The only reactants able to reach the inner layers of the deposit are H and methyl radicals.

Finally, it is relevant to observe that this dissolution presents strong analogies with a condensation process discussed and stressed by several authors (Cai *et al.*, 2002) as being responsible for coke formation/deposition in the TLE tube outlet section at operating temperatures of 350–450°C. Indeed this mechanism can be explained on the basis of the solubility of heavy species of the process fluid phase in the soft polymer. There has also been research into the computer generation of a network of elementary steps for coke formation during steam cracking process (Wauters and Marin, 2002).

B. EVOLUTION OF STRUCTURE AND PROPERTIES OF THE DEPOSIT

Once the initial and successive formation of the deposit is analysed, a further important aspect in the overall fouling process is the transformation of the deposit. Due to the thermal degradation of the polymer, the deposit goes from rubbery to glassy and solid state with structural variations over time. The part of the deposit being considered here is the layer between the initial catalytic polymer (near the metal wall) and the one just generated by the radical mechanism close to the process interface (see Fig. 13 panel c). The morphology and properties of the deposit in this intermediate layer are similar to those of a glassy or solid polymer; the material is amorphous and rather rigid. Relatively disordered graphite with cata-condensed aromatic rings is the asymptotic structure, characterized by condensed aromatic rings, with methyl substitution on the free boundary. This is due to the fact that aromatic poly-alkenes are highly reactive even at low temperatures; polystyrene (PS), for instance, will decompose in about 1 h at 360°C. This decomposition process is further enhanced if the aromatic poly-alkenes also contain alkyl or methyl substitutions. So when they are formed or dissolved in the rubber part of the deposit, they are promptly subjected to dealkylation reactions. Only methyl-aromatic structures are present in the inner layers of the deposit. Delayed coking and visbreaking processes' modelling has shown that the average probability of methyl substitution on the free boundary of the aromatic sheets is about 50%. A simple example of a typical poly-aromatic structure with methyl substitutions and methylene bridges is given in Fig. 17.

These aromatic structures are roughly the same for all the fouling processes with the exception of ethane pyrolysis. It is convenient to distinguish and define the different C-atoms and groups inside the deposit. As clearly shown in the previous figure, methyl (P_{CH_3}), methylene (P_{CH_2}), aromatic (P_A) and fused aromatic (P_{FUS}) positions can be identified. Inside the rubbery polymer, initiation, H-abstraction and substitutive addition reactions form the corresponding

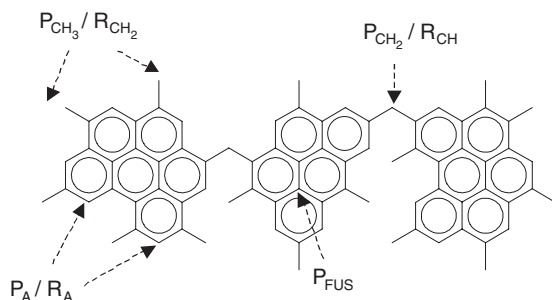


FIG. 17. Typical poly-aromatic structure of the deposit.

radical positions. Three different types of macro-radicals are formed: benzyl-like (R_{CH_2}), phenyl-like (R_A) and radicals on the methylene bridge (R_{CH}). Macro-radicals R_{CH_2} and R_{CH} are present in large amounts due to aromatic resonance but cannot move freely in the polymer. H and CH_3 radicals, on the other hand, can diffuse and react in the deposit porosity via the usual radical mechanism. H_2 , CH_4 , C_2H_6 are released in the gas phase as a result of H-abstraction, substitutive addition and termination reactions which form radical positions also in the glassy layers.

The H/C ratio of the deposit gradually decreases and, at high temperatures, the hard aromatic C–C and C–H bonds can be broken also. Initially, P_{CH_3} and P_{CH_2} are the preferred positions for H-abstraction reactions with the formation of R_{CH_2} and R_{CH} macro-radicals. Less stable radicals are generated next. All the radicals are active either in H-abstraction or in substitutive additions; otherwise, they recombine with each other.

The deposit from ethane cracking is more compact than the ones derived from other feeds. Practically, all of the growth is due solely to the very ordered additions of ethylene and vinyl radicals. Successive cyclization and dehydrogenation reactions complete the formation of well-organized aromatic structures. This leads to the formation of a more ordered and compact deposit: unlike the case of different feedstocks, large molecules or radical additions are of less importance. Thus, the material produced during ethane pyrolysis is equivalent to disordered graphite, and P_{CH_3} positions are practically absent even though the methylene bridges and a similar aromatic structure are maintained.

1. Kinetic Modelling

Thermal conductivity, H/C ratio, specific volume and specific heat vary during the chemical evolution of the deposit. Unfortunately, there is very small quantity of data in the literature on thermal conductivity. In fact, what little there is refers to coke or bitumen and provides limited or sometimes contradictory information because of the high dependency on the structure and composition of the solid. More reliable data refer to disordered graphite, similar to an aged deposit, without hydrogen and with a low porosity. The available experimental data on the time evolution of pressure drop and tube metal temperature in pyrolysis coils of ethylene crackers only permit rough estimates of the overall and average thickness and thermal conductivity of the deposit.

For this reason, the evolution of the thermal conductivity can be obtained on the basis of a group contribution method, mainly based on the concentration of P_{CH_3} , P_{CH_2} , P_A and P_{FUS} positions.

It is quite clear that the thermal conductivity is heavily dependent on the H/C ratio and structural properties, such as the void fraction. Porosity (i.e. free volume) is an important characteristic. Dehydrogenation and dealkylation reactions progressively reduce the molar volume of the deposit, with the

formation of fused aromatic carbons. This reduction brings the density of the deposit to about $1,600 \text{ kg/m}^3$. Further volume contractions generate fractures and increase the void fraction but the apparent density remains about constant. The temporal and spatial evolution of the deposit depends mainly on temperature, but temperature evolution and distribution are difficult to describe too. The different equipment and operating conditions greatly influence the thickness and physico-chemical properties of the deposit. Even a rough initial description of this evolution would involve a large number of species and reactions. Consequently, the appropriate lumping techniques are applied once again in this case. Important reactions are grouped into different classes, to be considered as equivalent reactions between positions and radicals, with their kinetic constants. The evolution of the deposit is the result of a radical degradation mechanism based on the following steps:

- Initiation reactions: $P_i \rightarrow R_1 \cdot + R_2 \cdot$
- Propagation reactions (H-abstraction or substitutive addition): $R_1 \cdot + P_1 \rightarrow R_2 \cdot + P_2$
- Termination reactions: $R_1 \cdot + R_2 \cdot \rightarrow P_i$

P_i and R_j are molecular species (or positions) and radicals, respectively.

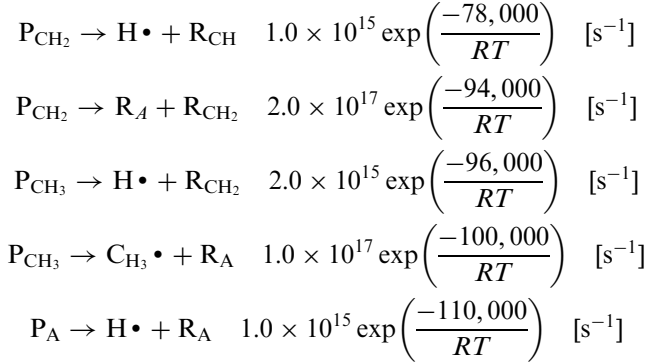
In order to give an example of the main reactions involved in this modelling, let us consider the conditions when the local evolution in the bulk of the deposit is such that the H/C ratio is less than about 0.8. The deposit mostly consists of polycyclic aromatic structures connected by methylenic bridges and only a few methylated positions are present on the aromatic edge. As already mentioned, these structures are quite stiff (glassy or solid), and the movements of the large macromolecules are more or less limited to vibrations and small-width oscillations. Under these conditions, only small species radicals and molecules react effectively, i.e. $H \cdot$, $CH_3 \cdot$, H_2 and CH_4 . The average free volume in the layer (about 30% of the total deposit) is made up of "nanochannels" in which the gas radicals and molecules diffuse. Consequently, the mobility of the $H \cdot$ and $CH_3 \cdot$ radicals is very similar to that typical of the gas phase. The same thing happens for their H-abstraction or substitutive addition reactions on P_{CH_3} , P_{CH_2} and P_A macromolecular positions.

Radical chain terminations are dominated by $H \cdot$ and $CH_3 \cdot$ recombinations into the void volume: these are typical three-body reactions where the third body is generally made up of the close rigid walls of the polymeric material.

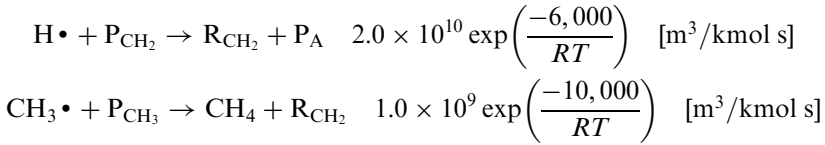
Due to the lack of reliable experimental data on fouling rates, kinetic parameters of these reactions were first obtained by means of *a priori* prediction methods. The H/C data published by Lohr and Dittman (1978) relating to several TLE deposit samples provided the first kinetic validation of the model. A further confirmation of these kinetic data relied on experimental data on bituminous coals (Van Krevelen, 1961).

A sample of the kinetic constants involved in this process includes:

Initiation



Propagation



High-pressure limits are assumed for the termination reactions of small radicals.

The local H and C content of the deposit is directly obtained from the concentration of the different positions (P_A , P_{CH_2} and P_{CH_3}). After the first evolution steps, P_{CH_2} and P_{CH_3} concentrations decrease. As P_A positions become dominant, the successive reactions transform P_A into P_{FUS} . The concentration of aliphatic C-atoms drastically decreases during degradation. [Figure 18](#) shows a typical evolution of the H/C ratio as predicted by the model at about 900 K.

Ethane and methane are released in the first part of this evolution. With a rapid decrease in P_{CH_3} positions, the H/C ratio reaches an intermediate value of about 0.5. The successive dehydrogenation process evolves at a lower kinetic rate. Of course, methane decreases and the gaseous phase is made up mainly of hydrogen.

The initial H/C ratio in the more ordered deposit obtained from ethane pyrolysis is lower than that in a non-compact structure. Due to its more ordered structure, the kinetic rate of successive dehydrogenation reactions of the ethane deposit is lower too.

The evolution of the H/C ratio of the bulk of deposit is extremely important because it affects the void fraction, specific gravity and thermal conductivity of the solid. For ethane cracking, an asymptotic value for H/C, slightly larger than the one yielded by heavy feeds, is obtained at low and intermediate temperatures (700–900 K). At low temperatures (700 K), the deposit mostly loses methyl

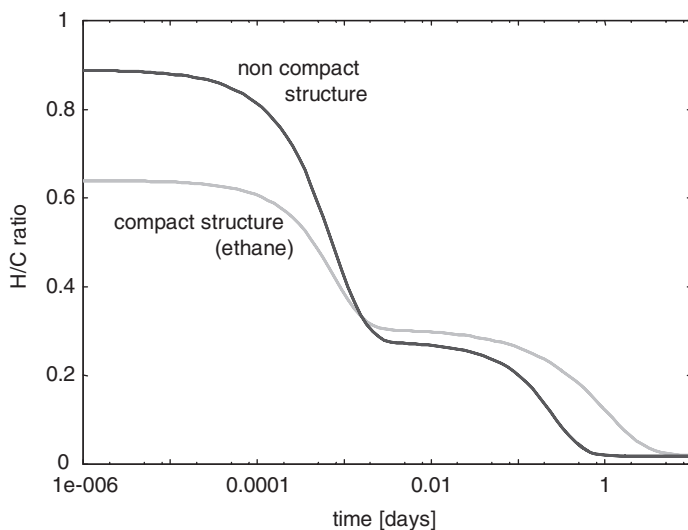


FIG. 18. Time evolution of the H/C ratio of carbonaceous deposits from pyrolysis of naphthas and ethane feed.

positions after about 100 days. The dehydrogenation of P_A positions in favour of P_{FUS} formation requires an higher activation energy. A more or less extended flat region can then be observed. The value of H/C ratio in the flat region and its time dependence vary with local temperature. The total carbon concentration is larger in the ordered deposit because of the different formation mechanism and asymptotic specific gravity. In addition to this, the carbon making up the deposit is mainly aromatic so that the carbon loss is limited.

The evolutions of thermal conductivity vs. H/C ratio for the compact and non-compact deposit morphologies are reported in Fig. 19. The asymptotic value for compact deposit, after deep dehydrogenation, is about 4 kcal/m/h/K (similar to the value of disordered graphite) while for the non-compact deposit, the maximum value is about 2.2 kcal/m/h/K, typical of coke.

It is interesting to observe that the gas released during the aging of the deposit generates micro-bubble in the softer and rubber-like external layers. Some of these bubbles are then trapped in the material and leave micro-spherical cavities and voids close to the process fluid interface. This microscopic aspect of the deposit is strictly connected to the “*bubbling*” phenomenon.

As a consequence of the more ordered and compact structure, the volume contractions due to the dehydrogenation and dealkylation reactions of carbon deposits from ethane crackers are less important. The deposit maintains a limited void fraction, the density is higher and decoking process is more difficult.

Of course, during the decoking process, the void fraction increases with the time because of the decrease in the solid fraction.

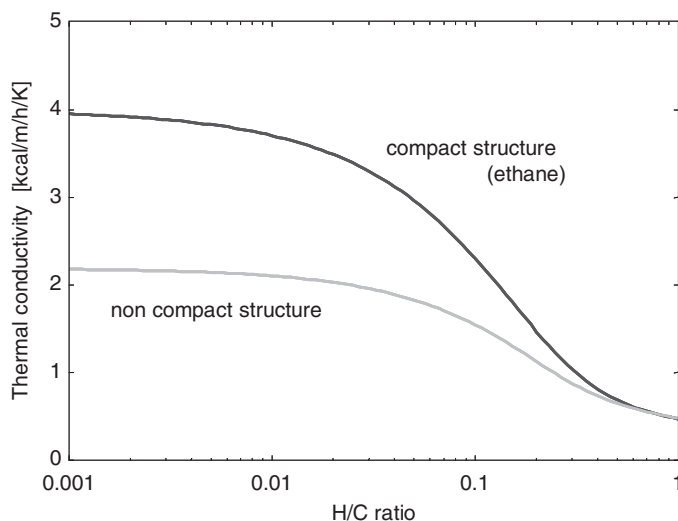


FIG. 19. Thermal conductivity as a function of the H/C ratio for compact and non-compact deposit.

2. Comparisons with Experimental Data

Lohr and Dittman (1978) studied the fouling of TLE in heavy gasoil pyrolysis and their experimental data provided the H/C ratios for three different deposit samples. Sample A at TLE inlet near the process fluid interface (H/C about 0.024); Sample B at TLE outlet near the metal wall (H/C about 0.365) and Sample C at TLE outlet near the process fluid interface (H/C about 0.224). The on-stream time of the TLE was 60 days. The deposit close to the process fluid was exposed throughout the running time at a temperature of about 730–750°C, similar to the furnace outlet temperature; Sample A was exposed to these temperatures for only 3–4 h, after which time the temperature dropped due to the shutdown of the furnace. Sample B was exposed to a more or less constant temperature for 60 days; in this case the temperature was a few degrees higher than the cooling process fluid (boiling water near critical temperature). Sample C, on the other hand, was exposed to rising temperatures due to the progressive thickening of the deposit. Nevertheless, the temperature of Sample C was also fairly constant and equal to that of the process fluid interface (about 600–630°C when the process fluid is made up of heavy gasoil and in the range of 400–430°C in the case of naphtha cracking).

The model predictions for Sample A after 3 h at 1,000 K are very close to the experimental value. Assuming a deposit growth of 5 mm/month, 20 μ m are obtained after 3 h; this value is compatible with the scraped amounts taken for the analysis.

There are some uncertainties in the case of sample B, mostly relating to the size of the sample drawn for analysis. Near the metal surface, the deposit is

grown via the catalytic mechanism with micro-fibres and highly porous structures. The drawn material is therefore limited and the sample had to be quite thick to ensure that an adequate amount had been obtained. Furthermore, the low thermal conductivity of this fibrous layer induces a sharp increase in temperature near the tube wall. In the case of a typical Borsig heat exchanger, a temperature increase of about 25 K is estimated in the 50 μm near the wall; the temperature to be assumed is therefore in the region of 650 K. With this temperature constant for the 60 days of run length, the model prediction ($\text{H/C} \approx 0.38$) agrees quite well with the experimental measurements. Lastly, the model predicts the proper H/C value for sample C too when 3 h of exposure at about 600°C is assumed.

A second set of comparisons refers to the H/C ratio of the coke obtained in a delayed coking process. This material remains inside the coking drums for about 24 h and its final H/C ratio becomes about 0.5 (de Freitas Sugaya, 1999). The model is able to predict this ratio both by maintaining about 700 K for 24 h and also by decreasing the temperature profile (from 715 K to 690 K) according to the temperature evolution of the coking drum.

Further experimental data and further model comparisons relate to the rapid pyrolysis of different coals. In the absence of air, this experimental device heats and converts small coal particles (10–200 μm) in gas and distillates. Figure 20 shows a very satisfactory agreement between experimental data relating to a bituminous coal and model results at 1,260 K. It is noteworthy that despite the strong differences between carbon deposit and bituminous coal, the characteristic times for the dehydrogenation processes are practically the same. Further data on this subject, as well as a detailed model for the analysis of the pyrolysis and devolatilization process of coal particles, are available in a recent paper (Migliavacca *et al.*, 2005).

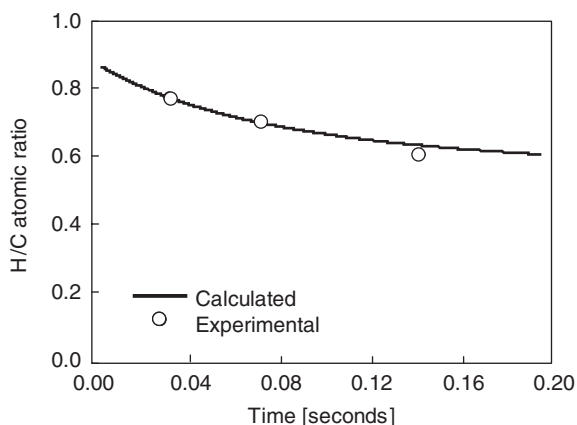


FIG. 20. Comparison with “Rapid Pyrolysis” data.

C. SOOT FORMATION

High-temperature pyrolysis reactions of hydrocarbons are responsible for the production of PAH and solid carbon black particles, soot. This phenomenon is common in diffusion flames where, at high temperatures and without oxygen, hydrocarbon fuel aggregates follow pyrolysis and condensation paths with the formation of heavy aromatic structures. Many PAH's identified in aerosols have been found to be mutagenic and are certainly important soot precursors. This formation of carbonaceous particles has recently become one of the main topics in chemical reaction engineering, especially in the field of pyrolysis and combustion of hydrocarbon fuels. This interest rises from environmental concerns about PAH and soot particle emissions because of their dangerous impact on the human health (Oberdorster *et al.*, 2004).

As already reported in Glasman's book (Glasman, 1996), soot characteristics were clearly described by Palmer and Cullis (1965). On an atomic basis, the carbon formed in flames generally contains a considerable proportion of hydrogen and corresponds to an empirical formula C_8H . When examined under the electron microscope, the deposited carbon consists of a number of roughly spherical particles strung together rather like pearls on a necklace. Figure 21 provides a representative image of the soot formed in rich flames.

Despite minor differences (Alfè *et al.*, 2005), young soot particles formed from ethylene and from benzene flames clearly show very similar morphologies. The diameters of the small spherical particles range from 10 to 20 nm. Each particle is made up of a large number of crystallites. Each crystallite consists of several aromatic sheets with interlayer spacing of about 0.34 nm, similar to the spacing of ideal graphite (0.335 nm).

Several kinetic mechanisms have been proposed in the literature for modelling the formation and growth of soot particles (Appel *et al.*, 2000; Balthasar and Frenklach, 2005; D'Anna *et al.*, 2001a; Frenklach and Wang, 1994; Richter *et al.*, 2005). All these mechanisms agree that the process can be described in terms of the following major steps:

- formation of the first aromatic rings
- growth of PAH structures
- homogeneous nucleation of particles
- particle coagulation
- particle surface growth
- particle agglomeration

Figure 22 (Bockhorn, 1994) clearly summarizes the evolution from light molecules to heavy aromatic structures and finally to carbon particles and aggregates. The transition of the species in the gas phase to aerosols and solid particles is possibly the least understood process.

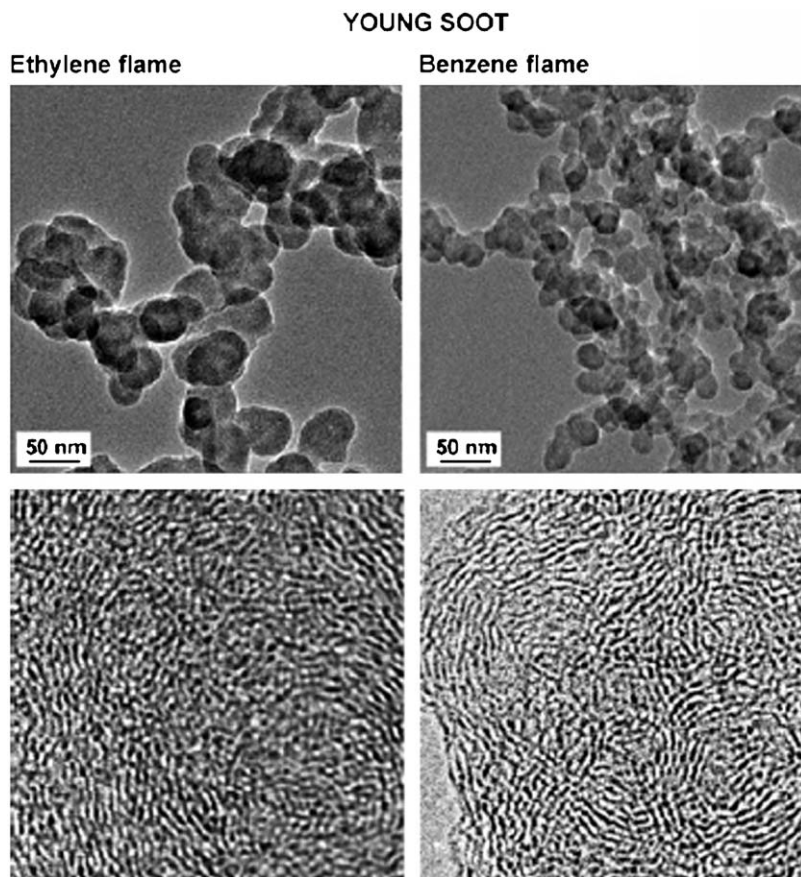


FIG. 21. TEM and HR-TEM of soot particles from ethylene and benzene flames (Alfè *et al.*, 2005).

The very first hypotheses regarding soot inception attributed a key role to ionic (Calcote, 1981) or polyacetylene species (Homann and Wagner, 1967). Recent studies all agree that PAH are the precursors of soot formation (Haynes and Wagner, 1981). Several alternative mechanisms were also discussed as part of the hypothesis. These considered different paths of PAH growth, involving condensed rings (Frenklach and Wang, 1994), aromatic sheets with methylenic or aliphatic bridges (D'Anna *et al.*, 2001b) or, lastly, polyynic pathways (Krestinin, 2000).

There are several analogies between the soot formation mechanism and the fouling mechanism, even though the typical temperatures are higher, and, as a result, more dehydrogenated species and different reactions dominate the process.

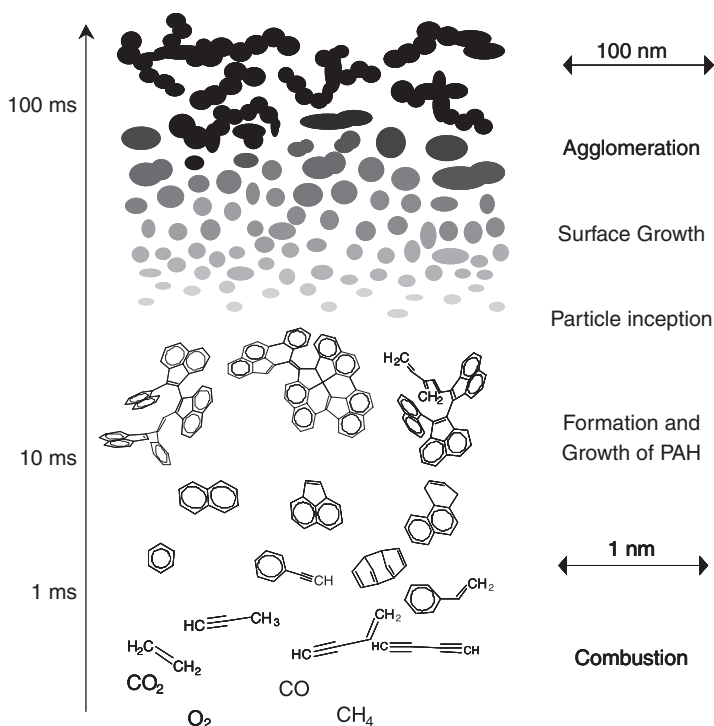
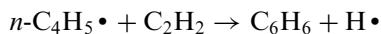


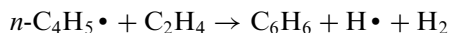
FIG. 22. Reaction steps toward soot formation (Adapted from Bockhorn, 1994).

1. Formation of the First Aromatic Rings and Aromatic Growth

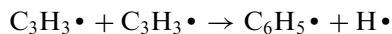
The first step in the soot formation mechanism is the formation of the first aromatic ring when aromatic species are not directly present in the feed. Thus, the formation mechanisms of benzene and the first aromatic species in hydrocarbon pyrolysis, particularly at high temperatures, have been investigated in great depth. Nevertheless, several uncertainties about these formation paths remain. Due to the high temperatures, acetylene addition reactions on unsaturated radicals play a key role (Frenklach and Wang, 1994):



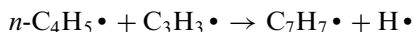
Similarly, at lower temperatures, the following reaction also contributes to benzene formation when there is a significant amount of ethylene in the reacting system:



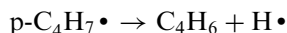
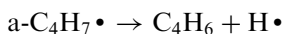
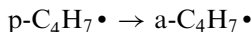
In addition to these reactions of even carbon atoms, odd pathways involving the resonantly stabilized propargyl radical (C_3H_3) have also been identified as relevant contributions to benzene formation (Miller and Melius, 1992):



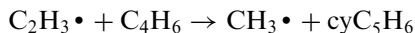
Although propargyl recombination is not an elementary reaction and most probably passes through the linear C_6H_6 compound (Miller, 2001), it can be conveniently lumped into a single equivalent reaction (Appel *et al.*, 2000). Similarly, C_3H_3 can also react with methyl-allenyl ($n\text{-C}_4\text{H}_5$) to form toluene or H and benzyl radical:



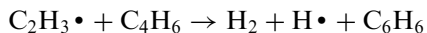
At intermediate temperatures, vinyl, allyl, methyl-allyl ($a\text{C}_4\text{H}_7$), cyclopentadienyl radicals as well as cyclopentadiene are involved in a relevant subset of addition reactions (Faravelli *et al.*, 1998). Vinyl addition to ethylene, through the intermediate $p\text{C}_4\text{H}_7$ and $a\text{C}_4\text{H}_7$ radicals, easily forms butadiene.



The allyl type and more stable $a\text{C}_4\text{H}_7\cdot$ can also add to C_2H_4 giving rise to cyclopentene (cyC_5H_8) and methyl-cyclopentene. Successive dehydrogenation and dealkylation reactions explain the formation of cyclopentadiene. cyC_5H_6 is also formed by the addition of vinyl radical to butadiene

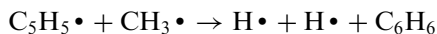
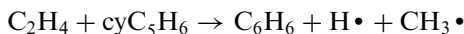


This reaction, which is very important to butadiene disappearance, competes with benzene formation.



At moderate temperatures, further important sources of benzene are the *cyclo*-addition of ethylene to cyC_5H_6 (Dente *et al.*, 1979) and the radical

recombination reaction between cyclopentadienyl and methyl radicals (Ikeda *et al.*, 2000; Moskaleva *et al.*, 1996)

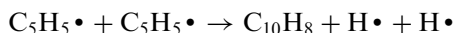


Cyclopentadienyl ($\text{C}_5\text{H}_5\cdot$) is another important resonantly stabilized radical originating from cyclopentadiene or formed by the *cyclo*-addition of propargyl on C_2H_2



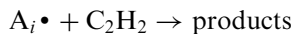
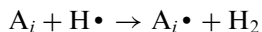
This initial cyclization is similar to the one from propargyl recombination. However, due to the formation of a five-membered ring, it is less favoured from the kinetic point of view: the rate constant is about 30 times lower (Frenklach, 2002). Depending on the operating conditions, this lower reactivity may often be compensated for by the larger amount of C_2H_2 with respect to $\text{C}_3\text{H}_3\cdot$.

For several years now (Dente *et al.*, 1979), the critical role of C_5H_5 radicals in the formation of heavy species, and typically of naphthalene has been defined as



The kinetic parameters of the reactions involved in the formation of the first aromatic rings are summarized in Table X.

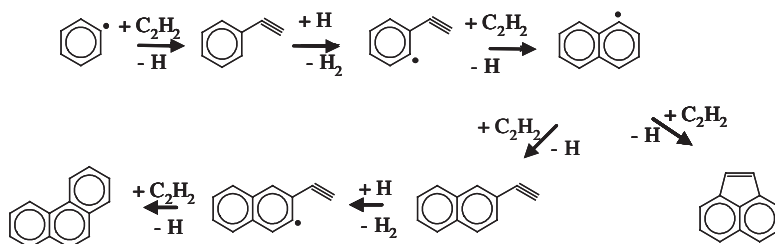
A reliable and well-defined model for describing the successive growth of aromatic species comes from Frenklach and Wang and is the so-called HACA mechanism (Frenklach and Wang, 1990). This acronym stands for the sequence of two main repetitive reactions, i.e. H-abstraction and C_2H_2 addition. This mechanism explains the successive growth of aromatic structures. The H-abstraction from the generic aromatic with i condensed rings (A_i) forms the corresponding aromatic radical ($\text{A}_i\cdot$). The successive addition reaction of $\text{A}_i\cdot$ on acetylene is the first growing step.



The successive repetition of these reactions with parallel cyclization and dehydrogenation reactions easily yields condensed aromatic structures with high molecular weights

TABLE X
RATE CONSTANTS OF REACTIONS INVOLVED IN FIRST AROMATIC RING FORMATION (UNITS ARE KMOL,
M³, K, KCAL)

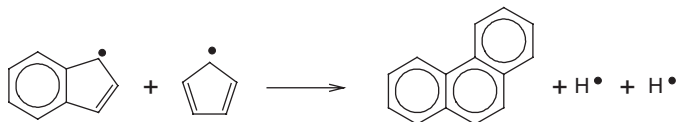
$n\text{-C}_4\text{H}_3\cdot + \text{C}_2\text{H}_2 \rightarrow \text{C}_6\text{H}_5\cdot$	7.01×10^{11}	-0.86	6,379	Westmoreland <i>et al.</i> (1989)
$n\text{-C}_4\text{H}_5\cdot + \text{C}_2\text{H}_2 \rightarrow \text{C}_6\text{H}_6 + \text{H}\cdot$	1.60×10^{13}	-1.33	5,400	Appel <i>et al.</i> (2000)
$n\text{-C}_4\text{H}_5\cdot + \text{C}_2\text{H}_4 \rightarrow \text{C}_6\text{H}_6 + \text{H}\cdot + \text{H}_2$	3.00×10^8	0.00	7,000	Faravelli <i>et al.</i> (1998)
$\text{C}_3\text{H}_3\cdot + \text{C}_3\text{H}_3\cdot \rightarrow \text{C}_6\text{H}_5\cdot$	3.00×10^8	0.00	0.00	Miller and Melius (1992)
$\text{C}_3\text{H}_3\cdot + \text{C}_3\text{H}_3\cdot \rightarrow \text{C}_6\text{H}_5\cdot + \text{H}\cdot$	3.00×10^8	0.00	0.00	Miller and Melius (1992)
$n\text{-C}_4\text{H}_5\cdot + \text{C}_3\text{H}_3\cdot \rightarrow \text{C}_7\text{H}_8$	1.00×10^9	0.00	0.00	Faravelli <i>et al.</i> (1998)
$n\text{-C}_4\text{H}_5\cdot + \text{C}_3\text{H}_3\cdot \rightarrow \text{C}_7\text{H}_7 + \text{H}\cdot$	1.00×10^9	0.00	0.00	Faravelli <i>et al.</i> (1998)
$\text{C}_2\text{H}_3\cdot + \text{C}_2\text{H}_4 \rightarrow p\text{-C}_4\text{H}_7\cdot$	4.00×10^8	0.00	6,500	Dente <i>et al.</i> (1979)
$p\text{-C}_4\text{H}_7\cdot \rightarrow a\text{-C}_4\text{H}_7\cdot$	2.50×10^{12}	0.00	36,000	Dente <i>et al.</i> (1979)
$a\text{-C}_4\text{H}_7\cdot \rightarrow \text{C}_4\text{H}_6 + \text{H}\cdot$	1.00×10^{14}	0.00	51,000	Dente <i>et al.</i> (1979)
$p\text{-C}_4\text{H}_7\cdot \rightarrow \text{C}_4\text{H}_6 + \text{H}\cdot$	2.50×10^{13}	0.00	38,000	Dente <i>et al.</i> (1979)
$\text{C}_2\text{H}_3\cdot + \text{C}_4\text{H}_6 \rightarrow \text{CH}_3\cdot + \text{cyC}_5\text{H}_6$	3.40×10^9	0.00	3,000	Dente <i>et al.</i> (1979)
$\text{C}_2\text{H}_3\cdot + \text{C}_4\text{H}_6 \rightarrow \text{H}_2 + \text{H}\cdot + \text{C}_6\text{H}_6$	6.00×10^8	0.00	3,000	Dente <i>et al.</i> (1979)
$\text{C}_2\text{H}_4 + \text{cyC}_5\text{H}_6 \rightarrow \text{C}_6\text{H}_6 + \text{H}\cdot + \text{CH}_3\cdot$	3.00×10^8	0.00	30,000	Dente <i>et al.</i> (1979)
$\text{C}_5\text{H}_5\cdot + \text{CH}_3\cdot \rightarrow \text{H}\cdot + \text{H}\cdot + \text{C}_6\text{H}_6$	2.00×10^9	0.00	0.00	Ikeda <i>et al.</i> (2000)
$\text{C}_3\text{H}_3\cdot + \text{C}_2\text{H}_2 \rightarrow \text{C}_5\text{H}_5\cdot$	1.00×10^8	0.00	0.00	Frenklach (2002)
$\text{C}_5\text{H}_5\cdot + \text{C}_5\text{H}_5\cdot \rightarrow \text{C}_{10}\text{H}_8 + \text{H}_2$	5.00×10^8	0.00	0.00	Dente and Ranzi (1983)



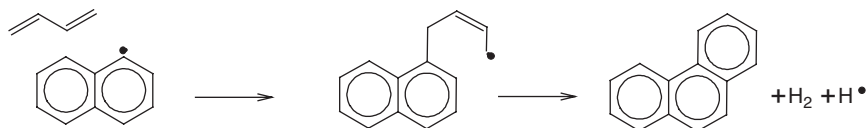
This recursive sequence of reactions progressively increases the number of rings in the poly-aromatic structure whilst always referring to a fixed number of similar species, and makes the adoption of a method of moments for the modelling of this process convenient (Frenklach and Wang, 1994).

Besides acetylene, which is important due to its great abundance in pyrolytic environments at high temperatures, there are also several other components which contribute to aromatic growth. In fact, the RSR (like C_3H_3 , C_4H_5 or C_4H_3 , C_5H_5 etc. ...) can either recombine with aryl radicals or they can add on the five- or six-membered rings (mainly five) and contribute to the growth of these aromatic structures. Analogous to C_5H_5 recombination, different cyclopentadienyl-like structures also contribute to the successive growth of

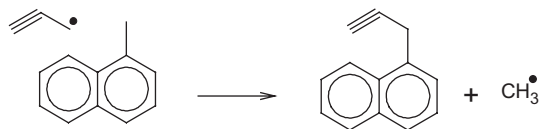
PAH (D'Anna *et al.*, 2001b)



Moreover, aryl radicals can add on unsaturated molecules forming radical intermediates whose successive fate is dehydrogenation and cyclization.

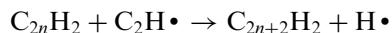


A further important reaction class refers to the substitutive addition reactions which were already discussed in the pyrolytic mechanism of deposit formation. During PAH formation and growth, there are alkyl substitutions (mainly methyl) on the edge surface too. Active radicals add on the aromatic structures with a simultaneous dealkylation. This results in an increase in the molecular weight and dehydrogenation of the aromatics.



Successive addition and condensation reactions of large aromatic molecules and radicals or recombination of large aromatic radicals further contribute to the growth of aromatic structures. As clearly shown in Fig. 23, five-membered ring compounds also play a significant role in this process (D'Anna *et al.*, 2001b).

This mechanism involves the formation of ring–ring aromatics, interconnected by aliphatic chains, which after successive dehydrogenation reactions progressively organize ordered graphite structures. Vlasov and Warnatz (2002) propose a competitive role for the polyne molecules as important soot precursors. The polyne pathway is derived from the works of Krestinin (2000) and assumes that these species grow rapidly with successive additions of C_2H radicals



Polyne molecules were not supposed to grow above certain mass ranges in line with the experimental observations of Homan and Wagner (1967) who analysed the composition of large PAH and soot. Their data on average soot composition indicated H/C ratios of about 0.1–0.12 with molecular weights in

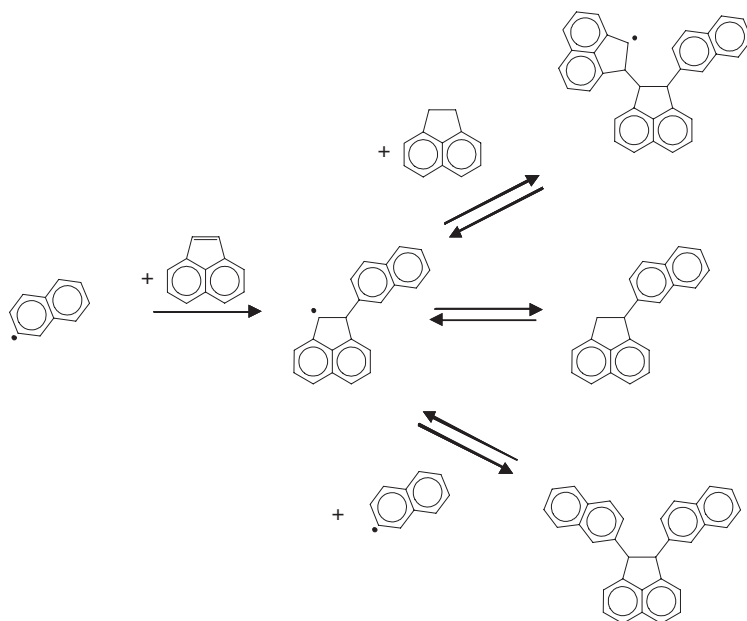
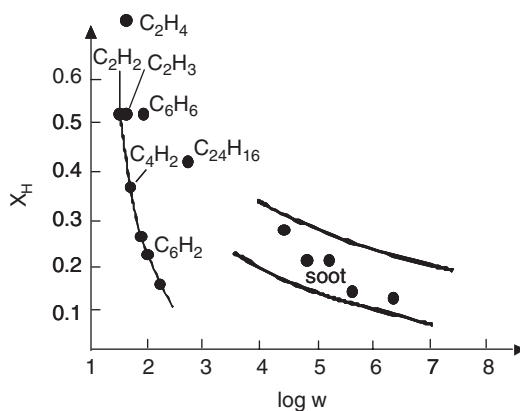
FIG. 23. Growth of PAH structures (D'Anna *et al.*, 2001b).

FIG. 24. Hydrogen content in hydrocarbons and soot as function of molecular weight adapted from Homan and Wagner (1967).

the order of 10^5 – 10^6 while polyene species quickly move to lower hydrogen content, as shown in Fig. 24. In the Krestinin mechanism, polyene molecules can generate heavier PAH structures through radical addition on unsaturated bonds and the formation of cross-linked structures. The polyenes are also thought to be successively responsible for major soot growth via surface reactions (Krestinin, 2000).

2. Soot Inception and Growth

Nucleation is a crucial step in the whole process of carbonaceous particle formation. According to Frenklach and Wang (1990, 1994), nucleation is controlled mainly by the sticking of PAH sheets during their collisions. Physically bound clusters of PAH are then formed and successively evolve toward aerosol, solid particles and crystallites. As shown in Fig. 25, different polycyclic aromatic layers can form more or less regularly ordered graphite structures, all of which have interlayer distances of about 0.35 nm. These two to four-layer structures are assumed as the threshold of the formation of the solid phase; particle inception typically takes place at molecular masses of 1,000–2,000 amu.

A partially different approach assumes that the transition from the gas to the condensed phase simply occurs as a sequence of successive addition reactions, with the formation of large poly-aromatic structures. Once again, above a certain molecular weight PAH becomes aerosol or soot particles (D'Anna *et al.*, 2001b; Richter *et al.*, 2005; Sarofim and Longwell, 1994).

The kinetic modelling of soot formation processes refer to gross simplifications and the use of lumped pseudospecies aimed at describing the physico-chemical evolution of heavy PAH towards soot particles with molecular weight of more than 10^6 – 10^7 . The discrete sectional method (DSM) is commonly adopted to solve this problem. Soot formation is described in the usual form of gas-phase kinetics (Granata *et al.*, 2005; Richter *et al.*, 2005) and a limited number of lumped pseudospecies is selected. Large PAH species and particles are grouped into sections (equivalent components, here referred to as BINs), each of these has an average mass, mass range and defined H/C ratio. The first BIN corresponds to coronene, $C_{24}H_{12}$, but either lighter (pyrene) or heavier aromatics can be adopted. The next BIN has twice the average mass and mass range, i.e. BIN₂ has an average mass of 600 amu and a mass range of

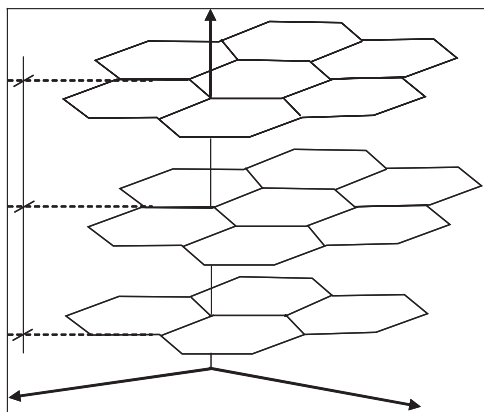


FIG. 25. Three-layer PAH cluster with ordered structure and interlayer distances of about 0.35 nm.

401–800 amu. This exponential sectional approach saves on computation time whilst still offering a good description of the low-molecular weight components. The largest BIN reaches nominal species with more than 10^6 C-atoms and H/C ratios lower than ~ 0.125 in line with the experimental measurements.

Large BINs, i.e. heavier than 2,000–2,500 amu, are considered to be soot or solid particles and therefore interact like aerosol particles. Kinetic rates are scaled to account for the variation in the collision frequency with reactant sizes. Particle diameter and collision interactions are usually based on the assumption of spherical structures.

Nascent soot particles are formed via reactions between PAH radicals or between stable PAHs and their radicals. The kinetic rates are evaluated on the basis of the analogy with the first phenyl radical and benzene reactions. Frequency factors are scaled on the basis of the change in collision frequencies relative to those of benzene addition on phenyl or phenyl recombination. These reactions are treated as irreversible. BIN radicals are formed via H-abstraction, mainly by H radicals, with both forward and reverse reactions assumed. Unimolecular hydrogen loss from parent BINs and the corresponding reverse reaction also occur.

Surface growth mainly takes place via reactions with acetylene, PAH and PAH radicals to soot nuclei activated by H-abstraction as well as PAH radicals to parent BINs. Soot particle coagulation is the result of addition reactions between BINs and BIN radicals, recombination reactions of BIN radicals and, lastly, interactions between heavy BIN species.

This modelling approach allows the description not only of the overall soot volume fraction but also of the distribution of the equivalent diameters of the carbon particles. Figure 26 shows a sample of comparisons between model

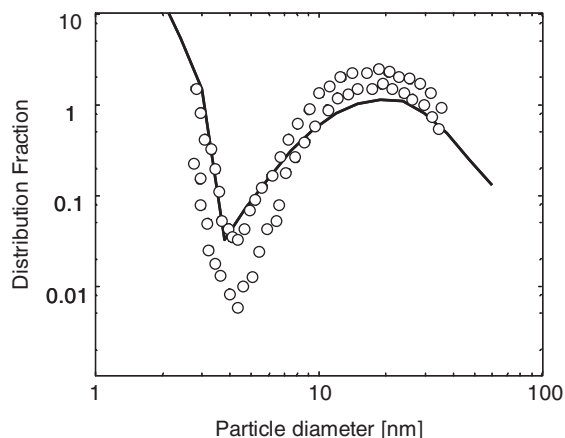


FIG. 26. Distribution of particle diameters in an ethylene sooting flame. Comparison between model predictions and the experimental data (Zhao *et al.*, 2003).

predictions and the experimental data of Zhao *et al.* (2003) relating to an example of this distribution of particle diameters in an ethylene sooting flame.

IV. Applications

This chapter presents the industrial applications and validations of certain detailed models which refer to the kinetics analysed earlier. The steam cracking process will be analysed first followed by visbreaking and delayed coking processes. Last of all, the method will be applied to the thermal degradation of plastic waste.

A. STEAM CRACKING PROCESS AND PYROLYSIS COILS

Thermal cracking is a well-known and widely accepted method of olefin production. A steam cracker can be conveniently divided into three sections: pyrolysis, quenching and product separation. Of course, the pyrolysis section is the heart of the steam cracker process. Hydrocarbons first enter the convection section of the pyrolysis furnace and are preheated to about 600–650°C. Then, the vaporized steam is mixed with superheated steam and passed into long pyrolysis coils with typical diameters in the range of 30–125 mm. The pyrolysis reactions mostly take place in the radiant section of the furnace where tubes, usually made of chromium nickel alloys, are heated externally to about 1,100°C by floor and/or wall burners. Depending on the cracking severity, free radical reactions lead to the formation of ethylene and light olefins with different selectivities. The hot gases are then quenched in the TLE to 450–650°C to reduce the effect of successive reactions and generate high-pressure steam at the same time. As already described in the previous paragraphs, pyrolysis coils and heat exchangers are prone to fouling and therefore have to be periodically shut down (Ren *et al.*, 2006).

In the primary fractionation section, gasoline and fuel oil streams are quenched by oil and fractionated. The liquid fraction is extracted and the gaseous products are cooled in the quench tower by a circulating water stream. The gaseous fraction is then compressed and cooled down to remove acid gases, carbon dioxide and water. The final product separation essentially involves distillation, refrigeration and extraction. The equipment used includes chilling trains, where methane and hydrogen are separated at cryogenic temperatures, and a sequence of several fractionation towers. Ethane and propane are usually recycled as feedstock. The product yield from steam cracking process varies greatly according to the feed and operating conditions.

Regular decoking is required to deal with coke deposits in both pyrolysis coils and the TLE. The furnace is shut down and high-pressure steam and air are fed

in to burn off the coke deposit on the inner surfaces of the walls. The coke deposit in the TLE is washed away with high-pressure water or is removed mechanically. Depending on the feedstock, coil configuration and severity, this decoking process must be carried out every 10–70 days and can take 20–40 h.

In order to maximize ethylene yield and selectivity, the pyrolysis process should take place at high temperatures, under low pressure and with low contact times. In fact, high temperatures favour decomposition reactions, low pressures inhibit condensation reactions, and low residence times avoid successive reactions of ethylene and derived products. Mostly for this last reason, the geometry of pyrolysis coils has been changed from the long, large-diameter coils used in the past to the current small-diameter and shorter coils (10–20 m). Today the focus is also on coil configurations and geometries capable of not only improving ethylene yields but also increasing the on-stream time of the furnaces.

As an example of recent efforts to improve overall coil performance, Fig. 27 shows the new coils recently patented by Kubota (Magnan *et al.*, 2004). MERT (Mixing Element Radiant Tube) is a centrifugal cast radiant tube with a helical mixing element on the inside diameter for use in cracking furnaces. It works by inducing high turbulence and disrupting the inside boundary layer of hydrocarbons, thus increasing the effective internal heat transfer coefficient. The high

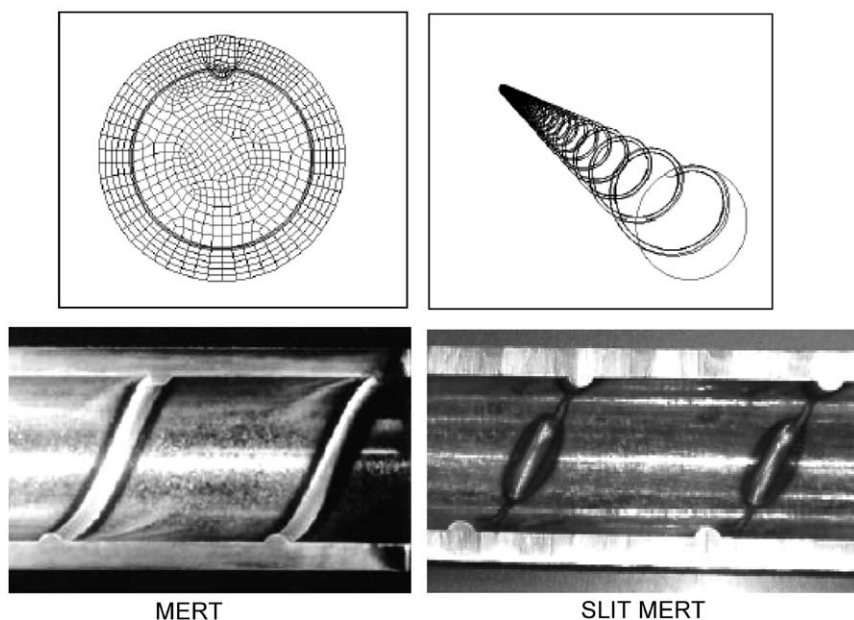


FIG. 27. (a) CFD representation of MERT. (b) Longitudinal cross-section of MERT and SLIT MERT.

turbulence and mixing improves cracking performance and provides a more uniform hydrocarbon temperature throughout the tube cross-section. However, the increased friction factor does also have certain detrimental effects. In fact, the geometry was recently modified to achieve a lower friction factor yet maintain the same mixing effect and internal heat transfer coefficient. The new coils (SLIT MERT) are similar to the previous helical finned ones except for the fact that the element is applied intermittently. The volume fraction of the element is reduced, but since the alignment of the segments is maintained, the swirl mixing effect continues throughout the length of the tube.

Engineering companies always are interested in work aimed at improving coils and furnace arrangements, regardless of whether the focus is on design or revamping. Pyrolysis coil selectivity and yields are being continuously improved by changing from older large bore tubes to smaller tubes with very short residence times. An example of these design improvements is provided by [Evans *et al.* \(2002\)](#) who observes that the key factor in minimizing investment and operation costs without sacrificing performance is larger capacity per single furnace, as would be the case with the re-introduction of the staggered or two-lane coil. The compactness of the new design decreases firebox size while maintaining high cracking furnace availability, thus lowering the investment and operating cost of the cracking furnaces. Although a staggered coil layout is not typical in modern coil design, a feasible design was obtained by minimizing the inherent drawback of the staggered design, i.e. the higher peak-to-average heat flux ratios. A new furnace design (GK6) was compared to a previous one (GK5). The staggered GK6 design has an 8–8 cracking coil configuration with the inlets and outlets of the cracking coil entering and leaving the radiant section through the roof. The tubes are arranged in two lanes: each inlet tube in one lane is connected to an outlet tube in the other lane. The bottom jump overlies the same plane as the in and outlet tubes. This means that there are no horizontal forces in the GK6 design, which avoid bowing of the radiant tubes. Feedback from operating units confirmed that the cracking performance of the GK6 is equal to or slightly better than that of a leading cracking coil arrangement, the GK5 coil design. Improvements in run length and the expected tendency to bowing have been confirmed too.

1. Coil Model and Model Validation

A mathematical model to simulate the cracking process in the pyrolysis coils contains a set of differential equations describing material, energy and momentum balances. Additional features are also included, such as the fouling process, the associated dynamic behaviour of the coke deposit in the pyrolysis coils and the rising pressure drops in the coil and in the TLE. A monodimensional model is usually adopted, although several two-dimensional description projects have been attempted ([Heynderickx *et al.*, 1992, 2001](#); [Van Geem *et al.*, 2004](#)). There is less benefit to such an approach, however, than might be gained

with a proper description of the pyrolysis mechanisms and the corresponding overall kinetic scheme.

The previous description of the kinetic approach to pyrolysis, as well as the fouling phenomena, have been adopted for the development of a mechanistic model and simulation program (Dente *et al.*, 1970, 1992, 2005) which has been extensively used and tested in industry since the 80s.

About 250 real and lumped components, molecules and radicals are considered in the overall kinetic model which aims to describe the pyrolysis chemistry of gaseous and liquid feeds up to heavy gasoils and condensate fractions. Figure 28 shows the distribution of these components (real and lumped species) as a function of the number of carbon atoms and of the dehydrogenation degree Z , in accordance with the formula C_nH_{2n-Z} . The families of alkanes as well as several alkyl-aromatics are singled out and the vertical lumping of the heavy homologous compounds at 25, 30 and 35 carbon atoms is also quite clear. It is worthwhile noting too that the heaviest dehydrogenated species with about 40 C-atoms maintain an H/C ratio of about 0.7. This dehydrogenation level allows the gas-phase formation of the cracking fuel oil and heavy pyrolysis fractions to be described.

Careful, in-depth validation of the overall kinetic model across a wide range of operating conditions was carried out over long periods on the basis of industrial data. The resulting pyrolysis model thus gives accurate and reliable yields predictions and is a significant reference for the ethylene producers.

Figure 29 shows a scatter diagram relating to the deviations of ethylene yields predicted by two rival models. The experimental data refer to about 300 different cases. High and low cracking severities are considered, and the data refer to

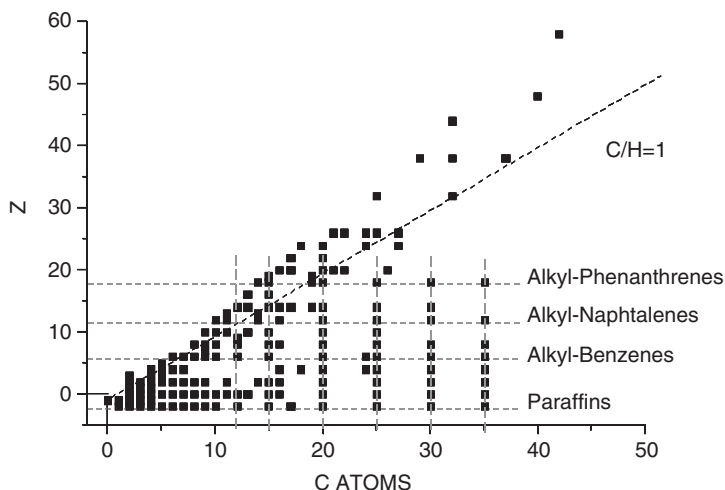


FIG. 28. Distribution of reference compounds involved in the pyrolysis model.

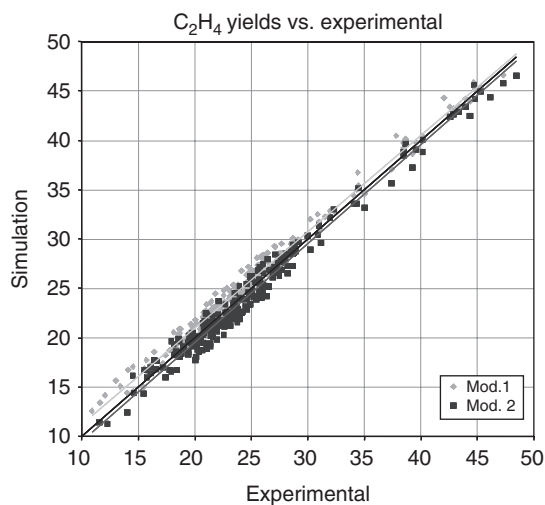


FIG. 29. Validation of the model. Comparison of two rival models. Scatter diagram of ethylene yields.

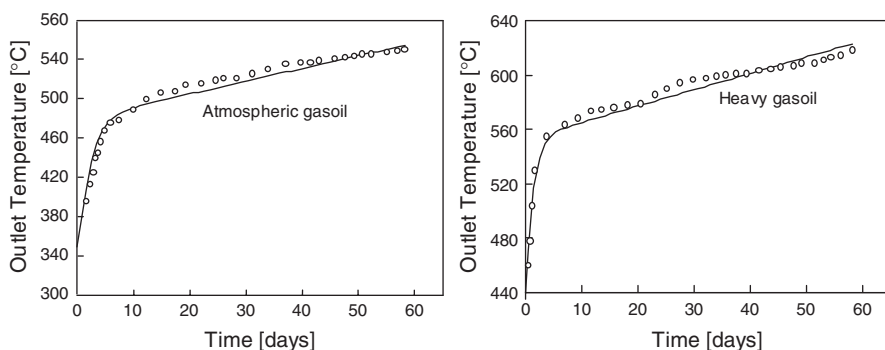


FIG. 30. Non-conventional TLE. Outlet temperature vs. time. Comparisons of predicted and experimental measurements (Lohr and Dittman, 1978).

commercial plant or pilot and laboratory-scale devices. Feedstocks range from light naphtha to virgin and hydrotreated gasoil with final boiling points of over 500°C.

Fouling process models for both pyrolysis coils and the TLE were also verified against experimental data. Figure 30 reports a comparison between model predictions and the experimental data reported by Lohr and Dittman (1978). The time evolution of the outlet temperature from the TLE indicates that the efficiency of the heat exchangers is penalized. In the case of both an atmospheric gasoil and a vacuum one, the temperature of the process gases from the TLE

increases by more than 200 K in 50 days. The very sharp, net initial temperature increase is due both to the catalytic growth and to the low thermal conductivity of the initial deposit.

B. VISBREAKING AND DELAYED COKING PROCESSES

Liquid-phase pyrolysis of oil streams is widely used in refinery: visbreaking and delayed coking processes are typical examples. The feeds are made up of residues of atmospheric or vacuum crude distillation. The typical temperatures ($440\text{--}490^\circ\text{C}$) and the high pressures ($> 10\text{ bar}$), together with the nature of the feedstock, indicate that these processes essentially take place in the liquid phase. Visbreaking and delayed coking are extensively used to upgrade refinery residues or heavy streams to increase distillate production: gas, gasoline, kerosene, light, heavy and vacuum gasoils. Visbreaking is widespread in Europe and the Far East while delayed coking is more popular in the US and the other parts of the world.

As shown in Fig. 31a, a visbreaking reactor consists of very long coils inserted into a radiating furnace. The effluent often passes into the extra adiabatic

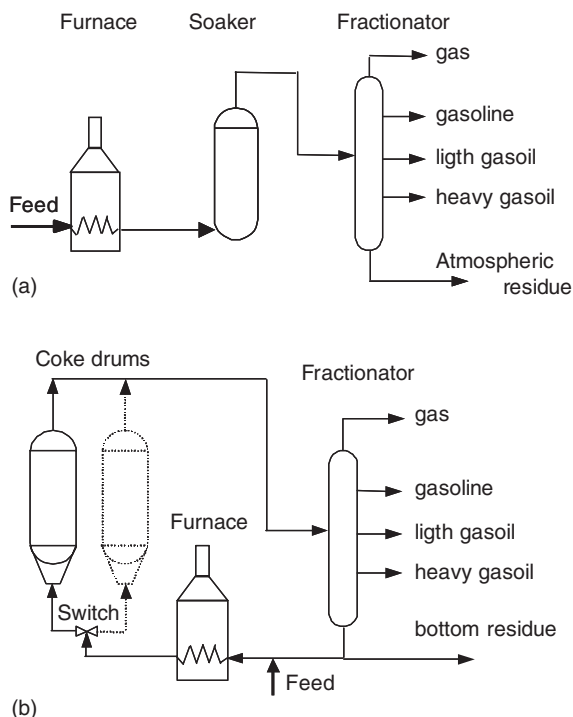


FIG. 31. (a) Visbreaking process. (b) Delayed coking process.

reaction volume of the soaker. This makes it possible to decrease the furnace outlet temperature and reduce the fouling inside the coils. One or more fractionators are aimed to the different streams recovering.

A simplified delayed coking process scheme is shown in Fig. 31b. The feed, mixed with part of the bottom of the fractionator, is preheated and partially vaporized in the coils of the furnace. The latter is connected to a system of two or more large coke drums that operate alternatively semi-batchwise, like adiabatic reactors. The liquid and the mesophase (i.e. the colloidal system precursor of coke) gradually fill the drum and the released vapours exit through the top. When the proper level of condensed phase is reached (60–70% of drum volume), the feed is progressively switched to the other drum. Steam is injected to complete the stripping and the recovery of the lighter fractions still contained into the drum. Last of all, coke removal begins.

Simplified macro-kinetic models (Del Bianco *et al.*, 1993; Filho and Sugaya, 2001) are usually proposed in the literature: these are limited because are not able to cover the complete range of operating conditions and feedstocks. A detailed kinetic model together with reliable feed characterization, on other hand, gives a flexible representation of the process.

1. Kinetic Mechanism

The whole kinetic mechanism is essentially characterized by initiation, β -scission, H-abstraction, internal isomerization of radicals, substitutive addition of radicals onto unsaturated molecules and radical recombination reactions.

H-abstraction and β -scission reactions are the main effective propagation steps of the chain.

H-abstractions on pseudocomponents give rise to radicals which can either (re)abstract H-atoms from other molecules or undergo β -scission reactions. Due to the relative activation energies and to the high concentration of neighbouring H-atoms in the liquid phase, the H-abstractions are much, much faster. Therefore, β -scission reactions constitute the rate-determining step of the overall decomposition process. In fact, the radicals produced through β -scissions rapidly generate their products before undergoing a new β -scission. The final consequence of these considerations is that the decomposition fate of every pseudocomponent can be simply described using a lumped equivalent reaction whose stoichiometry takes into account the relative probability of the scission of different bonds. The stoichiometric coefficients, which vary slightly with temperature, are conveniently evaluated at a reference temperature of 700 K.

As already mentioned, frequency factors and activation energies of all these reactions are derived from the equivalent ones in the gas phase, by applying the additive corrections of activation energies and entropies for their transposition in the condensed state.

The substitutive addition reactions of poly-aromatic radicals on methyl and alkyl positions of aromatic species produce poly-aromatic structures, as

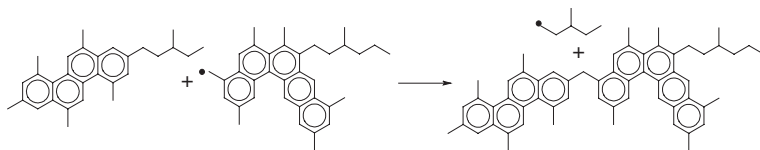


FIG. 32. Substitutive addition reaction.

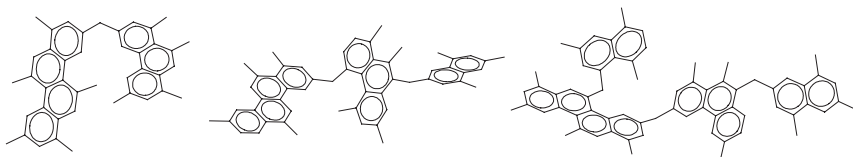


FIG. 33. Poly-aromatic species.

reported in Fig. 32. The net effect of these addition reactions with successive dealkylation is a polymerization of aromatic molecules characterized by multiple aromatic sheets connected by methylene bridges (see Fig. 33).

The index of multiplicity (i.e. the number of aromatic sheets) ranges from two to four. The maximum of four in the multiplicity index is justified mainly by two considerations. The first is that the predicted amount of the four-sheet molecules is already negligible compared with those of lower index. This simply means that further interactions, which would produce larger multi-sheet structures, become even more negligible. The second consideration refers to geometrical structure and to the increasing sterical hindrance which drastically reduces the possibility of further radical additions to the methyl sites of the molecule. During these substitutive addition reactions, the release of large alkyl radicals is more favoured than the release of methyl or even H radicals. These small radicals abstract H-atoms from the substrate forming alkanes, methane or H_2 .

These reactions are very important, principally in the delayed coking process because of the high residence time in the drum of up to 24 h. There is, therefore, a clearer need for appropriate lumping in the case of delayed coking.

As a function of the different sites, reference kinetic constants for these substitutive additions in the aromatic ring, are

- alkyl site $k_{ADD} = 5 \times 10^8 \exp(-24,000/RT)$ [$m^3/kmol\ s$]
- methyl site $k_{ADD} = 5 \times 10^8 \exp(-26,000/RT)$ [$m^3/kmol\ s$]
- aromatic hydrogen position ($C_{ar}-H$)
 $k_{ADD} = 5 \times 10^8 \exp(-28,000/RT)$ [$m^3/kmol\ s$]

Further dehydrogenation and demethylation reactions contribute to the formation of coke precursors, as shown in Fig. 34.

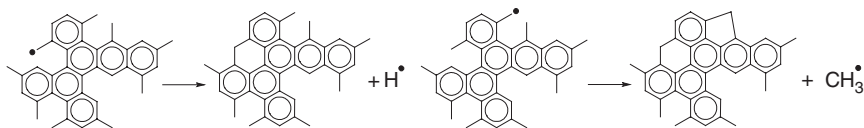


FIG. 34. Examples of internal dehydrogenation and demethylation of poly-aromatic radicals.

Significant amounts of methane and hydrogen are thus released in the gaseous products while the H/C ratio of the heavy residue gradually decreases to 0.6–0.4 and the hydrocarbon mesophase progressively becomes coke. In fact, the liquid containing the dispersed mesophase becomes more and more viscous and termination reactions become very difficult. As a consequence, poly-aromatic radical concentrations rise continuously with time and gas production is observed. The production of light fractions increases at the expense of the other distillates, such as gasoline and gasoils. This mechanism is clearly supported by experimental data and measurements relating to the kinetics of residue degradation (Del Bianco *et al.*, 1993). After about half an hour in the drum, the average size of the alkyl side chains in poly-aromatic species is so drastically reduced that addition, dehydrogenation and demethylation become the predominant reactions. Details of the kinetic models including the description of the several hundreds of real and lumped components and equivalent reactions contained therein are available in Bozzano *et al.* (1995, 2005).

2. Stability of the Visbroken Residue and Pyrolysis Severity

A further important aspect in visbreaking process modelling is the stability of the residue that rules the operating conditions or process severity. The asphalt-henes, which are present in the feed and formed during the cracking reactions, can flocculate forming a sort of mud, especially in systems with a vacuum distillation unit. This mud affects residue quality and therefore constitutes a limit to visbreaking severity. Asphaltenes are defined as the hydrocarbons that precipitate after the addition of *n*-heptane or *n*-pentane. An early discussion of the chemical species representative of asphaltenes is found in Algelt and Boduszynski's very comprehensive book (Altgelt and Boduszynski, 1994). Asphaltenes are best defined as high-molecular weight poly-aromatic species, containing cata-condensed aromatic sheets with methyl or short side chains and heteroatoms (mainly S, but also small amounts of N and O). Thus, the whole aromatic fraction can be considered to consist of asphaltenes and the remaining part of poly-aromatics with long alkyl side chains which also contain polar and resin compounds. Residue stability and asphaltenes flocculation are discussed in detail elsewhere (Bozzano and Dente, 2005; Bozzano *et al.*, 1995; Dente *et al.*, 1997). Only the essential aspects are reported here. Poly-aromatics with side chains decompose during the pyrolysis process and contribute to increase the asphaltene content in the visbreaking residue.

The reacting mixture can thus be represented by two phases. The first, the maltenic phase, is made up of aromatics, alkanes, alkenes, *cyclo*-alkenes and naphthenes. Aromatics and asphaltenes are contained in the second phase. Reciprocal compatibility is related to the solubility parameter that is in the range of $7\text{--}8(\text{cal}/\text{cm}^3)^{1/2}$ for alkanes and alkenes, $8\text{--}9(\text{cal}/\text{cm}^3)^{1/2}$ for naphthenes and *cyclo*-alkenes, $8.8\text{--}10(\text{cal}/\text{cm}^3)^{1/2}$ for aromatics and $11\text{--}12(\text{cal}/\text{cm}^3)^{1/2}$ for asphaltenes. It is worth noting too that the closer the solubility parameter of the two phases, the more resistant the system is to flocculation. All the asphaltenic molecules are supposed to be surrounded by aromatics, deposited as “sheets” over the asphaltenic “sheet”, constituting a molecular aggregate equivalent to an adsorbed phase. This coverage improves the solubility parameter and compatibility with the maltenic phase of the aggregate with respect to pure asphaltenes. The non-asphaltenic aromatics are supposed to be distributed between the maltenic and adsorbed phase. Their distribution ratio is estimated on the basis of the activity coefficients of the aromatic class inside the two phases and depends on the temperature and composition of the two phases. Activity coefficients are estimated using the solubility parameters. Precipitation occurs when, as a result of dilution (e.g., with cetane), the total concentration of aromatics in the maltenic phase is so low that it results in the desorption of the aromatics deposited on asphaltenes. *Cyclo*-alkane and *cyclo*-alkene components increase the stability of the visbreaking residue at the same severity level. In fact, their presence increases the global solubility parameter of the maltenic phase and a smaller amount of aromatics is needed to cover the asphaltenes. This phenomenological model allows the estimation of the peptisation value of the mixture commonly adopted in refineries to control the severity of the process.

3. Model Validation and Comparisons with Experimental Data

Some interesting examples of industrial visbreaker performance with comparisons between experimental data and model predictions are reported in Table XI. Three different feedstocks and process conditions are considered. About 60% of the total residence time is inside the soaker. These data also show the increase in stability due to the presence of naphthenes. Feed 1 is richer in *cyclo*-alkanes while the third feed is more aromatic.

Likewise, Table XII reports a comparison of delayed coking models with industrial plant data for five different feedstocks covering a large range of different gasoil recycle ratios. The coil outlet temperature is in the range of 490°C and coil outlet pressure is about 5 ata. The results obtained confirm the reliability of this model.

Further interesting kinetic data, obtained from a batch isothermal lab reactor across a wide range of temperatures and residence times, are also discussed (Del Bianco *et al.*, 1993). The feedstock is a Belaym vacuum residue with the following properties: specific gravity (15/4) 1.028, kinematic viscosity at 100°C

TABLE XI
COMPARISON OF EXPERIMENTAL AND CALCULATED YIELDS AND PROPERTIES FOR A VISBREAKER

		1		2		3	
Feed properties							
AEBPI (°C)		424		485		495	
Sp. Gr.15/4		1.018		1.010		1.042	
K.V. cSt (100°C)		2,086		1,200		13,300	
CCR		13.7		15.5		23	
S wt%		2.97		2.75		3.2	
Operating conditions							
Coil outlet temperature (°C)		448		448		450	
Coil outlet pressure (ata)		11.5		11.5		11.5	
Residence time (min)		15.4		16.2		17.0	
Effluents		Exp.	Model	Exp.	Model	Exp.	Model
Gas	H ₂ S wt%	0.15	0.12	0.16	0.12	0.18	0.15
	Yield wt%	0.82	0.95	1.10	1.04	1.16	1.21
	Yield wt%	5.30	4.9	5.36	5.04	6.8	6.4
Naphtha	ASTM D86 (°C)	22–165	23–168	36–167	27–168	32–191	34–195
	Sp. Gr. (15/4)	0.717	0.719	0.718	0.719	0.738	0.731
	Sulphur wt%	0.76	0.85	0.82	0.85	1.00	0.94
	Br. Number	84	86	101	87	80	88
	Yield wt%	7.86	7.96	8.27	8.69	5.0	5.7
Gasoil	ASTM D86 (°C)	195/325	200/324	195/331	200/324	200/300	200/321
	Sp. Gr. (15/4)	0.843	0.840	0.843	0.841	0.852	0.847
	K.V. at 50°C cSt	1.8	1.6	1.96	1.8	1.9	1.7
	Sulphur wt%	1.91	1.68	1.39	1.47	2.1	1.84
	Br. Number	44	44	40	44	45	47
	Yield wt%	86.02	86.19	85.27	85.23	87.04	86.69
	AEBP (°C)	> 340	> 340	> 340	> 340	> 320	> 320
Visbroken residue	Sp. Gr. (15/4)	1.028	1.027	1.021	1.020	1.049	1.051
	K.V. at 100°C cSt	450	644	310	427	1414	2300
	P.V.	1.2	1.20	1.10	1.15	1.20	1.10
	Sulphur wt%	2.97	3.0	2.35	2.78	3.20	3.30
	CCR wt%	24	22.0	21.0	19.0	27.0	25.0

5230 cSt, CCR 20.8, *n*-heptane asphaltenes 18.6(wt%). The comparisons between the experimental and predicted distillate yields are shown in Fig. 35. The maximum observed in the yields is related to the partial pressure of the distillates increasing with the time in the batch unit, so that partial condensation of heavy fractions is possible. At high temperatures and residence times, thermal degradation of the heavy fractions takes place in the gas phase; these reactions increase the gasoline and gas at the expense of heavy gasoil.

As previously discussed, fouling is an important aspect in the visbreaking process too. The adiabatic reactor volume of the soaker allows the run length of

TABLE XII
COMPARISONS OF EXPERIMENTAL AND CALCULATED YIELDS AND PROPERTIES IN A DELAYED COKING
UNIT

		1	2	3		4		5				
Feed properties												
AEBPI (°C)		360	360	480		370		470				
Sp. Gr. 15/4		0.998	1.044	1.065		0.98		1.026				
S wt%		4.83	8.3	8.8		3.3		4.0				
CCR		9.1	17	20		14		20				
K.V. cSt (50°C)		30	400,000	25,000,000		1,100		400,000				
Gasoil recycle (% feed)			0		6		15		6		15	
Effluents			Exp. Mod		Exp. Mod		Exp. Mod		Exp. Mod		Exp. Mod	
Gas ($\leq C_4$)	Yield wt%	6.72	6.9	9.6	9.2	11.3	10.7	6.6	7.0	9.0	8.5	
	H ₂ S	1.4	1.56	3.4	3.1	3.9	3.7	1.3	1.1	1.6	1.5	
	CH ₄ + H ₂ + C ₂ [±]	3.0	3.31	3.7	2.4	4.3	2.8	3.1	2.2	4.3	2.8	
	C ₃ [±]	1.4	1.0	1.1	1.2	1.4	1.3	1.0	1.1	1.4	1.3	
	C ₄ ^{±a}	1.0	1.5	1.4	2.6	1.7	2.9	1.2	2.4	1.7	2.9	
L. Gasoline (C ₅ /80°C)	Yield wt%	2.91	2.94	4.6	4.4	4.2	4.6	4.8	4.3	4.2	4.4	
H. Gasoline (80/180°C)	Yield wt%	10.6	10.5	7.5	8.0	6.8	7.0	7.9	8.1	6.8	7.0	
	Sp. Gr. 15/4	0.777	0.775	0.76	0.77	0.76	0.76	0.75	0.76	0.75	0.75	
	Sulphur wt%	2.1	1.5	3.0	3.2	3.3	3.1	1.2	1.3	1.5	1.3	
L. Gasoil (180/350°C)	Yield wt%	31.8	31.9	27.7	29.0	24.0	26.4	32.5	32.4	26.2	26.1	
	Sp. Gr. 15/4	0.90	0.91	0.88	0.87	0.88	0.86	0.86	0.85	0.86	0.85	
	Sulphur wt%	3.0	2.6	4.3	4.5	4.8	4.1	2.0	1.9	2.5	1.9	
H. Gasoil (> 350°C)	Yield wt%	30.1	30.5	24.4	23.8	22.8	22.4	26.1	26.7	22.8	22.7	
	Sp. Gr. 15/4	0.96	0.96	0.96	0.97	0.96	0.97	0.94	0.94	0.94	0.95	
	Sulphur wt%	3.3	3.0	4.5	5.0	5.0	4.8	2.6	2.2	3.0	2.2	
Coke	Yield wt%	17.8	17.7	25.5	25.4	30.2	28.9	21.4	21.5	30.3	31.3	
	Sulphur wt%	6.1	5.95	8.0	9.0	10.0	9.5	3.3	3.7	3.3	3.8	

^aIn the industrial cases part of the C₄ are entering into the light gasoline fraction.

the furnace to be increased up to about one year. Figure 36 shows the comparison between experimental and predicted external tube skin temperatures at the coil outlet in the case of an industrial visbreaking furnace. Moreover, the fouling also takes place in different areas of the visbreaking plant, such as the vacuum distillation tower or the heat exchangers, via the same mechanism.

Finally, it is worth pointing out that the modelling was strongly supported by a large amount of laboratory and industrial experimental data which allowed further tuning and verification of model assumptions and kinetic parameters. Detailed results of this, together with a discussion of the kinetic parameters, are reported in several papers (Bozzano and Dente, 2005; Dente *et al.*, 1997).

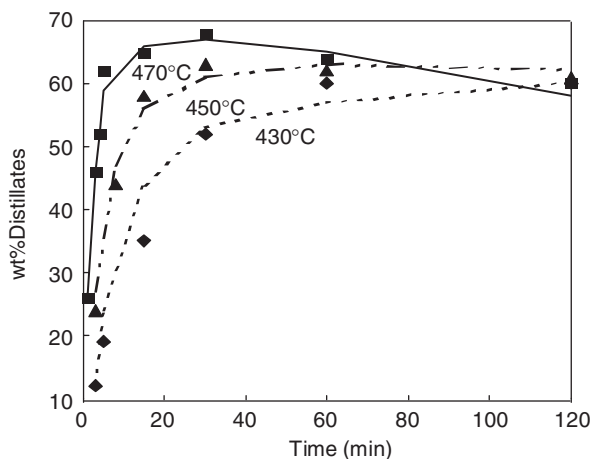


FIG. 35. Distillate yields in a batch lab reactor (Del Bianco *et al.*, 1993). Prediction (line) vs. experimental points.

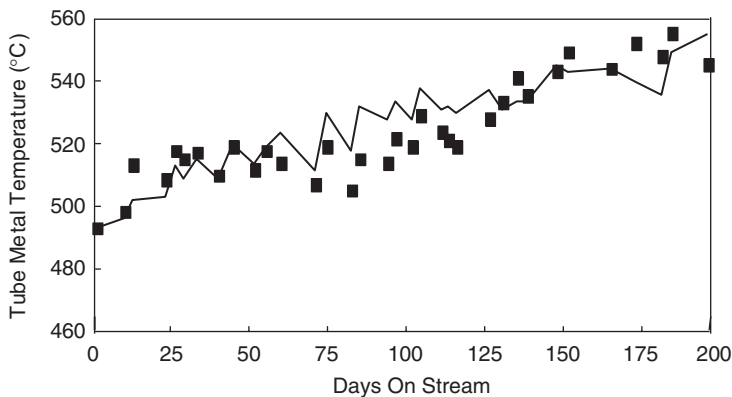


FIG. 36. External tube skin temperature at coil outlet in a visbreaking furnace. Prediction (line) vs. experimental points.

C. THERMAL DEGRADATION OF POLYMERS

Polyvinyl polymers, such as polyethylene (PE), polypropylene (PP), polystyrene (PS) and polyvinyl chloride (PVC), are widely used in packaging and make up the main components of plastic waste in domestic refuse. Gaining a full understanding of their decomposition is therefore of great relevance to the environment. Waste recycling processes are always based on complex chain radical mechanisms taking place in the molten phase. These follow the same kinetic rules already discussed and analysed for visbreaking and delayed coking.

The scientific and technical literature on pyrolysis and gasification of plastics includes several papers, for instance, on PE (Anderson and Freeman, 1961; Miranda *et al.*, 2001; Westerhout *et al.*, 1997) on PP (Gambiroza-Jukic and Cunko, 1992), on PS (Lattimer and Kroenke, 1982; Madorsky, 1952) and on PVC (Bockhorn *et al.*, 1999a; Knumann and Bockhorn, 1994; Miranda *et al.*, 2001). The primary goal of most of these works is the evaluation of the overall rate of weight loss in thermal decomposition (Borchardt and Daniels, 1957; Coats and Redfern, 1964; Flynn and Wall, 1966; Friedman, 1963). The conventional power law model is commonly used for describing the conversion α

$$\frac{d\alpha}{dt} = k_0 \times \exp\left(-\frac{E_{\text{att}}}{RT}\right) \times (1 - \alpha)^n$$

where n is the reaction order and E_{att} and k_0 are the activation energy and the pre exponential factor. The kinetic parameters relating to the same polymer and obtained from different experimental works differ significantly. The frequency factor spans several orders of magnitude whilst the activation energy can span ± 50 kJ/mol; this happens even when considering selected experiments in which transport phenomena limitations are negligible (Westerhout *et al.*, 1997). These differences could be partially linked to either the presence of additives (which can display catalytic activity) or weak bonds in the original polymers. Consequently, a clearer understanding of the degradation process might be gained from a detailed kinetic model.

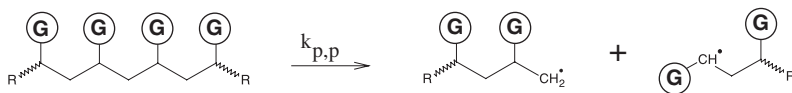
1. Mechanism Considerations

PE, PP and PS in their molten state decompose according to a liquid-phase radical chain mechanism which mainly involves the cleavage of the chain backbone while the side groups are not significantly removed from the polymer structure. Once again, the free chain radical reactions are simply described by the usual sequence of initiation, propagation and termination reactions. The same reaction classes as ever allow the pyrolysis process of the three different polymers to be explained. For the sake of simplicity, we can represent the polymers through a simplified notation in which the “side chain” (**G**) can be either H, CH₃ or phenyl in the case of PE, PP or PS, respectively. An exception must be considered for the specific case of PE in which the side group (**G**) undergoes the same reaction classes shown here for only one hydrogen atom.

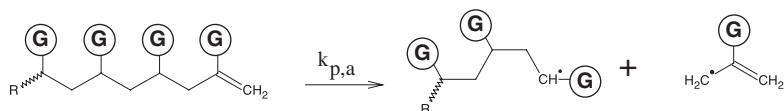
The overall mechanism can be reduced to the usual reaction classes:

1. Initiation reactions, to produce radicals from molecules:

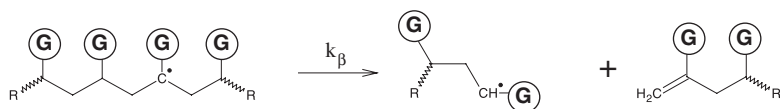
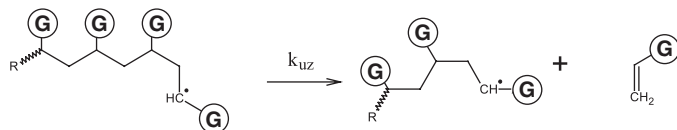
(1A) Random scission of polymer backbone



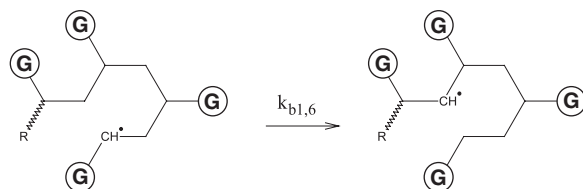
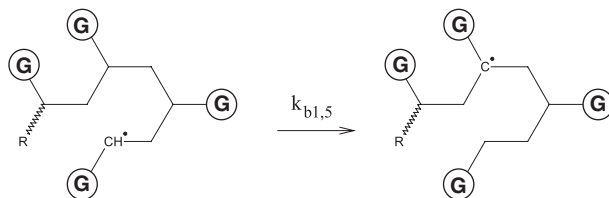
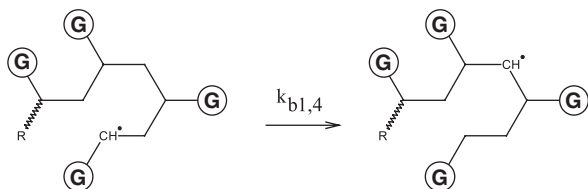
(1B) Terminal scission



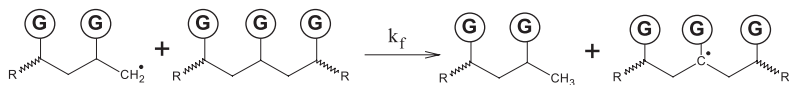
2. Propagation reactions of intermediate radicals:

(2A) β -scission of radicals to form unsaturated molecules and smaller radicals(2B) β -scission in specific position, including unzipping reactions

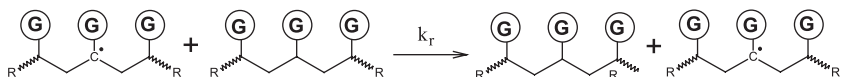
(2C) Alkyl radical isomerization via (1,4), (1,5) and (1,6) H-transfer



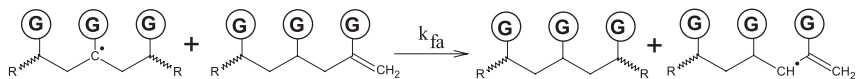
(2D) H-abstraction (metathesis) reaction on the polymer chain due to terminal radicals



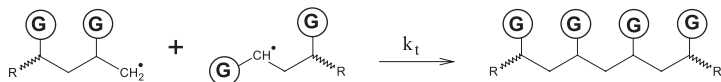
(2E) H-abstraction (metathesis) reaction on the polymer chain due to mid-chain radicals



(2F) H-abstraction (metathesis) reaction on a specific position

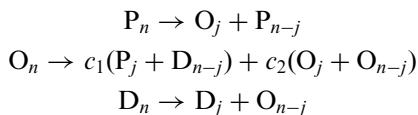


3. Termination by radical recombination reactions



The thermal degradation of PE, PP and PS proceeds with the progressive formation of unsaturations at the end chain of the molecules. Each species in the melt, characterized by molecules or radicals, differs mostly for the type of end and tail unsaturation (Faravelli *et al.*, 1999, 2001, 2003; Ranzi *et al.*, 1997a). Smaller radicals and unsaturated species are formed through β -scission reactions of the radicals produced by H-abstraction reactions.

Thus, alkene backbones can be formed from alkyl radicals or also from unsaturated radicals. Similarly, α - ω dialkene backbone species are produced from parent radicals of heavier alkenes and dialkenes. By using P, O and D respectively to indicate the whole amount of alkane, alkene and α - ω dialkene backbone molecules, the resulting stoichiometry of the process is the following:



where j varies along the carbon chain of total length n . The two constants c_1 and c_2 depend on the presence of resonant position and intramolecular backbiting reactions (Faravelli *et al.*, 1999). The average molecular weight of the melting

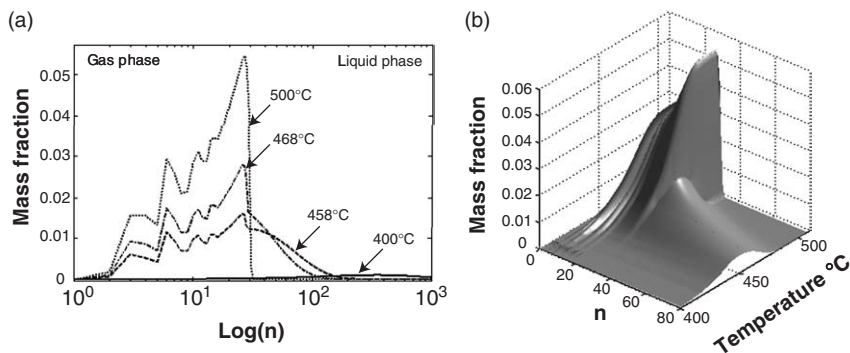


FIG. 37. Simulation of the instantaneous molecular weight distribution of PE during pyrolysis, expressed in term of repeated units n : heating rate $10^\circ\text{C}/\text{min}$, pressure 1 atm. Panel (a) Total mass fraction of chains nearby the border range of evaporable compounds at different temperature levels; panel (b) temperature profiles of components in the gas and the nearest liquid phase.

phase is progressively reduced due to the reiteration of these reactions. Ultimately, light decomposition products evaporate and leave the condensed phase without further reactions (Poutsma, 2003). The increase in the gas phase when the temperature rises and the simultaneous consumption of the melt is clear in the simulations reported in panel a of Fig. 37. Consequently, the gas released is fully described by the surface reported in Fig. 37b. During the thermal degradation process the initial molecular weight distribution (MWD) is affected by the shortening of the polymeric chains and the concentration of molecules close to the evaporation limit drastically increases. It is therefore necessary to consider a gas–liquid equilibrium at the interface and to account for mass balances in the gas and liquid phase. The simple approach considers all the components with boiling points lower than the system temperature as instantaneously entering the gas phase.

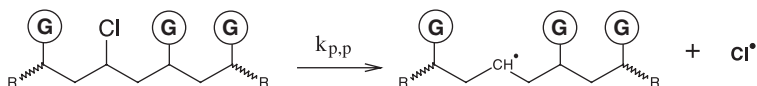
Two additional phenomena contribute to the thermal degradation mechanism and can determine the formation of the relative maximum and minimum in the characteristic surface of the gaseous MWD as shown in Fig. 1. In the backbiting process, the end of polymer chain can also react to form gaseous products with a non-random distribution through a sequence of isomerization and β -scission reactions. Finally, monomer units can also be released by an unzipping process through β -scission of the terminal radicals.

Even though PVC thermal degradation is a free chain radical mechanism in the liquid phase, it partially differs from what observed for PS, PP and PE. In fact, PVC pyrolysis involves the cleavage of the C–Cl bond of the side chain, instead of just decomposing the polymer chain. The result of this process is the formation of a large quantity of double bonds due to successive β -scissions and the formation of poly-aromatic structures as a result of the consequent cross-linking reactions.

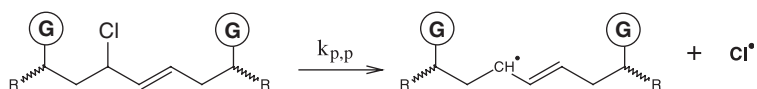
The polymer structures involved in PVC pyrolysis can be represented using the same previously mentioned, simplified notation in which the side chain (**G**) can be either H, Cl or PAH clusters. The free chain radical reactions are simply described by the following reaction classes:

1. Initiation reactions, to form chlorine radical:

(1A) Random scission of C–Cl bonds

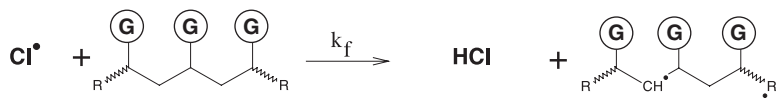


(1B) Specific scission in allyl position

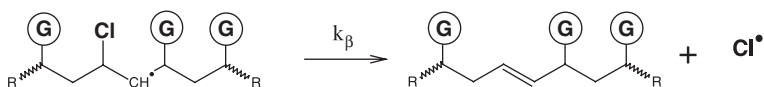


2. Propagation reactions of intermediate radicals:

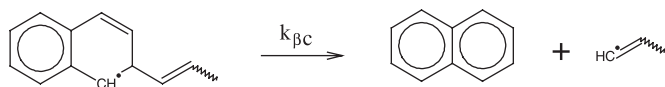
(2A) H-abstraction (metathesis) reaction on the polymer chain, mainly due to chlorine



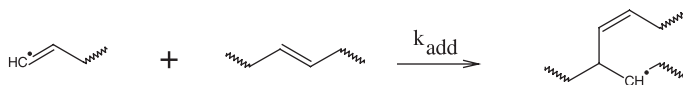
(2B) β -scission of radicals to form double bonds and chlorine radical



(2C) β -scission of radicals forming tar compounds

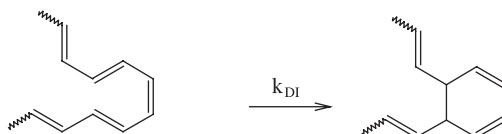


(2D) Radical addition on double bonds

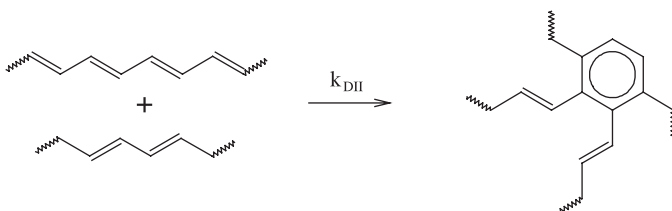


3. Molecular reactions:

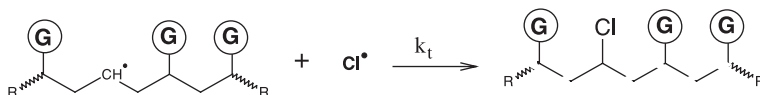
(3A) Intramolecular Diels–Alder



(3B) Intermolecular Diels–Alder



4. Termination or radical recombination reactions.

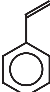
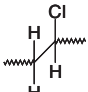
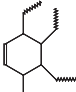
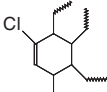
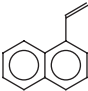
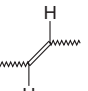
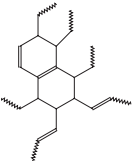
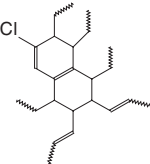
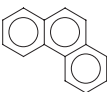
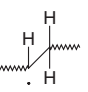
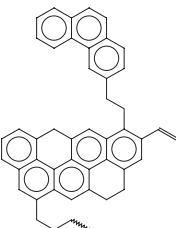
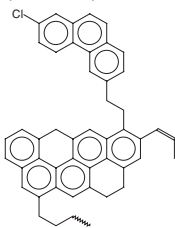
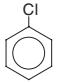
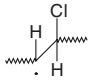
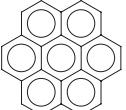
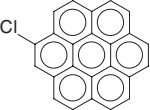


A sequence of H-abstractions due to the very reactive chlorine radical and β -decomposition gives rise to the formation of polyene molecules and HCl which is released from the melting phase. Cross-linking reactions between polyenes lead to alkyl aromatic intermediates which can further decompose, releasing tar compounds and/or can polymerize with char formation. These transformations are experimentally observed as a second weight loss in PVC thermo gravimetric analysis.

This mechanism is more complex with respect to other vinyl polymer ones and demands specific simplifications. One proposed approach carefully analyses all the reactions of the single monomer unit in the polymer chain ([Marongiu *et al.*, 2003](#)). The initial PVC polymer is simply represented by the chlorinated reference unit $\text{P}-(\text{CH}_2\text{CHCl})-\text{P}$. The successive steps of degradation form polyene molecules and these species, which have different molecular weights, are represented by the alkene reference unit: $\text{P}-(\text{CH}=\text{CH})-\text{P}$. The reference species (reported in bold characters in the brackets) are the reacting units and are placed inside the polymer chain, represented here by the P at the beginning and end.

The resulting semi-detailed kinetic mechanism thus consists of real species and a limited number of pseudocomponents (molecules and radicals) which are representative of the whole system. They characterize the typical structures

TABLE XIII
REFERENCE COMPONENTS IN THE KINETIC MODEL OF PYROLYSIS OF PVC

Real species	Linear pseudo species	Aromatic and char pseudo species	
 C_8H_8	 $P-(CH_2CHCl)-P$	 $P-(C_{10}H_{10})-P$	 $P-(C_{10}H_9Cl)-P$
 $C_{12}H_{10}$	 $P-(CH=CH)-P$	 $P-(C_{18}H_{16})-P$	 $P-(C_{18}H_{15}Cl)-P$
 $C_{14}H_{10}$	 $P-(CH_2\bullet CH)-P$	 $P-(C_{47}H_{36})-P$	 $P-(C_{47}H_{35}Cl)-P$
 C_6H_5Cl	 $P-(\bullet CHCHCl)-P$	 CHAR	 CHARC

involved in the different degradation phases in terms of polymer reference pseudospecies, aromatic and char components. Table XIII provides a sample of the different components involved in PVC degradation model.

Intermediate species during the dehydrochlorination phase are other reference units which present either Cl or double bonds in the structure. H or Cl abstractions from these pseudocomponents form the corresponding radicals. Cross-linking reactions between polyene molecules lead to alkyl aromatic intermediates which can further condensate and grow into char. Reference lumped components are then introduced according to the different number of aromatic rings and the possible presence of Cl. The thermal degradation of this and similar polymers is always described on the basis of the same reaction classes, and always with a small set of reference kinetic parameters (Marongiu *et al.*, 2003; Mehl *et al.*, 2004).

Independently of the adopted approach for the mechanism formulation, the estimation of the rate constants for all the reaction classes involved in the pyrolysis process of PE, PP, PS and PVC is of critical importance in model development. As already mentioned, the kinetic parameters of the condensed-phase reactions are directly derived from the rate parameters of the analogous gas-phase reactions, properly corrected to take into account transposition in the liquid phase (e.g., Section II.D).

2. Balance Equations

Mass balance equations are expressed in a very general form:

$$\rho \frac{dy_n}{dt} = \sum_{j=1}^{NRC} v_{n,j} \cdot R_j \cdot W_n$$

where y is the mass fraction and NRC the number of chemical reactions. R_j is the reaction rate of disappearance or formation, $v_{n,j}$ is the corresponding stoichiometric coefficient and W_n the molecular weight of the component. The density ρ is assumed constant during the degradation. The first difficulty in developing the kinetic model for thermal degradation of polymers is to properly simplify the system to reduce and control the overall dimensions.

Three different approaches are briefly discussed here. They refer to the steady state assumption of propagating radicals, the discrete section method and the method of moments.

a. Continuously varying steady state (CVSS). The continuously varying steady state (CVSS) assumption can be conveniently applied to the pyrolysis of PE, PP and PS. The concentration of all the propagating radicals is proportional to that of a lumped single radical R^\bullet .

$$[R^\bullet] = \sqrt{\frac{\sum_i k_{pp,i} [BP]_i}{k_t}}$$

where k_t is the rate constant of self-recombination reaction $R + R$; $k_{pp,i}$ are the rate constants of the different initiation acts; $[BP]_i$ are the total concentrations of backbone reacting positions of alkanes, alkenes and dialkenes.

Because of the lower activation energy of their initiation reactions, the rising concentration of double bonds inside the polymer enhances the radical concentration and favours the pyrolysis process. This radical concentration is then used to evaluate the rate of formation and disappearance of all the species in the system. Thus, the production of the alkene O_j is simply expressed as

$$\frac{d[O_j]}{dt} = k_\beta [R_n^\bullet] = k_\beta \frac{k_r [R^\bullet] [S_n]}{k_f \{H\} + k_\beta} = k_{app} [R^\bullet] [S_n]$$

where k_{app} is the rate constant of the apparent propagation reaction. This is the proper combination of the decomposition (k_β) and abstraction rate constants (k_f and k_r). The total concentration of H-atoms is

$$\{H\} = n_H \frac{\rho}{W_0}$$

where ρ is the density of the polymer, W_0 the molecular weight of the monomer and n_H the number of available H for each monomer unit. Of course, CVSS and the assumption of the single lumped radical results in a significant reduction of the total number of balance equations (Dente *et al.*, 1979; Faravelli *et al.*, 1999, 2001, 2003; Ranzi *et al.*, 1997a).

b. Discrete section method. A further possible reduction of the overall dimension of the problem can be addressed with appropriate lumping procedures (Ebert *et al.*, 1982). This approach is equivalent to the discrete sectional model, which has been widely adopted in particle distribution research for many years and already discussed in the soot formation paragraph (Gelbard *et al.*, 1980; Wulkow, 1996). The method approximates the MWD of polymer molecules by a finite number of sections or lumped components, typically called BINs, which represent groups of species. By dividing the entire MWD into sections and dealing only with a representative pseudospecies inside each section, the number of conservation equations is reduced to the number of sections.

Using a finite element type formulation, the concentration of the discretized element B_i is

$$B_i = \sum_{n=n_{i,\min}}^{n_{i,\max}} S_n$$

where S_n is the molar concentration of each molecule in the section between $n_{i,\min}$ and $n_{i,\max}$. Below $n_{1,\min}$ no clustering is introduced and each real species is taken into account. The lumped pseudospecies can be either equispaced or spaced linearly in $\ln(n)$, separated by a constant factor Δ : the exponential sectional approach saves on computation time whilst still maintaining a good description of the low molecular weight components.

During polymer decomposition, whenever a species is formed with a molecular weight not equal to that of a pseudocomponent, its amount is linearly distributed between the adjacent bins (B_i, B_{i+1}). This lumping procedure or discrete section method was successfully applied to the thermal degradation of PS (Faravelli *et al.*, 2001).

c. Method of moments. The method of moments is a very effective mathematical tool when it comes to dealing with the complexity of regular systems. In fact, the MWD of different families of species can be conveniently described by

a continuous expression (Frenklach *et al.*, 1984). Moment equations describe the time evolution of the statistical parameters characteristic of the MWD of molecules and radicals in the liquid and gas phases. The zero-order moment represents the molar concentration, the first and second moments stand for the average MW and its variance (Abramowitz and Stegun, 1968). This method involves a small number of equations and drastically reduces the computing times for the solution of the problem. McCoy and co-workers have extensively applied the method of moments and developed various models with different mechanistic details (Madras and McCoy, 2002; Madras *et al.*, 1996; McCoy and Wang, 1994). Kruse and Broadbelt apply the method of moments to the thermal degradation of PS, PP and their binary mixture (Kruse *et al.*, 2002, 2003, 2005).

The polymer species in the liquid phase span from L to N_{\max} , where L represents the minimum number of units for species in the liquid phase and N_{\max} is the corresponding maximum, thereby limiting the mass MWD to 99.9%. Monomers and oligomers up to $L-1$ units are in the gas phase. Frenklach (1985) and Bockhorn (1999b) assume the following definition of statistical moments of the size distribution of the polymer species:

$${}^k\mu_{P,l} = \sum_{n=L}^{N_{\max}} n^k \cdot P_n$$

The left superscript k denotes the order of moment, the right subscript represents the family of the different species (alkanes, alkenes, ...); l indicates the liquid phase and n is the number of repeated units. The distribution of volatile species is defined as follows:

$${}^k\mu_{P,v} = \sum_{n=1}^{L-1} n^k \cdot P_n$$

where subscript v denotes the gas phase. Moment equations properly describe all the typical reactions involved in the thermal degradation process of the different polymers. The kinetic expression ruling the moment variation can be calculated for each reaction class, starting from the molar balances of the different species. This formulation of the system permits a mechanistic identification and description of the thermal decomposition of polymers in both isothermal and non-isothermal pyrolysis, where L changes with the time (Marongiu, 2006).

To deduce the moment equations, the balance equations of the different species must be summed up to group the contributions of the different reaction classes. The overall contribution kR_j for each reaction class to the different moment equations, k , is simply analytically calculated with the proper sum of all the corresponding terms for the liquid and the vapour phase:

$${}^kR_{j,l} = \sum_{n=L}^{N_{\max}} n^k \cdot v_{n,j} \cdot R_j \quad {}^kR_{j,v} = \sum_{n=1}^{L-1} n^k \cdot v_{n,j} \cdot R_j$$

The following system of differential equations is obtained by considering all the reaction classes and families of species in the kinetic scheme:

$$\frac{d^k \mu_{i,l}}{dt} = \sum_{j=1}^{NRC} v_{i,j} \cdot {}^k R_{j,l} \quad i = 1, \dots, NSP$$

$$\frac{d^k \mu_{i,v}}{dt} = \sum_{j=1}^{NRC} v_{i,j} \cdot {}^k R_{j,v} \quad i = 1, \dots, NSP$$

where NRC is the total number of reactions, $v_{i,j}$ the stoichiometric coefficient and NSP the number of families of species.

3. Model Validation and Comparisons with Experimental Data

A few comparisons between experimental measurements and model predictions are reported to show the reliability of the different models, to investigate the relative reactivity of the different polymers and, finally, to allow a brief discussion of the different numerical approaches.

Figure 38 shows the comparisons of model predictions and experimental measurements of thermal decomposition of PS (panel a), PP (panel b) and PE (panel c). These experiments refer to three dynamic TGA's with different heating rates (Anderson and Freeman, 1961; Ranzi *et al.*, 1997a). The agreement between model predictions and experimental data is quite good. Figure 38a shows the dynamic thermal degradation of PS under vacuum 1 mmHg and heating rate 5°C/min. Thermal decomposition proceeds with a single step and the mass loss is due to the evaporation of small fragments of the polymer (monomers, dimers and trimers). Of course, for all the polymers, the shortening of the polymer chain requires the formation of double bonds before the initial weight loss. The behaviour of the three different degradation curves in Fig. 38 confirms the relative reactivity of the three polymers: PS > PP > PE, as expected from thermo kinetic analysis of the polymers structures.

As already mentioned, different modelling approaches were applied; (a) the complete system of balance equations of all the species with QSSA for the single propagating radical; (b) discrete section method; (c) the method of moment. These comparisons demonstrate the equivalence between these techniques, not only with respect to total mass loss, but also in terms of intermediate liquid components (alkanes, alkenes and α - ω dialkenes).

Figure 39 presents the characteristic three phases of PVC decomposition very clearly. The initial dehydrochlorination reactions form HCl and polyene structures. During this phase, benzene and some naphthalene and phenanthrene are also formed through Diels–Alder reactions and the successive dealkylation of polyene molecules. Then, when Cl has been quantitatively released

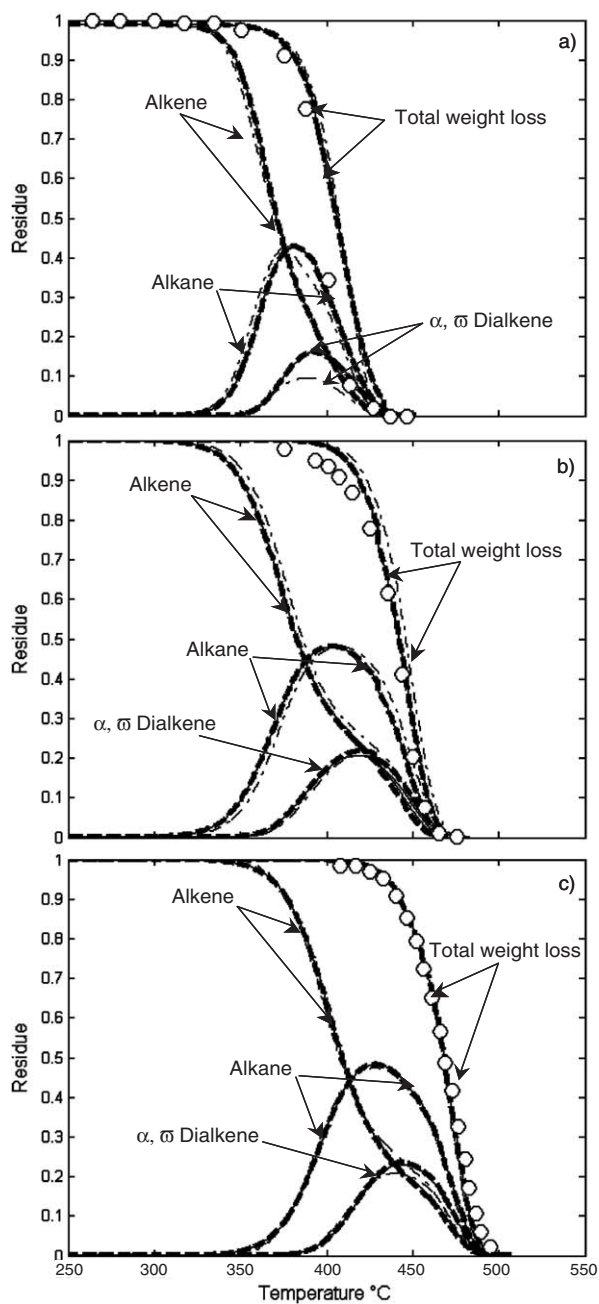


FIG. 38. Total weight loss and main species in the liquid phase during dynamic thermal decomposition. (a) Pyrolysis of polystyrene (Anderson and Freeman, 1961) (5°C/min, 1 mmHg). (b) Thermal decomposition of polypropylene (Ranzi *et al.*, 1997a) (10°C/min, 1 atm). (c) Pyrolysis of polyethylene (Ranzi *et al.*, 1997a) (10°C/min, 1 atm). Discrete model (Dashed) and Moment model (—).

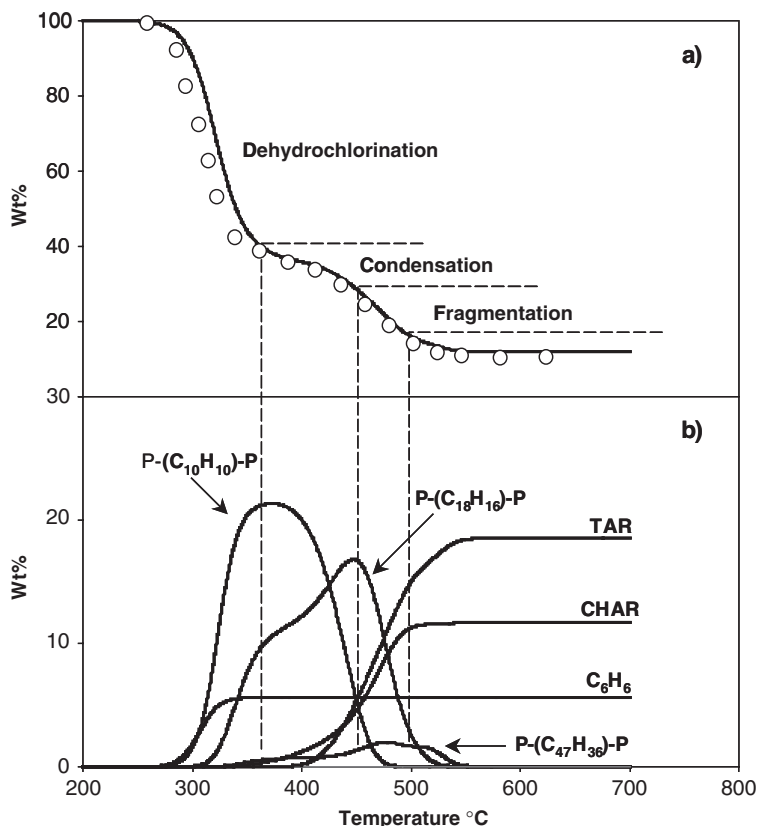


FIG. 39. Predicted dynamic TGA of PVC with an heating rate of 10°C/min, experimental data (Marks) (Montaudo and Puglisi, 1991). Panel (a) Residue (%wt) behaviour and identification of the main thermal decomposition phases. Panel (b) Benzene, PAH and char formation profiles. The TAR fraction represents the total amount of volatile aromatics.

from the melt, the polyene molecules rearrange and, through cyclization and cross-linking reactions, form alkyl aromatic hydrocarbons and char residues. The model agrees quite well with the experiments in all the different phases. Similar agreement can be found for different heating rates (Marongiu *et al.*, 2003).

As a final consideration, it is relevant to discuss the behaviour of mixtures of different plastics. In fact, one possible process for recovering valuable chemical and petrochemical products from plastic waste is the stepwise thermal degradation of polymer mixtures. This potentially allows the step-by-step simultaneous separation of the different fractions generated by the polymers of the blend. The effect of the mixing scale of PE and PS and their interactions in the melt on the basis of several hypotheses was recently investigated (Faravelli *et al.*, 2003). The first and simplest approach was a completely segregated model which

directly combines the results from pure plastics. The opposite solution is a completely mixed model assuming a single melt phase with a homogeneous and perfectly mixed composition. Neither of these asymptotic models is correct because it is necessary to refer to the real solubility, miscibility and mass-transfer among the polymers, even though a completely segregated model is a reasonable approximation which allows easy extension to more complex mixtures.

V. Conclusions

The kinetic aspect common to all the topics discussed in this chapter is the pyrolysis reactions. The same kinetic approach and similar lumping techniques are conveniently applied moving from the simpler system of ethane dehydrogenation to produce ethylene, up to the coke formation in delayed coking processes or to soot formation in combustion environments. The principles of reliable kinetic models are then presented to simulate pyrolysis of hydrocarbon mixtures in gas and condensed phase. The thermal degradation of plastics is a further example of these kinetic schemes. Furthermore, mechanistic models are also available for the formation and progressive evolution of both carbon deposits in pyrolysis units and soot particles in diffusion flames.

Detailed kinetic schemes also consist of several hundreds of species involved in thousands of reactions. Once efficient tools for handling the correspondingly large numerical systems are available, the extension of existing kinetic models to handle heavier and new species becomes quite a viable task. The definition of the core mechanism always remains the most difficult and fundamental step. Thus, the interactions of small unsaturated species with stable radicals are critical for the proper characterization of conversion and selectivity in pyrolysis processes. Parallel to this, the classification of the different primary reactions involved in the scheme, the definition of their intrinsic kinetic parameters, the automatic generation of the detailed primary reactions and the proper simplification rules are the important steps in the successive extension of the core mechanism. These assumptions are more relevant when the interest lies in the pyrolysis of hydrocarbon mixtures, such as naphtha, gasoil and heavy residue, where a huge number of isomers are involved as reactant, intermediate and final products. Proper rules for feedstock characterizations are then required for a detailed kinetic analysis.

Due to the complexity of these kinetic schemes, an accurate model validation must always refer to different experimental devices and to the widest possible range of operating conditions and feed varieties.

In spite of the different models present in the technical literature and discussed here to some extent, not all the problems have been solved yet and much theoretical and experimental work still remains to be done. New experimental data will allow further improvements in the kinetic assumptions or suggest new

hypotheses for a deeper understanding of the detailed chemistry of pyrolysis and fouling processes.

LIST OF SYMBOLS

A	matrix of the stoichiometric coefficients
B_i	concentration of the discretized element i
$[BP]_i$	total concentrations of backbone reacting positions of alkanes, alkenes and dialkenes
C_{AS}	concentration of radical A in liquid phase S
D_{AS}	diffusivity of radical A in liquid phase S
D_j	set of decomposition reactions
E_{ATT}	activation energy
f	total molar fraction of the liquid phase containing from n_{CMIN} to n_C carbon atoms
$F(n_C)$	correction of activation energy
h	Planck constant
$\Delta H^\#$	molar enthalpy variation in the transition state
ΔH_{ev}	molar heat of vaporization of liquid or polymer unit of flow
k	kinetic constant
k_0	frequency factor
k_{coll}	collision constant
K	Boltzmann constant
I_j	set of isomerization reactions involving radical j
n_C	number of carbon atoms
$n_{CMIN},$ $n_{C,AV}$	minimum and average number of carbon atoms
O_j	olefin concentration
P_j	concentration of reacting position into the deposit layer
\dot{P}_j	total production rate of the component j
\dot{P}_0	vector of the initial production rate
r_A	distance among atoms in A + A recombination
R	gas constant
R_j	set of decomposition reactions forming the j th product
S_n	molar concentration of molecules pertaining to section n
$\Delta S^\#$	molar entropy variation in the transition state
T	absolute temperature
\tilde{V}_s	molar volume of liquid or polymer unit of flow
V_{coll}	collision rate per unit volume and time in liquid phase
X_i	molar concentration of the radical i
\vec{X}	vector of the radical concentration
y_n	mass fraction of component n

Z_i	concentration of the radical decomposed in the reaction i th
W_0	molar mass of the monomer unit
W_n	molecular weight of the n component
W_S	molar mass of the liquid or of the unit of flow
α	conversion in polymer degradation
ϕ_{AA}	orientation factor
$v_{n,j}$	stoichiometric coefficient of component n in reaction j
μ_S	viscosity of the liquid S
$\mu_{p,l}^k$	k moment of polymer distribution in the liquid phase
$\mu_{p,v}^k$	k moment of polymer distribution in the vapour phase
ρ	polymer density

Appendix 1. MAMA Program: Automatic Generation of Primary Lumped Reactions

The aim of this mechanism generator is to evaluate the set and weights of the end products obtained by the decomposition of a large, heavy radical. Starting with an initial radical, the propagation path includes isomerization and decomposition/dehydrogenation reactions with the formation of final products. The assumptions made in the generation of the primary propagation mechanism correspondingly define the structure of the algebraic system, which once solved, gives the distribution of the primary decomposition products. This subject will be dealt with first in the next paragraph. Due to the large number of components that can be involved in a propagation path, the concept of lumping of components as well as the classes of components which need to be lumped, will be then discussed.

The generation of a propagation path requires computing time which rapidly increases with the carbon number of the initial radical. However, the resulting generated pathway of a specific radical is independent from the formation mechanism of the radical itself, and therefore there is a clear need to save the path in a database. The description of the database structure will include details on the molecule representation as well as on the way the reaction path is stored and recorded. Finally, before the functioning of the MAMA Generator is summarized, the algorithm for molecule homomorphism will be described in brief.

A.1. EVALUATION OF END-PRODUCT COMPOSITION

The automatic generation of the primary product distributions is based on the assumption that the propagation reactions of radicals are described with an autonomous system, i.e. H-abstraction, radical addition and termination

reactions and any interactions of the intermediate radicals with the reacting mixture are disregarded. Consequently, the end products of this propagation mechanism are small radicals and unsaturated components (UC). The total production rate \dot{P}_j of the j th product is simply expressed in the form:

$$\dot{P}_j = \sum_{i \in R_j} k_{i,j}^D Z_i + \dot{P}_{j0} \quad (\text{A.1})$$

where \dot{P}_{j0} is the initial production rate of the j th component j (normally = 0 for end products), $k_{i,j}^D$ is the production rate in the i th reaction, Z_i is the concentration of the radical decomposed in the reaction i , and R_j is the set of decomposition reactions forming the j th product. For all the intermediate radical components, assuming quasi-steady conditions, mass balance equations are written in the form:

$$X_j \left(\sum_{i \in I_j} k_{j,i}^I + \sum_{i \in D_j} k_{j,i}^D \right) = \sum_{i \in I_j} k_{i,j}^I \cdot X_i + \dot{P}_j \quad (\text{A.2})$$

where X_j = concentration of the j th component; I_j = set of isomerization reactions involving the j th radical component; D_j = set of decomposition reactions involving the j th radical component; $k_{j,i}^I$ = isomerization rate constant of the j th radical component to form the i th radical component; $k_{i,j}^I$ = isomerization rate constant of the i th radical component to form the j th radical component; $k_{j,i}^D$ = decomposition rate constant of the j th radical component in the reaction i ; \dot{P}_j = total production rate of the j th radical component as described in Eq. (A.1), with $Z \in X$.

The left side of Eq. (A.2) represents the depletion of j th component due to its isomerization and decomposition. The right side is the formation contribution to j th component coming both from the isomerization of i th radical and from the decomposition of larger radicals.

At fixed temperature, the material balances turn into a system of linear equations in radical concentrations.

$$\overline{A} \vec{X} - \vec{P}_0 = 0 \quad (\text{A.3})$$

where \overline{A} is the coefficient matrix (size n,n), \vec{X} the vector of radical concentrations (size n), \vec{P}_0 the vector of the initial production rates (size n), n the number of the intermediate radical components.

It is worth to notice the following properties of this linear system:

- The size of the system rapidly increases with the carbon number of the initial radical, reaching values of several hundred thousands when studying the primary propagation path of unsaturated components, such as alkenes and cyclo-alkanes with more than 14–15 carbon atoms,

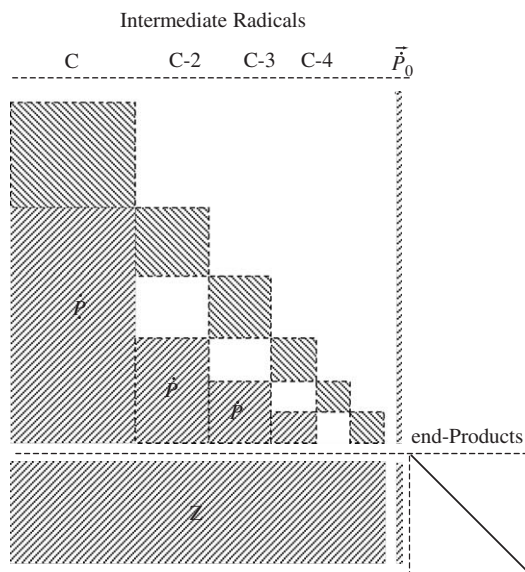


FIG. A1. Structure of the system (3) with end-product production rate.

- The system is dominantly sparse with a few tens of unknowns in each Eq. (A.2),
- The overall system may be decomposed into subsystems of reduced size as shown in Fig. A1.

Once the linear system is solved and the intermediate radical concentrations are known, the end product distribution (Eq. (A.1)) is directly obtained.

The upper part of Fig. A1 shows the structure of the system (3) while the set of Eq. (A.1) giving the total production of end products, is in the lower part. As previously mentioned, the two portions are solved disjointed, in sequence with the upper portion followed by the lower one.

In the system (3), the unknowns are ordered according by decreasing carbon number C . It should be stressed that a radical with C_n carbon atoms can only decompose generating radicals with C_{n-2} , C_{n-3} , ... carbon atoms. In fact, β -decomposition does not allow the formation of a radical with C_{n-1} carbon atoms. This explains the presence of empty blocks in the structure of the system. The equations are ordered by decreasing carbon number too. The resulting structure of the system in Fig. A1 suggests the most effective solution. By its nature, the block including the equations with the highest carbon number does not contain any production term (see Eq. (A.1)) except the initial values \dot{P}_{j0} , i.e. the set of decomposition reactions R_j is empty. This block can be solved and the calculated values of the unknowns factorize the vertical band " \dot{P} ". " \dot{P} " contains the production terms of smaller radicals. The factorization renders as known all the production terms of the successive block with the highest C

number. This block is solved and the results allow the factorization of the related vertical band. This procedure is then repeated until the end of the system. Finally, the production of the end products is easily calculated as all the related unknowns are available courtesy of the previous system solutions.

One important aspect derives from the initial assumption made: each radical evolves without interacting with the surrounding environment. In other words, the decomposition reactions are considered irreversible which results in the linearity of the algebraic system: the end product composition of an initial radical is not dependent on the initial composition of any other intermediate radical.

In fact if $X_j(.., \dot{P}_{j0}, ..)$ and $X_i(.., \dot{P}_{i0}, ..)$ stand for the solution vectors of the above system (3) for a null vector \dot{P}_0 except, respectively, for the initial production rates of components j and i , a trivial property of linear systems gives

$$X_{j,i}(... \dot{P}_{i0}, .. \dot{P}_{j0} ..) = X_i(.., \dot{P}_{i0}, ..) + X_j(.., \dot{P}_{j0}, ..)$$

This property applied to the problem at hand turns into the statement that, given a mixture of initial radicals at $\dot{P}_{10}, \dot{P}_{20}, \dots \dot{P}_{R0}$, their product distribution is equal to the sum of the distributions of each single radical. The advantage of this result is that the product distributions of each radical can be considered to be independent of the mixture it belongs to, such as, for example, the initiation reactions which generated it. This fact anticipates an item relevant to the invariance of the propagation paths in the face of the problem in which they are included. The propagation paths are built once for all and stored in a database and they are ready to be analysed for any class of problems that requires them.

A.2. LUMPING OF COMPONENTS

The evaluation of the end product composition in a propagation chain may require the solution of linear systems involving a large number of unknowns referring to the concentrations of intermediate radicals. The number of end products may be so large that they are almost of the same magnitude.

Figure A2 shows the number of components involved in the primary propagation reactions of normal alkenes. These data clearly indicate that this number rapidly becomes very large, increasing the carbon number of the initial alkene. This fact justifies the need to turn to the component lumping when dealing with detailed and mechanistic models describing the hydrocarbons pyrolysis of such heavy species.

However, the following conclusions may help to make the solution of this complex problem more viable:

- The amount of alkenes and unsaturated components in the end products is large and strongly suggests the introduction of lumping of components, as it will be described below.

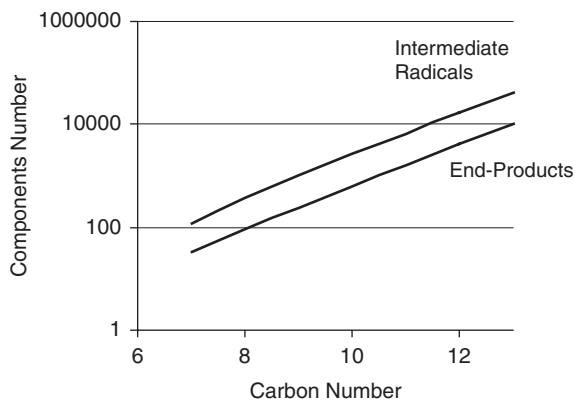


FIG. A2. Components number in the primary propagation reactions of normal-alkenes.

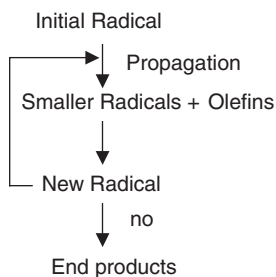


FIG. A3. Schematic propagation reaction chain of radical decomposition and formation of end products.

- As the end products consist of an initial radical not dependent on the initial composition of any other intermediate radical, the simplification and lumping procedures will not refer to such components.
- The amount of small and stabilized radicals in the end products is rather limited compared to the amount of the remaining components so that the lumping might be avoided for this class or applied to a small portion of it.

If just a single radical is considered (see Fig. A3), propagation reactions produce a smaller and/or stabilized radical and an olefin and/or UC. Each new radical is then processed according to its primary propagation reactions (isomerization and decomposition) which results in the production of new olefin or UC and a smaller radical. The olefins produced define the whole set of components involved in this chain so that the lumping technique conveniently applies only to them.

The grouping or lumping of components does not refer to unique rules, but it is only dependent on the successive uses of the kinetic scheme. Consequently,

the Automatic Generator does not contain any lumping rule. Nevertheless, the resulting final products may be conveniently lumped according to pre-assigned rules.

A.3. DATABASE STRUCTURE

As already anticipated, a key feature of the automatic generator is a database storing the propagation paths of initial radicals. The choice of which radical has to be considered is dependent, as mentioned above, on the mathematical model (say steam cracker simulator) which will include the generator results. Provided that all the possible isomers of hydrocarbons up to six carbon number are limited to few hundred, it can be assumed that the database already stores the propagation paths of all the radicals included in this set. This means that the propagation path of a C7 hydrocarbon will produce new isomerization reactions and products with seven carbon atoms while the remaining reactions and products with a lower number of C-atoms are already present in the existing database (so that there is no need to further describe them). Thus the database is enlarged to contain only the new portion created by this component, as it shown in Fig. A4.

It will take some effort to enlarge the database to include all the possible isomers with seven carbon number as the isomers are still acceptably limited in their number. However, this becomes rather difficult and practically impossible with higher carbon numbers due to the rapid increase of the involved isomers set. A compromise is therefore required between the comprehensiveness and the size of the whole database.

Within the context of a steam cracker simulator, experience has shown that the accumulation of propagation paths in the database by starting with mixture of radicals obtained by H-abstraction reactions of normal paraffins and normal olefins (with progressively increased carbon number), produces a whole

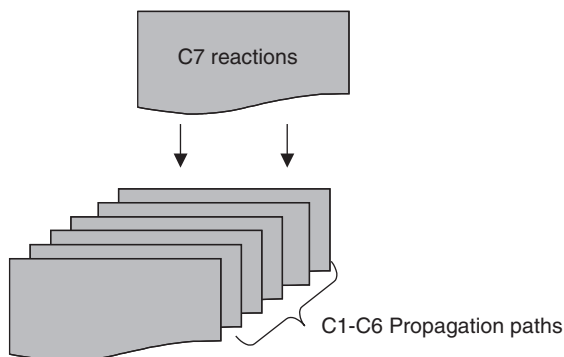


FIG. A4. Sketch of the accumulation of new portions in the database.

information set which covers the description of a good percentage of components present in the kinetic scheme. The rationale for this comes from the fact that isomerization reactions produce (via successive ring formation) and then break a set of isomers of alkenyl and *cyclo*-alkyl radicals which is close to the complete theoretical one. Dehydrogenation reactions therefore increase the total number of end products with a definite finger print of all the intermediate radicals.

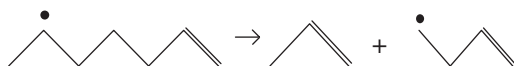
The computing time required to create reaction paths is similar to that reported in Fig. A2: only few seconds are required for radicals with carbon atoms lower than five to six while almost a week is needed for olefins with carbon number larger than 16.

Because of the rapid increase in components and the consequent practical problem of storing all the data in an efficient way, it is also worth mentioning the technique adopted for this purpose.

As the propagation path is a sequence of reactions steps, the basic elements for the description of the whole path are those ones which can describe a single reaction:

- Description of the components molecular structure
- Indication of the products and related reactions associated with the component.

For instance, the decomposition reaction of 6-hepten-2-yl radical



is characterized by the description of the molecular structures of the three components, the type of the reaction and the distinction between the reactant and the products.

As the components are normally involved in several different reactions, it is more convenient to collect all the component descriptions in a list, and to address their position in that list.

Similarly, the reactions too may be grouped in a proper list.

Figure A5 provides an example of a possible presentation of the cited reaction as a sequence of addresses:

k (reactant), **i** (olefin product if any), **j** (radical) and **n** (reaction type).

The molecule description is based on a sequence of integers. In fact, in dealing with hydrocarbons the molecule is univocally characterized by the carbon-carbon bonds and the type of the carbons. For example, Table A1 reports the assumed correspondence between integer indexes and carbon types: they are used to represent a molecule, in a plane, as a sequence of integers.

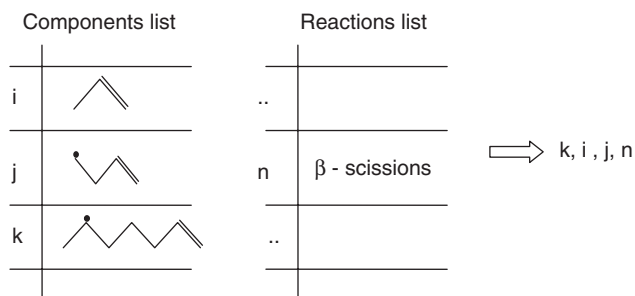
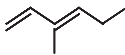


FIG. A5. Schematic structure of elements describing a reaction step.

TABLE A1

MOLECULE DESCRIPTION. CORRESPONDENCE BETWEEN INTEGER NUMBERS AND CARBON TYPES

 \rightarrow			21	22	23	22	2	1
			1					
1 \rightarrow C —	21 \rightarrow C =	31 \rightarrow C \equiv						
2 \rightarrow — C —	22 \rightarrow — C =	32 \rightarrow — C \equiv						
3 \rightarrow — C — 	23 \rightarrow — C = 	42 \rightarrow = C =						
4 \rightarrow — C — 								

Similarly, *cyclo*-alkane with five- or six- membered rings too may be put into correspondence with integers which contain information about the ring members and their connections to the molecule chain.

It is worth to noting that in this type of molecule representation, there is no need to specify the connections between C- and H-atoms any further ([Wauters and Marin 2001](#)).

A.4. MOLECULE HOMOMORPHISM ALGORITHM

Molecule homomorphism is a non-ambiguous and effective statement whether two molecule descriptions refer to the same product or not. The importance of, or rather, the necessity for such a statement is obvious. In a certain sense, it is the key statement on which the Automatic Generator is based. Inability to recognize identical structure may cause unnecessary calculations at the best of times but more commonly will lead to infinite loops of calculations.

The molecule homomorphism is based on a “branch and chain” algorithm. A branch is a linear portion (including rings), which is connected to the molecule

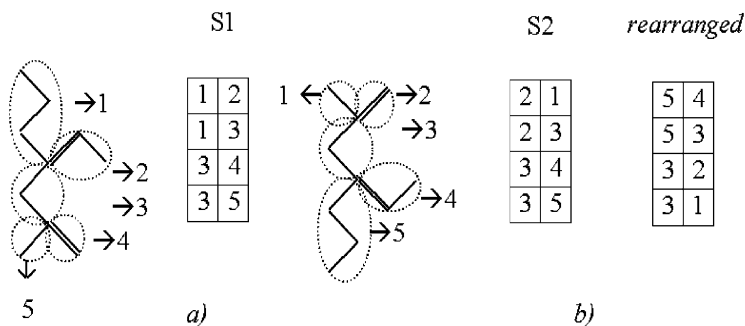


FIG. A6. (a) Molecule divided into branches and substitution matrix; (b) initial substitution matrix $S2$ of an equal molecule, and its content after rearrangement.

chain at its ends. A molecule is then divided into branches (see Fig. A6a). Due to its linearity, it is assumed that the branch homomorphism, i.e. the statement about two branches are identical, is a trivial problem. In fact, the two branches are checked for their length and position of possible unsaturated bonds. The molecule is represented as a graph whose nodes are the branches. The molecule homomorphism is then transformed into a graph homomorphism. Despite many algorithms present in literature, the one used by Steward (1965) for the definition of an admissible output set of an algebraic system of equations may be slightly modified to solve the problem at hand. For low interconnected graphs, substitution matrixes are an efficient method of representation (Fig. A6a). The homomorphism of two graphs analyses their representation with the matrixes $S1$ and $S2$ which start at the first row and column with a branch-edge, i.e. one of the two extreme points of a branch which is not connected to any other branch. While $S1$ description remains fixed, $S2$ is rearranged from top to bottom with the aim of creating a chain equal to $S2$ (Fig. A6b). The rearrangement involves an exhaustive analysis of all the possible chains obtained by connecting each branch of $S2$ with admissible branches, i.e. those which are equal to the corresponding one in $S1$.

A.5. SCHEMATIC FUNCTIONALITY OF THE KINETIC GENERATOR

The kinetic generator's functionality is based on three elements with three different functions (see Fig. A7).

- A pre-processor which prepares the kinetic data and the initial radical mixture according to specified user requirements (Initiation reactions, addition, ... etc.)
- The main processor that analyses each single radical of the mixture with the aim of calculating the composition of the end products. In the case of a

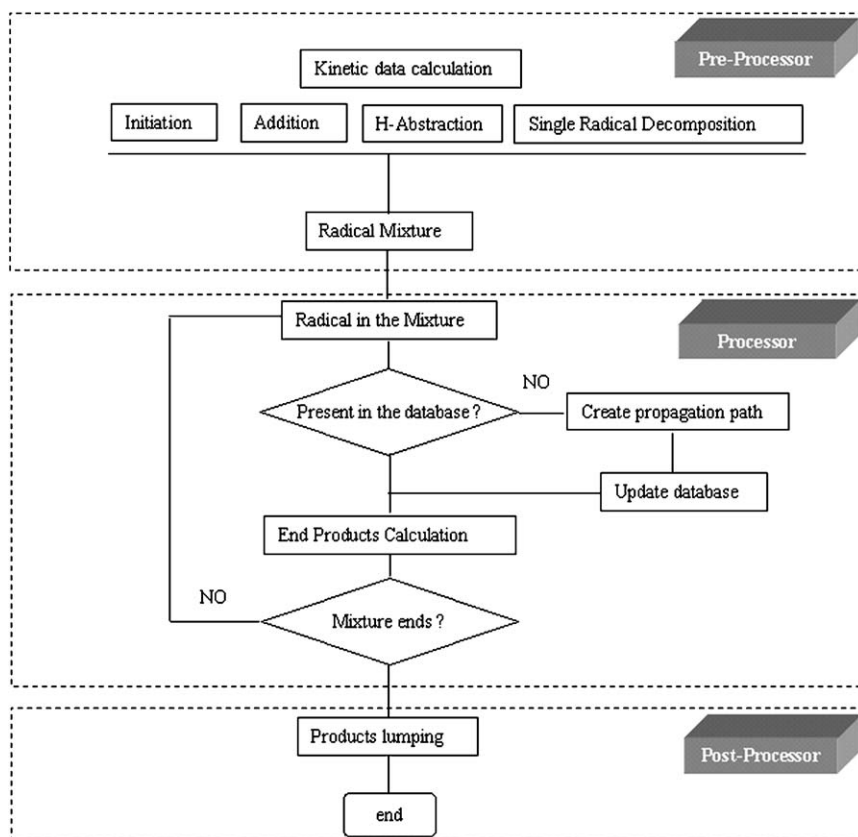


FIG. A7. Schematic functionality of the kinetic generator.

radical not present in the database, the propagation path of the radical is created for the portion not present in the database which is then updated with these new data.

- Lastly, a post-processor lumps the end products according with pre-assigned rules specified by the user.

REFERENCES

- Aalund, L. *Oil Gas J.* **29**(March), 98–122 (1976a).
 Aalund, L. *Oil Gas J.* **26**(April), 112–126 (1976b).
 Abramowitz, M., and Stegun, I. A., “Handbook of Mathematical Functions with Formulas, Graphs, and Mathematical Tables”. Dover Publications, New York, Chapter 26 (1968).
 Albright, L. F. *Ind. Eng. Chem. Res.* **41**, 6210–6212 (2002).

- Albright, L. F., and Marek, J. C. *Ind. Eng. Chem. Res.* **27**, 751–755 (1988).
- Albright, L. F., and Marek, J. C. *Ind. Eng. Chem. Res.* **31**, 14–20 (1992).
- Albright, L. F., McConnell, C. F., and Welther, K., in “Thermal Hydrocarbon Chemistry ACS 183” (A. G. Oblad, H. G. Davis, and R. T. Eddinger, Eds.), Chap. 10, pp. 175–191 (1979).
- Alfè, M., Apicella, B., Barbella, R., Ciajolo, A., Kennedy, L., Merchan-Merchan, W., Rouzaud, J. N., and Tregrossi, A. Proceedings of Italian Combustion Meeting, Napoli III-7, (2005).
- Ali, M. F., Hasan, M. U., Bukharl, A. M., Saleem, M. *Hydrocarb. Process.* February, 83–86 (1985).
- Altgelt, K. H., and Boduszynski, M. M., “Composition and Analysis of Heavy Petroleum Fractions”. Marcel Dekker, Inc, New York (1994).
- Anderson, D. A., and Freeman, E. S. *J. Polymer Sci.* **54**, 253 (1961).
- Appel, J., Bockhorn, H., and Frenklach, M. *Combust. Flame* **21**, 122–136 (2000).
- Bach, G., Zimmermann, G., Kopinke, F. D., Barendregt, D., Oosterkamp, P. V. D., and Woerde, H. *Ind. Eng. Chem. Res.* **34**, 1132 (1995).
- Balthasar, M., and Frenklach, M. *Combust. Flame* **140**, 130–145 (2005).
- Barendregt, S., Dente, M., Ranzi, E., and Duim, F. *Oil Gas J.* **6**(April) (1981).
- Battin-Leclerc, F., Fournet, R., Glaude, P. A., Judenherc, B., Warth, V., Come, G. M., and Scacchi, G. *P. Combust. Inst.* **28**, 1597–1605 (2000).
- Baulch, D. L., Cobos, C. J., Cox, R. A., Esser, C., Frank, P., Just, T., Kerr, J. A., Pilling, M. J., Troe, J., Walker, R. W., and Warnatz, J. *J. Phys. Chem. Ref. Data* **21**, 411–429 (1992).
- Baulch, D. L., Cobos, C. J., Cox, R. A., Frank, P., Hayman, G., Just, T., Kerr, J. A., Murrells, T., Pilling, M. J., Troe, J., Walker, R. W., and Warnatz, J. *J. Phys. Chem. Ref. Data* **23**, 847–1033 (1994).
- Benson, S. W., “The Foundations of Chemical Kinetics”. McGraw-Hill, New York (1960).
- Benson, S. W., “Thermochemical Kinetics”. 2nd ed. Wiley, New York (1976).
- Blaikley, D. C. W., and Jorgensen, N. *Catal. Today* **7**, 227 (1990).
- Blurock, E. S. *J. Chem. Inf. Comput. Sci.* **44**, 1336–1347 (2004).
- Bockhorn, H., “Soot Formation in Combustion”. Springer-Verlag, Berlin (1994).
- Bockhorn, H., Hornung, A., and Hornung, U. *J. Anal. Appl. Pyrolysis* **50**, 77–101 (1999a).
- Bockhorn, H., Hornung, A., Hornung, U., and Jakobstroer, P. *J. Anal. Appl. Pyrolysis* **49**, 53–74 (1999b).
- Borchardt, H. J., and Daniels, F. *J. Am. Chem. Soc.* **79**, 41 (1957).
- Bowman, C. T. *Combust. Flame* **25**, 343–354 (1975).
- Bozzano, G., and Dente, M. ESCAPE 15-Barcelona (2005).
- Bozzano, G., Dente, M., and Carlucci, F. *Comput. Chem. Eng.* **29**, 1439–1446 (2005).
- Bozzano, G., Dente, M., Faravelli, T., and Ranzi, E. *Appl. Therm. Eng.* **22**(8), 919–927 (2002).
- Bozzano, G., Dente, M., and Pirovano, C. *AIDIC Conference Series* **1**, 173–180 (1995).
- Bozzano, G., Dente, M., Sugaya, M., and Mcgreavy, C. “ACS-National Meeting—Boston” 43, p. 653 (1998).
- Bozzelli, J. W., and Dean, A. M. *J. Phys. Chem.* **94**, 3313–3317 (1990).
- Braun-Unkshoff, M., Frank, P., and Just, T. *Ber. Bunsen. Phys. Chem.* **94**, 1417–1425 (1990).
- Broadbelt, L. J., Stark, S. M., and Klein, M. T. *Ind. Eng. Chem. Res.* **33**, 790–799 (1994).
- Broadbelt, L. J., Stark, S. M., and Klein, M. T. *Ind. Eng. Chem. Res.* **34**, 2566–2573 (1995).
- Broadbelt, L. J., Stark, S. M., and Klein, M. T. *Comput. Chem. Eng.* **20**, 113–129 (1996).
- Brown, T. C., and King, K. D. *Int. J. Chem. Kinet.* **21**, 251 (1989).
- Cai, H., Krzywicki, A., and Oballa, M. C. *Chem. Eng. Proc.* **41**, 199 (2002).
- Calcote, H. C. *Combust. Flame* **42**, 215 (1981).
- Chan, K. Y. G., Inal, F., and Senkan, S. *Ind. Eng. Chem. Res.* **37**, 901 (1998).
- Chang, P., Oka, M., and Hsia, Y. P. *Energy Sources* **6**, 67–83 (1982).
- Chevalier, C., Warnatz, J., and Melenk, H. Proc. XII Task Leaders Meeting IEA (1988).
- Clymans, P. J., and Froment, G. F. *Comput. Chem. Eng.* **8**, 137–142 (1984).
- Coats, A. W., and Redfern, J. P. *Nature* **201**, 68 (1964).

- CONCAWE, "Gas oils (diesel fuels/heating oils)", Report 95–107 (1995).
- Curran, H. J., Gaffuri, P., Pitz, W. J., and Westbrook, C. K. *Combust. Flame* **114**, 149–177 (1998).
- D'Anna, A., D'Alessio, A., and Kent, J. H. *Combust. Flame* **125**, 1196–1206 (2001a).
- D'Anna, A., Violi, A., D'Alessio, A., and Sarofim, A. F. *Combust. Flame* **127**, 1995–2003 (2001b).
- de Freitas Sugaya, M., "Analysis of stresses in reactors for pyrolysis of petroleum residues", Ph.D. Thesis, Leeds University, Department of Chemical Engineering (1999).
- De Witt, M. J., Dooling, D. J., and Broadbelt, L. J. *Ind. Eng. Chem. Res.* **39**, 2228–2237 (2000).
- Dean, A. M. *J. Phys. Chem.* **89**, 4600 (1985).
- Del Bianco, A., Panariti, N., Anelli, M., Beltrame, P. L., and Carniti, P. *Fuel* **72**, 75–80 (1993).
- Dente, M., Bozzano, G., and Bussani, G. *Comput. Chem. Eng.* **21**, 1125–1234 (1997).
- Dente, M., Faravelli, T., Pierucci, S., Ranzi, E., Barendregt, S., and Valkenburg, P. AIChE Spring Meeting—Atlanta (2005).
- Dente, M., Pierucci, S., Ranzi, E., and Bussani, G. *Chem. Eng. Sci.* **47**, 2629 (1992).
- Dente, M., Ranzi, E., in "Pyrolysis: Theory and Industrial Practice" (L. F. Albright, B. L. Crines, and W. H. Corcoran Eds.), Academic Press, San Diego (1983).
- Dente, M., Ranzi, E., Antolini, G., and Losco, F. 97th event of the EFCE, Florence (1970).
- Dente, M., Ranzi, E., Barendregt, S., and Tsai, F. W. AIChE Meeting—Houston (1983).
- Dente, M., Ranzi, E., and Goossens, A. G. *Comput. Chem. Eng.* **3**, 61 (1979).
- Ebert, K. H., Ederer, H. J., Shroder, U. K. O., and Hamielec, A. W. *Makromol. Chem.* **183**, 1207 (1982).
- Edwards, T., and Maurice, L. Q. *J. Propul. Power* **17**, 461–466 (2001).
- Ellis, C., Scott, M. S., and Walker, R. W. *Combust. Flame* **132**, 291–304 (2003).
- Evans, B., Dupon, E. J. P., Overwater, J. A. S., and Laghate, A. S. TECHNIP-COFLEXIP Ethylene Conference (2002).
- Faravelli, T., Bozzano, G., Colombo, M., Ranzi, E., and Dente, M. *J. Anal. Appl. Pyrolysis* **70**, 761–777 (2003).
- Faravelli, T., Bozzano, G., Scassa, C., Perego, M., Fabini, S., Ranzi, E., and Dente, M. *J. Anal. Appl. Pyrolysis* **52**, 87–103 (1999).
- Faravelli, T., Goldaniga, A., and Ranzi, E. *P. Combust. Inst.* **27**, 1489–1495 (1998).
- Faravelli, T., Pinciroli, M., Pisano, F., Bozzano, G., Dente, M., and Ranzi, E. *J. Anal. Appl. Pyrolysis* **60**, 103–121 (2001).
- Filho, R. M., and Sugaya, M. *Comput. Chem. Eng.* **25**, 683–692 (2001).
- Flynn, J. H., and Wall, L. A. *J. Polym. Sci. Pol. Lett.* **4**(5), 323 (1966).
- Fournet, R., Battin-Leclerc, F., Glaude, P. A., Judenherc, B., Warth, V., Côme, G. M., Scacchi, G., Ristori, A., Pengloan, G., Dagaut, P., and Cathonnet, M. *Int. J. Chem. Kinet.* **33**, 574–586 (2001).
- Frenklach, M. *Chem. Eng. Sci.* **40**, 1843 (1985).
- Frenklach, M. *Phys. Chem. Chem. Phys.* **4**, 2028–2037 (2002).
- Frenklach, M., Clary, D. W., Gardiner, W. C., and Stein, S. E. *P. Combust. Inst.* **20**, 887–901 (1984).
- Frenklach, M., and Wang, H. *P. Combust. Inst.* **23**, 1559–1566 (1990).
- Frenklach, M., and Wang, H., "Soot Formation in Combustion". Springer-Verlag, Berlin (1994).
- Friedman, H. L. *J. Polym. Sci.* **6**, 183 (1963).
- Frisch, S., Hippler, H., and Troe, J. *Zeitschrift für Physikalische Chemie* **188**, 259–273 (1995).
- Froment, G. F. *Rev. Chem. Eng.* **6**, 293 (1990).
- Froment, G. F. *Chem. Eng. Sci.* **47**, 2163–2174 (1992).
- Gambiroza-Jukic, M., and Cunko, R. *Acta Polym.* **43**, 258–260 (1992).
- Gear, W., "Numerical Initial Value Problems in ODEs". Prentice-Hall, New Jersey (1968).
- Gelbard, F., Tambour, Y., and Seinfeld, J. H. *J. Colloid Interf. Sci.* **76**, 541–556 (1980).
- Glasman, I., "Combustion". Academic Press, San Diego (1996).
- Goossens, A. G., Dente, M., and Ranzi, E. *Oil Gas J.*, Sept. 4, 89–94 (1978).
- Granata, S., Cambianica, F., Zinesi, S., Faravelli, T., and Ranzi, E. ECM—Proceedings of European Combustion Meeting, Louvain-la-Neuve (2005).

- Green, W. H., Barton, P. I., Bhattacharjee, B., Matheu, D. M., Schwer, D. A., Song, J., Sumathi, R., Carstensen, H.-H., Dean, A. M., and Grenda, J. M. *Ind. Eng. Chem. Res.* **40**, 5362–5370 (2001).
- Grenda, J. M., Androulakis, I. P., Dean, A. M., and Green, W. H. *Ind. Eng. Chem. Res.* **42**, 1000–1010 (2003).
- Grenda, J. M., Dean, A. M., Green, W. H. J., and Peczak, P. K. Work-in-Progress Poster (WIPP) Session, at the 27th International Symposium on Combustion, Boulder, CO, Aug 2–7 (1998).
- Haynes, B. S., and Wagner, H. G. *Prog. Energ. Combust. Sci.* **7**, 229 (1981).
- Helveg, S., and Hansen, P. L. *Catal. Today* **111**(1–2), 68–73 (2006).
- Helveg, S., Lopez-Cartes, C., Sehested, J., Hansen, P. L., Clausen, B. S., Rostrup-Nielsen, J. R., Abild-Pedersen, F., and Norskov, J. K. *Nature* **427**(6973), 426–429 (2004).
- Heynderickx, G. J., Cornelis, G. G., and Froment, G. F. *AIChE J.* **38**, 1905–1912 (1992).
- Heynderickx, G. J., Oprins, A. J. M., Marin, G. B., and Dick, E. *AIChE J.* **47**, 388–400 (2001).
- Hillewaert, L. P., Dierickx, J. L., and Froment, G. *AIChE J.* **34**, 17–24 (1988).
- Homann, K. H., and Wagner, H. G. *P. Combust. Inst.* **11**, 371–379 (1967).
- Hudgens, J. W. Workshop on combustion simulation databases for real transportation fuels NIST Gaithersburg, MD (2003).
- Ikeda, E., Tranter, R. S., Kiefer, J. H., Kern, R. D., Singh, H. J., and Zhang, Q. *P. Combust. Inst.* **28**, 1725–1732 (2000).
- Kee, R. J., and Rupley, F. M. Sandia Report SAND87-8215 (1990).
- Knumann, R., and Bockhorn, H. *Combust. Sci. Technol.* **101**, 285–299 (1994).
- Kopinke, F. D., Zimmermann, G., and Nowak, S. *Carbon* **26**, 117 (1988).
- Krambeck, F. J. *Chemtech* **22**(5), 292–299 (1992).
- Krestinin, A. V. *Combust. Flame* **121**, 513–524 (2000).
- Kruse, T. M., Levine, S. E., Wong, H. W., Duoss, E., Lebovitz, A. H., Torkelson, J. M., and Broadbelt, L. J. *J. Anal. Appl. Pyrolysis* **73**, 342–354 (2005).
- Kruse, T. M., Wong, H. W., and Broadbelt, L. J. *Macromolecules* **36**, 9594–9607 (2003).
- Kruse, T. M., Woo, O. S., Wong, H. W., Khan, S. S., and Broadbelt, L. J. *Macromolecules* **35**, 7830–7844 (2002).
- Lattimer, R. P., and Kroenke, W. J. *J. Appl. Polym. Sci.* **27**, 1355–1366 (1982).
- Liguras, D. K., and Allen, D. T. *Ind. Eng. Chem. Res.* **28**, 665–673 (1989).
- Liguras, D. K., and Allen, D. T. *Ind. Chem. Res.* **31**, 45–53 (1992).
- Lobo, D. S., and Trimm, D. L. *J. Catal.* **29**, 15 (1973).
- Lohr, B., and Dittman, H. *Oil Gas J.* July 18, 73–77 (1978).
- Madorsky, S. L. *J. Polym. Sci.* **2**, 133 (1952).
- Madras, G., and McCoy, B. J. *J. Colloid Interf. Sci.* **246**, 356–365 (2002).
- Madras, G., Smith, J. M., and McCoy, B. J. *Polym. Degrad. Stabil.* **52**, 349–358 (1996).
- Magnan, J., Otsubo, K., Matsueda, S., and Fujiwara, M. ERTC Petrochemical Conference, Vienna (2004).
- Marongiu, A. “Thermal Degradation of Polymers”, Ph.D. Thesis, Politecnico di Milano, Department of Chemical Engineering (2006).
- Marongiu, A., Faravelli, T., Bozzano, G., Dente, M., and Ranzi, E. *J. Anal. Appl. Pyrolysis* **70**, 519–553 (2003).
- Matheu, D. M., Green, W. H., and Grenda, J. M. *Int. J. Chem. Kinet.* **35**, 95–119 (2003).
- McCoy, B. J., and Wang, M. *Chem. Eng. Sci.* **49**, 3773–3785 (1994).
- McGivervy, W. S., Manion, J. A., and Tsang, W. WIP 30th International Symposium on Combustion, Chicago, IL, USA July Paper 1F1-02, (2004).
- Mehl, M., Marongiu, A., Faravelli, T., Bozzano, G., Dente, M., and Ranzi, E. *J. Anal. Appl. Pyrolysis* **72**, 253–272 (2004).
- Merchan-Merchan, W., Saveliev, A. V., and Kennedy, L. A. *Combust. Sci. Technol.* **175**, 2217 (2003).

- Migliavacca, G., Parodi, E., Bonfanti, L., Faravelli, T., Pierucci, S., and Ranzi, E. *Energy* **30**, 1453–1468 (2005).
- Miller, J. A. *Faraday Discuss.* **119**, 461–475 (2001).
- Miller, J. A., and Melius, C. F. *Combust. Flame* **91**, 21–39 (1992).
- Miller, J. A., Pilling, M. J., and Troe, J. P. *Combust. Inst.* **30**, 43–88 (2005).
- Miranda, R., Pakdel, H., Roy, C., and Vasile, C. *Polym. Degrad. Stabil.* **73**, 47–67 (2001).
- Montaudo, G., and Puglisi, C. *Polym. Degrad. Stabil.* **33**, 229–262 (1991).
- Moskaleva, L. V., Mebel, A. M., and Lin, M. C. P. *Combust. Inst.* **26**, 521–526 (1996).
- Muller, C., Michel, V., Scacchi, G., and Côme, G. M. *J. Chim. Phys.* **92**, 1154 (1995).
- Oberdorster, G., Sharp, Z., Atudorei, V., Elder, A., Gelein, R., Kreyling, W., and Cox, C. *Inhal. Toxicol.* **16**, 437–445 (2004).
- Oka, M., Chang, P., and Gavales, G. R. *Fuel* **56**, 3–8 (1977).
- Palmer, H. B., and Cullis, H. F., “The Chemistry and Physics of Carbon”. Dekker, New York (1965).
- Pierucci, S., Ranzi, E., and Barendregt, S. ESCAPE 15, Barcelona (2005).
- Poutsma, M. L. *J. Anal. Appl. Pyrolysis* **54**, 5–35 (2000).
- Poutsma, M. L. *Macromolecules* **36**, 8931–8957 (2003).
- Quann, R. J., and Jaffe, S. B. *Ind. Eng. Chem. Res.* **31**, 2483–2497 (1992).
- Quann, R. J., and Jaffe, S. B. *Chem. Eng. Sci.* **51**, 1615–1635 (1996).
- Ranzi, E. *Energy Fuels* **20**, 1024–1032 (2006).
- Ranzi, E., Dente, M., Faravelli, T., Bozzano, G., Fabini, S., Nava, R., Cozzani, V., and Tognotti, L. *J. Anal. Appl. Pyrolysis* **40/41**, 305–319 (1997a).
- Ranzi, E., Dente, M., Faravelli, T., and Pennati, G. *Combust. Sci. Technol.* **95**, 1–50 (1994).
- Ranzi, E., Dente, M., Goldaniga, A., Bozzano, G., and Faravelli, T. *Prog. Energ. Combust.* **27**, 99–139 (2001).
- Ranzi, E., Dente, M., Pierucci, S., Barendregt, S., Cronin, P. *Oil Gas J.* Sept. 2, 49–52 (1985).
- Ranzi, E., Faravelli, T., Gaffuri, P., Garavaglia, E., and Goldaniga, A. *Ind. Eng. Chem. Res.* **36**, 3336–3344 (1997b).
- Ranzi, E., Faravelli, T., Gaffuri, P., and Sogaro, A. *Combust. Flame* **102**, 179–192 (1995).
- Ranzi, E., Frassoldati, A., Granata, S., and Faravelli, T. *Ind. Eng. Chem. Res.* **44**, 5170–5183 (2005).
- Ren, T., Patel, M., and Blok, K. *Energy* **31**, 425–451 (2006).
- Rice, F. O., and Herzfeld, K. F. *J. Am. Chem. Soc.* **55**, 3035–3040 (1933).
- Rice, F. O., and Herzfeld, K. F. *J. Am. Chem. Soc.* **56**, 284–289 (1934).
- Richter, H., Granata, S., Green, W. H., and Howard, J. B. *P. Combust. Inst.* **30**, 1397–1405 (2005).
- Ritter, E. R., and Bozelli, J. W. *Int. J. Chem. Kinet.* **23**, 767–778 (1991).
- Robaugh, D., and Tsang, W. *J. Phys. Chem.* **90**, 4159 (1986).
- Roth, W. R., Bauer, F., Beitat, A., Ebbrecht, T., and Wustefeld, M. *Chem. Ber.* **124**, 1453–1460 (1991).
- Saeyns, M., Reyniers, M. F., Marin, G. B., Van Speybroeck, V., and Waroquier, M. *J. Phys. Chem. A* **107**(43), 9147–9159 (2003).
- Saeyns, M., Reyniers, M. F., Marin, G. B., Van Speybroeck, V., and Waroquier, M. *AIChE J* **50**(2), 426–444 (2004).
- Saeyns, M., Reyniers, M. F., Van Speybroeck, V., Waroquier, M., and Marin, G. B. *ChemPhysChem* **7**(1), 188–199 (2006).
- Sarofim, A. F., and Longwell, J. P., “Soot Formation in Combustion”. Springer-Verlag, Berlin (1994).
- Savage, P. E. *J. Anal. Appl. Pyrolysis* **54**, 109–126 (2000).
- Seery, D. J., and Bowman, C. T. *Combust. Flame* **14**, 37–48 (1970).
- Smith, H. M., “Qualitative and Quantitative Aspects of Crude Oil Composition”. Bureau of Mines, Bartlesville (1968).
- Smoot, L. D., Hecker, W. C., and Williams, G. A. *Combust. Flame* **26**, 323–342 (1976).

- Steward, D. V. *Soc. Ind. Appl. Math. J.* **2B**, 345 (1965).
- Sundaram, K. M., and Froment, G. F. *Ind. Eng. Chem.* **17**, 174 (1978).
- Susnow, R. G., Dean, A. M., Green, W. H., Peczak, P., and Broadbelt, L. J. *J. Phys. Chem. A* **101**, 3731–3740 (1997).
- Touchard, S., Fournet, R., Glaude, P. A., Warth, V., Battin-Leclerc, F., Vanhove, G., Ribacour, M., and Minetti, R. *P. Combust. Inst.* **30** (2004).
- Tsang, W. *Int. J. Chem. Kinet.* **10**, 1119 (1978a).
- Tsang, W. *Int. J. Chem. Kinet.* **10**, 599 (1978b).
- Tsang, W. *Int. J. Chem. Kinet.* **10**, 821 (1978c).
- Tsang, W. *J. Phys. Chem. Ref. Data* **17**, 887 (1988).
- Tsang, W. *Ind. Eng. Chem.* **31**, 3–8 (1992).
- Tsang, W. *Data Sci. J.* **3**, 1–9 (2004).
- Van Geem, K. M., Heynderickx, G. J., and Marin, G. B. *AIChE J.* **50**, 173–183 (2004).
- Van Krevelen, D. W., “COAL, Typology, Chemistry-Physics-Constitution”. Elsevier, Amsterdam (1961).
- Van Krevelen, D. W., “Properties of Polymers, their Estimation and Correlation with Chemical Structure”. Elsevier, Amsterdam (1976).
- Van Nes, K., and Van Westen, H. A., “Aspects of the Constitution of Mineral Oils”. Elsevier Publ. Company, New York (1951).
- Vlasov, P. A., and Warnatz, J. *P. Combust. Inst.* **29**, 2335–2341 (2002).
- Warnatz, J., Rate coefficients in the C/H/O system, in “Combustion Chemistry” (W.C. Gardiner Ed.), Springer-Verlag, New York (1984).
- Warth, V., Battin-Leclerc, F., Fournet, R., Glaude, P. A., Côme, G. M., and Scacchi, G. *Comput. Chem.* **24**, 541–560 (2000).
- Watson, K. M., Nelson, E. F., and Murphy, G. B. *Ind. Eng. Chem.* **27**(12), 1460–1466 (1935).
- Wauters, S., and Marin, G. B. *Chem. Eng. J.* **82**(1–3), 267–279 (2001).
- Wauters, S., and Marin, G. B. *Ind. Eng. Chem. Res.* **41**, 2379 (2002).
- Weissman, M., and Benson, S. W. *Int. J. Chem. Kinet.* **16**, 307 (1984).
- Westbrook, C. K., and Dryer, F. C. *Prog. Energ. Combust. Sci.* **10**, 1–57 (1984).
- Westbrook, C. K., Mizobuchi, Y., Poinso, T. J., Smith, P. J., and Warnatz, J. *P. Combust. Inst.* **30**, 125–157 (2004).
- Westerhout, R. W. J., Waanders, J., Kuipers, J. A. M., and Van Swaaij, W. P. M. *Ind. Eng. Chem. Res.* **36**, 1955–1964 (1997).
- Westmoreland, P. R., Dean, A. M., Howard, J. B., and Longwell, J. P. *J. Phys. Chem.* **93**, 8171–8180 (1989).
- Wulkow, M. *Macromol. Theor. Simul.* **5**, 393 (1996).
- Yoneda, Y. *Bull. Chem. Soc. Jpn.* **52**, 8–14 (1979).
- Zhao, B., Yang, Z., Johnston, M. V., Wang, H., Wexler, A. S., Balthasar, M., and Kraft, M. *Combust. Flame* **133**, 173–188 (2003).
- Zimmerman, G., Dente, M., and Van Leeuwen, C. AIChE Meeting, Orlando (1990).
- Zou, R., Lou, Q., Liu, H., and Niu, F. *Ind. Eng. Chem. Res.* **26**, 2528 (1987).
- Zychlinski, W., Wynns, K. A., and Ganser, B. *Mater. Corros.* **53**, 30–36 (2002).